Calculation of Convective and Radiative Heating on the Forebody Heatshield of the Aeroassist Flight Experiment Vehicle

H. Harris Hamilton II

Robert B. Greendyke

May 1991

CALCULATION OF CONVECTIVE AND RADIATIVE HEATING ON THE FOREBODY HEATSHIELD OF THE AEROASSIST FLIGHT EXPERIMENT VEHICLE

H. Harris Hamilton II
Langley Research Center
Hampton, Virginia

and

Robert B. Greendyke
Analytical Services and Materials, Inc.
Hampton, Virginia

Introduction

In order to obtain the data necessary to design future aeroassisted space transfer vehicles, NASA is currently developing the Aeroassist Flight Experiment (AFE). The vehicle used in this experiment will be deployed from the Shuttle Orbiter (scheduled for 1996), make a data-gathering aeropass through the upper atmosphere, and then return to orbit for pickup by the shuttle. The primary purpose of the AFE is to obtain data in the flight regime where chemical and thermal nonequilibrium effects dominate the shock layer, because such effects may play a large role in the design of aeroshells for future aeroassisted space transfer vehicles. A review of aeroassist concepts is given by Walberg.[1]

The absence of applicable flight data and the inability of ground-based wind tunnels to simulate the low-density, high-energy flight environment[2,3] is the impelling force which dictates the need for the AFE. This lack of data also creates an uncertainty in the heat transfer predictions which are needed to design the AFE heatshield. Among the important factors which must be considered in the heating predictions are both chemical and thermal nonequilibrium, an extensive viscous region, small but finite wall recombination rates, nonequilibrium radiative heating, and three-dimensional effects due to a nonaxisymmetric heatshield geometry.

Rochelle et al.[4,5] have used an axisymmetric chemically reacting boundary layer code[6] to predict heating on the forebody heatshield of the AFE vehicle. However, a boundary-layer method does not properly account for the viscous-inviscid interaction and entropy-layer-swallowing effects.

Hamilton et al.[7] used an axisymmetric chemically reacting viscous-shock-layer code[8] at lower altitudes and a Navier Stokes code[9] at higher altitudes to calculate the stagnation point heating rate for a typical AFE trajectory. This approach automatically accounts for viscous-inviscid interaction effects not accounted for in the above boundary layer results. The effect of wall slip was also investigated at high altitudes, but it was found to be unimportant for

the AFE. Although this approach, provides the best set of heating calculations for the AFE vehicle's stagnation point it provides no information about heating for the remainder of the forebody heatshield.

The purpose of the present paper is to calculate the total (convective and radiative) heating over the entire forebody heatshield of the AFE vehicle. The convective heating is calculated using a three-dimensional Navier-Stokes code (LAURA) which includes both chemical and thermal nonequilibrium effects. The output from the flowfield calculation is then used to provide inputs to a nonequilibrium air radiation code (NEQAIR)[10] to calculate the nonequilibrium radiative heating. Results are presented at two points on the current Baseline 5A trajectory corresponding to the start of the primary data taking period and peak heating (near the end of the primary data taking period).

Symbols

M	Mach number
p	pressure, N/m^2
q	convective heating rate, W/cm^2
s	surface distance from nose along meridional plane, m
T	static temperature, deg K
V_∞	free-stream velocity, km/sec
x, y, z	cartesian coordinates (see Fig. 1), m
ϵ	emissivity
ϕ	meridional angle (see Fig. 1), deg
σ	Stefan-Boltzmann constant, $5.6696 \times 10^{-12} W/cm^2 K^4$
ρ	density, kg/m^3

Subscripts:

c	convective
r	radiative
req	radiative equilibrium
total	total
w	wall
∞	free stream

Vehicle and Trajectory

The aerobrake on the AFE vehicle (Fig. 1) is an elliptic cone, blunted with an ellipsoidal nose, and raked off at an angle of 17° relative to the cone axis. The ellipticity of the cone is such

as to produce a circular base in the rake plane which produces a highly three-dimensional stagnation region. A skirt is fitted tangent to the elliptic cone at the rake plane to reduce heating in this region. The aerobrake is made of a conventional aluminum structure covered with a thermal protection system with the outer layer consisting of tiles similar to those used on the Shuttle Orbiter.

The vehicle is deployed from the shuttle payload bay. It is maneuvered to its entry attitude and then driven into the outer fringes of the atmosphere at a high velocity by a solid rocket motor which is jettisoned prior to the data-collection phase of the experiment. The vehicle enters the atmosphere at approximately 9.9 km/sec and penetrates to a perigee of approximately 75 km where its Velocity has decreased to 8.7 km/sec (see Fig. 2) It is then maneuvered back into a higher Earth orbit using aerodynamic lift and is retrieved by the Shuttle Orbiter and returned to Earth. The most important part of the mission, from a scientific view point, is the entry phase from 90 km down to 75 km where several instruments will take data.

In the current paper, the heating is calculated at two points on the Baseline 5A trajectory: (1) peak heating and (2) the beginning of the quiescent period (see freestream flow conditions in Table I). The quiescent period is a period of approximately 30 sec when the attitude control jets are not fired (unless absolutely necessary to maintain control of the vehicle) so that data can be measured with minimum jet interference.

Computational Methods

In the present paper, convective heating to the AFE heatshield is computed using the LAURA code and radiative heating is computed using the NEQAIR code. A brief description of these codes is presented in this section.

LAURA

Gnoffo[11,12] has developed a three-dimensional, Navier-Stokes flowfield code, LAURA (Langley Aerodynamic Upwind Relaxation Algorithm), which includes both thermal and chemical nonequilibrium. The LAURA code is described in detail in Refs. 11 and 12. The version of the LAURA code used in the present paper is a three-dimensional, second-order accurate, finite-volume algorithm that solves the thin-layer Navier-Stokes equations for laminar flow. The code uses a two-temperature thermal model and an 11-species chemical model for air.[13] The thermodynamic and transport properties are taken from Ref. 14.

The governing equations are relaxed in "pseudo" time until the solution reaches steady-state. The treatment of the governing equations is described as point-implicit because variables at the cell center of interest are treated implicitly, while the latest available data are used for the left-hand-side numerics. With this strategy, updating cell-centered variables requires the inversion of only a 16 x 16 matrix and only one level of storage.

3

The solutions presented in the present paper were computed with a grid of which had 64 points between the body and the outer computational boundary. The grid on the body surface is shown in Fig. 3 where there were 42 points in the i direction and 21 points in the j direction. The surface grid was set up in this fashion instead of in meridional planes passing through the nose to avoid a "pole type" singularity at the nose.

NEQAIR

The NEQAIR[10] code is a nonequilibrium air radiation code that calculates the population distribution of atoms and molecules among their states by use of the quasi-steady-state assumption (QSS). The QSS assumes that the rates of population and depopulation of a given electronic state are much larger than the difference between the two rates, and the difference can be effectively ignored. Given the known population rates, the number densities of the excited and ground states can then be calculated from the predetermined thermodynamic state for any point in the flowfield. The NEQAIR code then calculates the intensity of radiative emission through a line-by-line integration over the spectral region in question.

For the purposes of this investigation, the gas was assumed to be opaque below 2000 angstroms and non-absorbing between 2000 and 15000 angstroms. Higher wavelengths were ignored. The total global emission was then integrated over the distance normal to the wall using the tangent-slab approximation to obtain the total radiative flux to the wall.

The data that was input to NEQAIR (the species number density and temperature profiles) is obtained from the converged flowfield.

Approach

The forebody heatshield of the AFE vehicle is subjected to high heating on the entry phase of the mission prior to perigee. In order to design a vehicle that can survive and perform its mission successfully, one must accurately predict the heating environment. The conditions are such that the flow within the shock layer is in both thermal and chemical nonequilibrium. The surface heating is primarily convective, but the nonequilibrium radiative heating is too large to ignore completely.

The LAURA code is used in the present paper to calculate the convective heating. Wall slip was neglected since it has been shown[7] that it is unimportant for these conditions. The surface of the aerobrake is covered with tile, made from the same material as that used on the shuttle orbiter, which has a small but finite chemical recombination rate. To account for this effect, the surface catalysis results of Stewart[15] have been used in the present calculations.

Once a converged flowfield solution has been obtained, the species number density and temperature profiles at a grid point on the body are input to the NEQAIR code and the

4

radiative heating at that grid point is computed. This process is repeated at every second grid point on the body (in both directions) until the entire heatshield surface has been covered. The radiative heating at the intervening surface grid points is obtained by interpolation.

The wall temperature used in the present analysis was the radiation equilibrium value ($T_{w,req}$) iteratively calculated from the following equation

$$T_{w,req} = [(q_{w,c} + q_{w,r})/\epsilon\sigma]^{1/4} \tag{1}$$

where the surface emissivity ϵ was assumed to 0.85.

The procedure for carrying out the computation was as follows:

1. A initial wall temperature is assumed (usually constant or from a previous converged solution at different flow conditions).

2. The LAURA code is run to obtain a flowfield solution and values for the convective heating rate ($q_{w,c}$).

3. Using the species-number-density and temperature profiles extracted from the flowfield solution, NEQAIR is run to obtain the radiative heating ($q_{w,r}$) at each body grid point. This step need only be done once during the iteration process since surface temperature has a very weak affect on radiative heating using the present uncoupled approach.

4. Equation (1) is now solved for a new value of wall temperature at each body grid point.

5. A check is made for overall convergence by comparing the new wall temperatures with those used in step 2.

6. If the wall temperature has not converged, go back to step 2 and repeat the process with the new wall temperature.

The iteration process for wall temperature is stopped when the maximum difference between input (at step 2) and output (at step 4) wall temperature is approximately 50°K. This required three passes for the results presented in the present paper.

Discussion of Results

Distribution of surface heating along meridional planes for the peak heating point on the trajectory are presented in Fig. 4. The vehicle was at $\alpha = 0°$. The flow conditions for this case is presented in Table I. On the lower portion of the body ($\phi \leq 0°$ - Figs. 4(a)-4(f)) the heating decreases as away from the stagnation point ($s \approx 0$), levels out over the conical

portion of the body and then rises again as near the beginning of the skirt. The rise in the heating near the beginning of the skirt is caused by the rapid acceleration of the flow in this region. On the upper portion of the body ($\phi > 0°$) the conical region decreases rapidly (see Fig. 1) and thus the tendency for the heating to level out on the conical segment of the body is less pronounced. The rise in heating at the beginning of the skirt is also less pronounced than it was on the lower portion of the body.

The wall temperatures along meridional planes for this case are presented in Fig. 5. These are the resulting wall temperatures after three iterations as discussed in the previous section. The heating contours and wall temperature contours for this case are presented in Figs. 6 and 7, respectively.

Distribution of surface heating along meridional planes for the beginning of the quiescent period are presented in Fig. 8. The vehicle was at $\alpha = 0°$. The flow conditions for this case is presented in Table I. The heating follows similar trends to the peak heating results discussed previously but the overall level is somewhat lower because the freestream density is lower.

The wall temperatures along meridional planes for this case are presented in Fig. 9. The heating contours and wall temperature contours for this case are presented in Figs. 10 and 11, respectively.

The surface heating rates have been interpolated onto the body point locations identified in the Aerothermodynamic Data Book[5] and these results are given in Tables II and III for the peak heating and beginning of the quiescent period, respectively. The results are provided in this form to assist with the heatshield design.

Concluding Remarks

The nonequilibrium convective and radiative heating rates on the heatshield of the AFE vehicle have been computed for two points (peak heating and the beginning of the quiescent period) on the baseline 5A trajectory. These results which are presented in both graphical and tabular form represent the most complete set of heating calculations available for the AFE vehicle.

References

1. Walberg, G. D., A Survey of Aeroassisted Orbit Transfer, Journal of Spacecraft and Rockets, Vol. 22, January-February 1985, pp. 3-18.

2. Jones, J. J., The Rationale for an Aeroassist Flight Experiment, AIAA Paper 87-1508, June 1987.

3. Walberg, G. D., Siemers, P. M. III, Calloway, R. L., and Jones, J. J., The Aeroassist Flight Experiment, Paper No. IAF-87-197, October 1987.

4. Rochelle, W. C., Ting, P. C., Mueller, S. R., Colovin, J. E., Bouslog, S.A, Curry, D. M., and Scott, C. D., Aerobrake Heating Rate Sensitivity Study for the Aeroassist Flight Experiment (AFE), AIAA Paper 89-1733, June 1989.

5. Rochelle, W. C., Ting, P. C., Mueller, S. R., Colovin, J. E., Data Book Documentation, AFE Aerobrake Aerothermodynamic Data Book for Baseline V Trajectory, Volume I - Pitch Plane and Volume II - Off Pitch Planes, Lockheed Engineering & Sciences Co., Houston, TX, LESC-26950 (JSC-23623), April 1989.

6. Tong, H., User's Manual, Nonequilibrium Chemistry Boundary Layer Integral Matrix Procedure, Aerotherm Corporation, Mountain View, CA, Aerotherm Report UM-73-37, Part I, July 1973.

7. Hamilton, H. H. II, Gupta, Roop N., Jones, Jim J., Flight Stagnation-Point Heating Calculations on Aeroassist Flight Experiment Vehicle, Journal of Spacecraft and Rockets, Vol. 28, No. 1, January-February 1991, pp. 125-128.

8. Gupta, R. N., and Simmons, A. L., Stagnation Flowfield Analysis for an Aeroassist Flight Experiment Vehicle, AIAA Paper 88-2613, June 1988.

9. Gupta, R. N., Navier-Stokes and Viscous Shock-Layer Solutions for Radiating Hypersonic Flows, AIAA Paper 87-1576, June 1987.

10. Park, C., Nonequilibrium Air Radiation (NEQAIR) Program: User's Manual, NASA TM 86707, July 1985.

11. Gnoffo, P. A., A Code Calibration Program in Support of the Aeroassist Flight Experiment, AIAA Paper 89-1673, June 1989.

12. Gnoffo, P. A., Gupta, R. N., Shinn, J. L. Conservation Equations and Physical Models for Hypersonic Air Flows in Thermal and Chemical Nonequilibrium, NASA TP-2867, February 1989.

13. Park, C., Assessment of Two-Temperature Kinetic Model for Ionizing Air, AIAA Paper 87-1574, June 1987.

14. Gupta, Roop N., Yos, Jerrold M., Thompson, Richard A., and Lee, Kam-Pui, A Review of Reaction Rates and Thermodynamic and Transport Properties for an 11-Species Air Model for Chemical and Thermal Nonequilibrium Calculations to 30,000 K, NASA Reference Publication 1232, August 1990.

15. Stewart, D. A. and Kolodziej, P., Wall Catalysis Experiment on AFE, AIAA Paper 88-2674, June 1988.

7

Table I. Freestream flow conditions.

Case	α deg	ρ_∞ kg/m^3	V_∞ km/sec	T_∞ ^oK	p_∞ N/m^2
Beginning of Quiescent Period	0	2.176×10^{-5}	9.715	196.8	1.227
Peak Heating	0	3.741×10^{-5}	9.306	198.9	2.134

Table II. - Heating rates on body at peak heating.

No	x	y	z	q_r	q_c	q_t	T_w
	m	m			W/cm^2		K
100	0.30305E+00	0.00000E+00	0.00000E+00	0.57573E+01	0.43623E+02	0.49380E+02	0.17891E+04
101	0.32883E+00	-0.34036E+00	0.00000E+00	0.47447E+01	0.43492E+02	0.48237E+02	0.17787E+04
103	0.51326E+00	-0.88900E+00	0.00000E+00	0.20815E+01	0.35776E+02	0.37857E+02	0.16741E+04
105	0.82123E+00	-0.14224E+01	0.00000E+00	0.16740E+01	0.32354E+02	0.34028E+02	0.16301E+04
107	0.11292E+01	-0.19558E+01	0.00000E+00	0.18543E+01	0.30282E+02	0.32136E+02	0.16069E+04
109	0.15105E+01	-0.26162E+01	0.00000E+00	0.20710E+01	0.32914E+02	0.34985E+02	0.16414E+04
301	0.16302E+01	-0.28237E+01	0.00000E+00	0.20101E+01	0.28510E+02	0.30520E+02	0.15820E+04
303	0.19646E+01	-0.30168E+01	0.00000E+00	0.69467E+00	0.31450E+01	0.38396E+01	0.89803E+03
111	0.32883E+00	-0.33680E+00	-0.59411E-01	0.46835E+01	0.43478E+02	0.48162E+02	0.17780E+04
113	0.51326E+00	-0.88011E+00	-0.15517E+00	0.20531E+01	0.35916E+02	0.37969E+02	0.16754E+04
115	0.82123E+00	-0.14082E+01	-0.24828E+00	0.17046E+01	0.32416E+02	0.34120E+02	0.16312E+04
117	0.11292E+01	-0.19360E+01	-0.34138E+00	0.18869E+01	0.30543E+02	0.32430E+02	0.16106E+04
119	0.15105E+01	-0.25898E+01	-0.45667E+00	0.20926E+01	0.33665E+02	0.35758E+02	0.16504E+04
311	0.16119E+01	-0.27638E+01	-0.48732E+00	0.20395E+01	0.29067E+02	0.31107E+02	0.15860E+04
313	0.19456E+01	-0.29545E+01	-0.52098E+00	0.10676E+01	0.79920E+00	0.18668E+01	0.93121E+03
131	0.32883E+00	-0.30823E+00	-0.17795E+00	0.46407E+01	0.43503E+02	0.48144E+02	0.17778E+04
133	0.51326E+00	-0.80457E+00	-0.46452E+00	0.20247E+01	0.36854E+02	0.38878E+02	0.16852E+04
135	0.82121E+00	-0.12881E+01	-0.74369E+00	0.18522E+01	0.33230E+02	0.35082E+02	0.16426E+04
137	0.11292E+01	-0.17711E+01	-0.10226E+01	0.20704E+01	0.32321E+02	0.34391E+02	0.16344E+04
331	0.14736E+01	-0.23114E+01	-0.13345E+01	0.20450E+01	0.29000E+02	0.31045E+02	0.15908E+04
333	0.18017E+01	-0.24841E+01	-0.14342E+01	0.49518E+00	0.16939E+01	0.21891E+01	0.88635E+03
151	0.32883E+00	-0.24460E+00	-0.29162E+00	0.47357E+01	0.43564E+02	0.48300E+02	0.17792E+04
153	0.51333E+00	-0.63906E+00	-0.76170E+00	0.20969E+01	0.37859E+02	0.39955E+02	0.16968E+04
155	0.82123E+00	-0.10226E+01	-0.12187E+01	0.21216E+01	0.35231E+02	0.37352E+02	0.16685E+04
157	0.11292E+01	-0.14061E+01	-0.16757E+01	0.21335E+01	0.37895E+02	0.40028E+02	0.16975E+04
351	0.12384E+01	-0.15422E+01	-0.18379E+01	0.17374E+01	0.27408E+02	0.29146E+02	0.15550E+04
353	0.15547E+01	-0.16759E+01	-0.19973E+01	0.14816E+00	0.10686E+01	0.12167E+01	0.83202E+03

Table II. - Continued.

No	x	y	z	q_r	q_c	q_t	T_w
		m			W/cm^2		K
171	0.32883E+00	-0.13932E+00	-0.38280E+00	0.48363E+01	0.43610E+02	0.48446E+02	0.17806E+04
173	0.51326E+00	-0.36393E+00	-0.99985E+00	0.22786E+01	0.39308E+02	0.41586E+02	0.17139E+04
175	0.82123E+00	-0.58227E+00	-0.15998E+01	0.22154E+01	0.38962E+02	0.41177E+02	0.17097E+04
371	0.97917E+00	-0.69428E+00	-0.19075E+01	0.16031E+01	0.30826E+02	0.32429E+02	0.16079E+04
373	0.12770E+01	-0.76784E+00	-0.21097E+01	0.21736E+00	0.32056E+00	0.53792E+00	0.81988E+03
191	0.32883E+00	0.00000E+00	-0.41956E+00	0.49050E+01	0.43759E+02	0.48664E+02	0.17826E+04
193	0.51326E+00	0.00000E+00	-0.10959E+01	0.23206E+01	0.39816E+02	0.42136E+02	0.17196E+04
391	0.76695E+00	0.00000E+00	-0.16375E+01	0.16527E+01	0.38087E+02	0.39739E+02	0.16921E+04
393	0.10423E+01	0.00000E+00	-0.18527E+01	0.39915E+00	0.36264E+01	0.40255E+01	0.81930E+03
182	0.32883E+00	0.13932E+00	-0.38280E+00	0.51149E+01	0.43762E+02	0.48877E+02	0.17846E+04
184	0.51326E+00	0.36370E+00	-0.99924E+00	0.22243E+01	0.39935E+02	0.42159E+02	0.17198E+04
382	0.63043E+00	0.44691E+00	-0.12279E+01	0.16695E+01	0.40046E+02	0.41715E+02	0.17152E+04
384	0.88402E+00	0.51760E+00	-0.14221E+01	0.29857E+00	0.46397E+01	0.49383E+01	0.99230E+03
162	0.32883E+00	0.24470E+00	-0.29162E+00	0.52111E+01	0.43715E+02	0.48926E+02	0.17850E+04
164	0.51326E+00	0.63876E+00	-0.76124E+00	0.20656E+01	0.39600E+02	0.41666E+02	0.17148E+04
362	0.55547E+00	0.69169E+00	-0.82433E+00	0.16449E+01	0.39504E+02	0.41149E+02	0.17094E+04
364	0.79266E+00	0.81653E+00	-0.97310E+00	0.25630E+01	0.44479E+02	0.47042E+02	0.10066E+04
142	0.32883E+00	0.30823E+00	-0.17795E+00	0.52484E+01	0.43713E+02	0.48962E+02	0.17853E+04
342	0.51836E+00	0.81308E+00	-0.46944E+00	0.18798E+01	0.38871E+02	0.40751E+02	0.17052E+04
344	0.74524E+00	0.97168E+00	-0.56098E+00	0.30035E+00	0.73498E+01	0.76501E+01	0.11197E+04
122	0.32883E+00	0.33693E+00	-0.59411E-01	0.53237E+01	0.43669E+02	0.48992E+02	0.17856E+04
322	0.50317E+00	0.86274E+00	-0.15212E+00	0.20838E+01	0.39308E+02	0.41392E+02	0.17119E+04
324	0.72522E+00	0.10370E+01	-0.18285E+00	0.32528E+00	0.83066E+01	0.86319E+01	0.11504E+04
102	0.32883E+00	0.34036E+00	0.00000E+00	0.53999E+01	0.43631E+02	0.49031E+02	0.17859E+04
302	0.50142E+00	0.86850E+00	0.00000E+00	0.21191E+01	0.39418E+02	0.41537E+02	0.17134E+04
304	0.72291E+00	0.10447E+01	0.00000E+00	0.30007E+00	0.78185E+01	0.81185E+01	0.11339E+04
112	0.39980E+00	-0.63177E+00	-0.11085E+00	0.30941E+01	0.41585E+02	0.44680E+02	0.17445E+04

Table II. - Concluded.

No	x	y	z	q_r	q_c	q_t	T_w
		m			W/cm^2		K
132	0.39845E+00	-0.57478E+00	-0.33017E+00	0.31389E+01	0.42288E+02	0.45427E+02	0.17522E+04
152	0.39627E+00	-0.45212E+00	-0.53619E+00	0.32465E+01	0.42100E+02	0.45346E+02	0.17512E+04
172	0.39418E+00	-0.25527E+00	-0.69781E+00	0.33919E+01	0.42759E+02	0.46151E+02	0.17591E+04
177	0.91895E+00	-0.65156E+00	-0.17901E+01	0.18634E+01	0.37706E+02	0.39569E+02	0.16907E+04
192	0.39332E+00	0.00000E+00	-0.76218E+00	0.35810E+01	0.43303E+02	0.46884E+02	0.17661E+04
195	0.73162E+00	0.00000E+00	-0.15621E+01	0.19120E+01	0.41526E+02	0.43438E+02	0.17327E+04
183	0.39418E+00	0.25527E+00	-0.69779E+00	0.37220E+01	0.43365E+02	0.47087E+02	0.17680E+04
186	0.60038E+00	0.42568E+00	-0.11695E+01	0.18429E+01	0.40758E+02	0.42601E+02	0.17243E+04
163	0.39624E+00	0.45220E+00	-0.53619E+00	0.37994E+01	0.43050E+02	0.46849E+02	0.17658E+04
143	0.39845E+00	0.57475E+00	-0.33017E+00	0.37968E+01	0.42819E+02	0.46616E+02	0.17636E+04
123	0.39980E+00	0.63180E+00	-0.11085E+00	0.38176E+01	0.42668E+02	0.46486E+02	0.17623E+04

Table III. - Heating rates on body at beginning of quiescent period.

No	x	y	z	q_r	q_c	q_t	T_w
	m	m			W/cm^2		K
100	0.30305E+00	0.00000E+00	0.00000E+00	0.67713E+01	0.36680E+02	0.43451E+02	0.17328E+04
101	0.32883E+00	-0.34036E+00	0.00000E+00	0.59922E+01	0.36326E+02	0.42318E+02	0.17214E+04
103	0.51326E+00	-0.88900E+00	0.00000E+00	0.30896E+01	0.29958E+02	0.33048E+02	0.16182E+04
105	0.82123E+00	-0.14224E+01	0.00000E+00	0.23057E+01	0.28280E+02	0.30586E+02	0.15872E+04
107	0.11292E+01	-0.19558E+01	0.00000E+00	0.25568E+01	0.27877E+02	0.30434E+02	0.15853E+04
109	0.15105E+01	-0.26162E+01	0.00000E+00	0.29148E+01	0.28410E+02	0.31325E+02	0.15967E+04
301	0.16302E+01	-0.28237E+01	0.00000E+00	0.28437E+01	0.22432E+02	0.25276E+02	0.15070E+04
303	0.19646E+01	-0.30168E+01	0.00000E+00	0.13427E+01	0.14432E+02	0.27858E+01	0.93184E+03
111	0.32883E+00	-0.33680E+00	-0.59411E-01	0.59218E+01	0.36305E+02	0.42227E+02	0.17205E+04
113	0.51326E+00	-0.88011E+00	-0.15517E+00	0.30537E+01	0.30037E+02	0.33091E+02	0.16187E+04
115	0.82123E+00	-0.14082E+01	-0.24828E+00	0.23438E+01	0.28278E+02	0.30621E+02	0.15877E+04
117	0.11292E+01	-0.19360E+01	-0.34138E+00	0.26031E+01	0.27887E+02	0.30490E+02	0.15860E+04
119	0.15105E+01	-0.25898E+01	-0.45667E+00	0.29401E+01	0.29006E+02	0.31947E+02	0.16045E+04
311	0.16119E+01	-0.27638E+01	-0.48732E+00	0.28873E+01	0.23889E+02	0.26776E+02	0.15272E+04
313	0.19456E+01	-0.29545E+01	-0.52098E+00	0.10987E+01	0.21987E+02	0.32974E+01	0.91071E+03
131	0.32883E+00	-0.30823E+00	-0.17795E+00	0.58586E+01	0.36321E+02	0.42179E+02	0.17200E+04
133	0.51326E+00	-0.80457E+00	-0.46452E+00	0.29712E+01	0.30585E+02	0.33556E+02	0.16244E+04
135	0.82121E+00	-0.12881E+01	-0.74369E+00	0.25359E+01	0.28567E+02	0.31103E+02	0.15939E+04
137	0.11292E+01	-0.17711E+01	-0.10226E+01	0.28687E+01	0.28395E+02	0.31264E+02	0.15959E+04
331	0.14736E+01	-0.23114E+01	-0.13345E+01	0.28086E+01	0.23012E+02	0.25821E+02	0.15126E+04
333	0.18017E+01	-0.24841E+01	-0.14342E+01	0.44729E-01	0.84840E+00	0.89313E+00	0.76532E+03
151	0.32883E+00	-0.24460E+00	-0.29162E+00	0.59121E+01	0.36392E+02	0.42304E+02	0.17213E+04
153	0.51333E+00	-0.63906E+00	-0.76170E+00	0.30670E+01	0.31519E+02	0.34586E+02	0.16367E+04
155	0.82123E+00	-0.10226E+01	-0.12187E+01	0.29037E+01	0.30184E+02	0.33088E+02	0.16187E+04
157	0.11292E+01	-0.14061E+01	-0.16757E+01	0.30373E+01	0.31985E+02	0.35022E+02	0.16418E+04
351	0.12384E+01	-0.15422E+01	-0.18379E+01	0.24978E+01	0.21384E+02	0.23882E+02	0.14842E+04
353	0.15547E+01	-0.16759E+01	-0.19973E+01	0.73932E-01	0.18488E+01	0.19227E+01	0.78052E+03

Table III. - Continued.

No	x	y	z	q_r	q_c	q_t	T_w
		m			W/cm^2		K
171	0.32883E+00	-0.13932E+00	-0.38280E+00	0.59847E+01	0.36492E+02	0.42477E+02	0.17230E+04
173	0.51326E+00	-0.36393E+00	-0.99985E+00	0.32462E+01	0.32819E+02	0.36066E+02	0.16539E+04
175	0.82123E+00	-0.58227E+00	-0.15998E+01	0.30220E+01	0.32697E+02	0.35719E+02	0.16499E+04
371	0.97917E+00	-0.69428E+00	-0.19075E+01	0.22396E+01	0.24928E+02	0.27168E+02	0.15296E+04
373	0.12770E+01	-0.76784E+00	-0.21097E+01	0.62112E-01	0.46277E+00	0.52489E+00	0.89733E+03
191	0.32883E+00	0.00000E+00	-0.41956E+00	0.60606E+01	0.36675E+02	0.42735E+02	0.17257E+04
193	0.51326E+00	0.00000E+00	-0.10959E+01	0.33201E+01	0.33395E+02	0.36715E+02	0.16614E+04
391	0.76695E+00	0.00000E+00	-0.16375E+01	0.22604E+01	0.32067E+02	0.34328E+02	0.16309E+04
393	0.10423E+01	0.00000E+00	-0.18527E+01	0.17089E+00	0.26239E+01	0.27948E+01	0.95202E+03
182	0.32883E+00	0.13932E+00	-0.38280E+00	0.62425E+01	0.36668E+02	0.42910E+02	0.17274E+04
184	0.51326E+00	0.36370E+00	-0.99924E+00	0.32157E+01	0.33416E+02	0.36632E+02	0.16605E+04
382	0.63043E+00	0.44691E+00	-0.12279E+01	0.23356E+01	0.33933E+02	0.36268E+02	0.16563E+04
384	0.88402E+00	0.51760E+00	-0.14221E+01	0.19137E+01	0.38208E+01	0.40121E+01	0.98017E+03
162	0.32883E+00	0.24470E+00	-0.29162E+00	0.63571E+01	0.36579E+02	0.42936E+02	0.17277E+04
164	0.51326E+00	0.63876E+00	-0.76124E+00	0.30532E+01	0.33187E+02	0.36240E+02	0.16559E+04
362	0.55547E+00	0.69169E+00	-0.82433E+00	0.24462E+01	0.33268E+02	0.35714E+02	0.16499E+04
364	0.79266E+00	0.81653E+00	-0.97310E+00	0.38351E+00	0.62517E+01	0.66352E+01	0.10913E+04
142	0.32883E+00	0.30823E+00	-0.17795E+00	0.63752E+01	0.36546E+02	0.42922E+02	0.17275E+04
342	0.51836E+00	0.81308E+00	-0.46944E+00	0.27778E+01	0.32752E+02	0.35530E+02	0.16477E+04
344	0.74524E+00	0.97168E+00	-0.56098E+00	0.42489E+00	0.78723E+01	0.82972E+01	0.11835E+04
122	0.32883E+00	0.33693E+00	-0.59411E-01	0.64453E+01	0.36521E+02	0.42967E+02	0.17280E+04
322	0.50317E+00	0.86274E+00	-0.15212E+00	0.30322E+01	0.33174E+02	0.36206E+02	0.16555E+04
324	0.72522E+00	0.10370E+01	-0.18285E+00	0.62568E+00	0.76089E+01	0.82346E+01	0.11576E+04
102	0.32883E+00	0.34036E+00	0.00000E+00	0.65040E+01	0.36515E+02	0.43019E+02	0.17285E+04
302	0.50142E+00	0.86850E+00	0.00000E+00	0.30859E+01	0.33317E+02	0.36403E+02	0.16578E+04
304	0.72291E+00	0.10447E+01	0.00000E+00	0.60868E+00	0.74109E+01	0.80196E+01	0.11608E+04
112	0.39980E+00	-0.63177E+00	-0.11085E+00	0.43188E+01	0.34691E+02	0.39010E+02	0.16863E+04

Table III. - Concluded.

No	x	y	z	q_r	q_c	q_t	T_w
		m			W/cm^2		K
132	0.39845E+00	-0.57478E+00	-0.33017E+00	0.43557E+01	0.35063E+02	0.39418E+02	0.16910E+04
152	0.39627E+00	-0.45212E+00	-0.53619E+00	0.44817E+01	0.35121E+02	0.39603E+02	0.16931E+04
172	0.39418E+00	-0.25527E+00	-0.69781E+00	0.45841E+01	0.35642E+02	0.40226E+02	0.16997E+04
177	0.91895E+00	-0.65156E+00	-0.17901E+01	0.26101E+01	0.31729E+02	0.34339E+02	0.16327E+04
192	0.39332E+00	0.00000E+00	-0.76218E+00	0.48021E+01	0.36255E+02	0.41057E+02	0.17084E+04
195	0.73162E+00	0.00000E+00	-0.15621E+01	0.26016E+01	0.34995E+02	0.37596E+02	0.16713E+04
183	0.39418E+00	0.25527E+00	-0.69779E+00	0.49411E+01	0.36262E+02	0.41203E+02	0.17100E+04
186	0.60038E+00	0.42568E+00	-0.11695E+01	0.25922E+01	0.34261E+02	0.36853E+02	0.16630E+04
163	0.39624E+00	0.45220E+00	-0.53619E+00	0.50860E+01	0.35920E+02	0.41006E+02	0.17079E+04
143	0.39845E+00	0.57475E+00	-0.33017E+00	0.50577E+01	0.35676E+02	0.40734E+02	0.17050E+04
123	0.39980E+00	0.63180E+00	-0.11085E+00	0.50950E+01	0.35529E+02	0.40624E+02	0.17039E+04

(a) Side view.

(b) Front view.
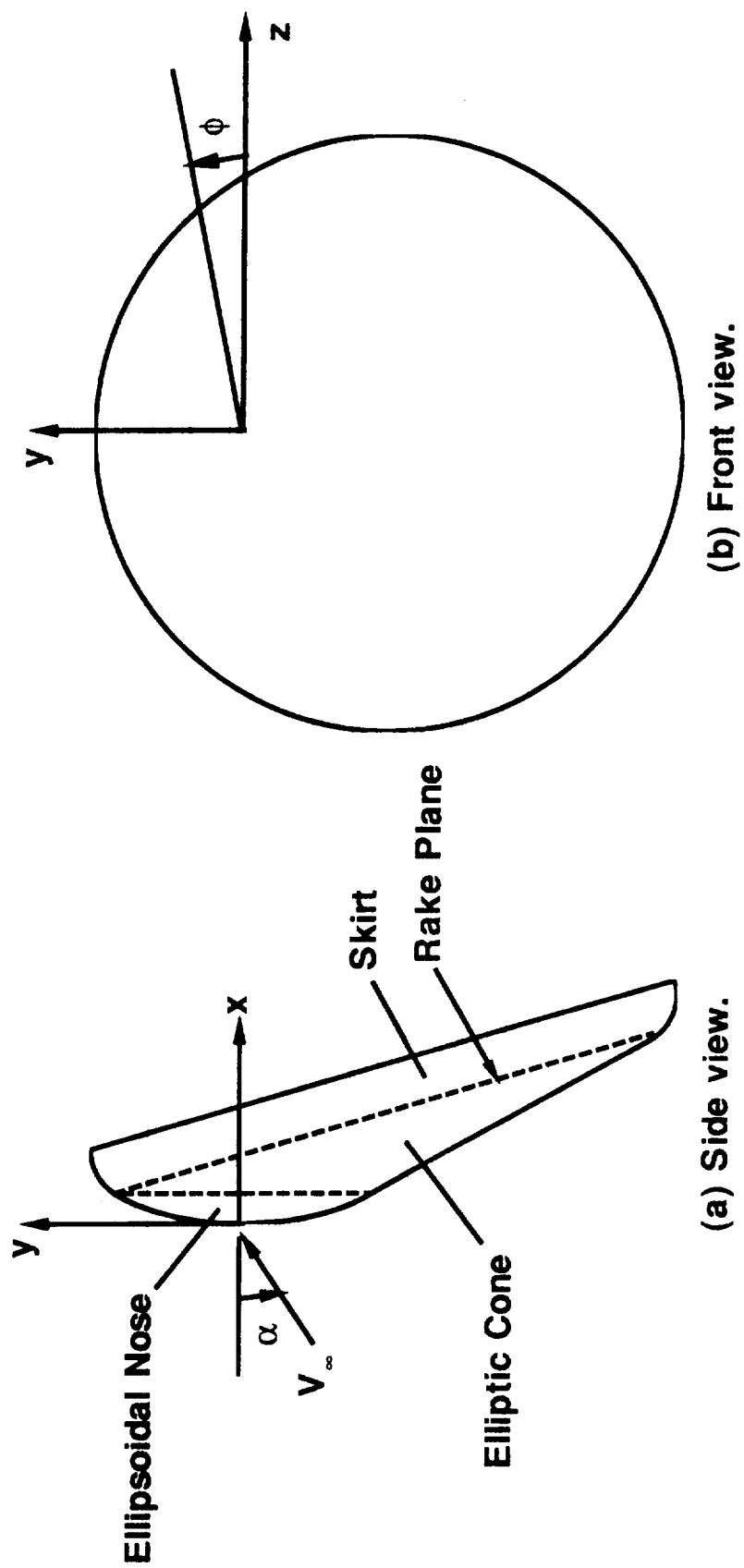
Figure 1. - AFE vehicle geometry.
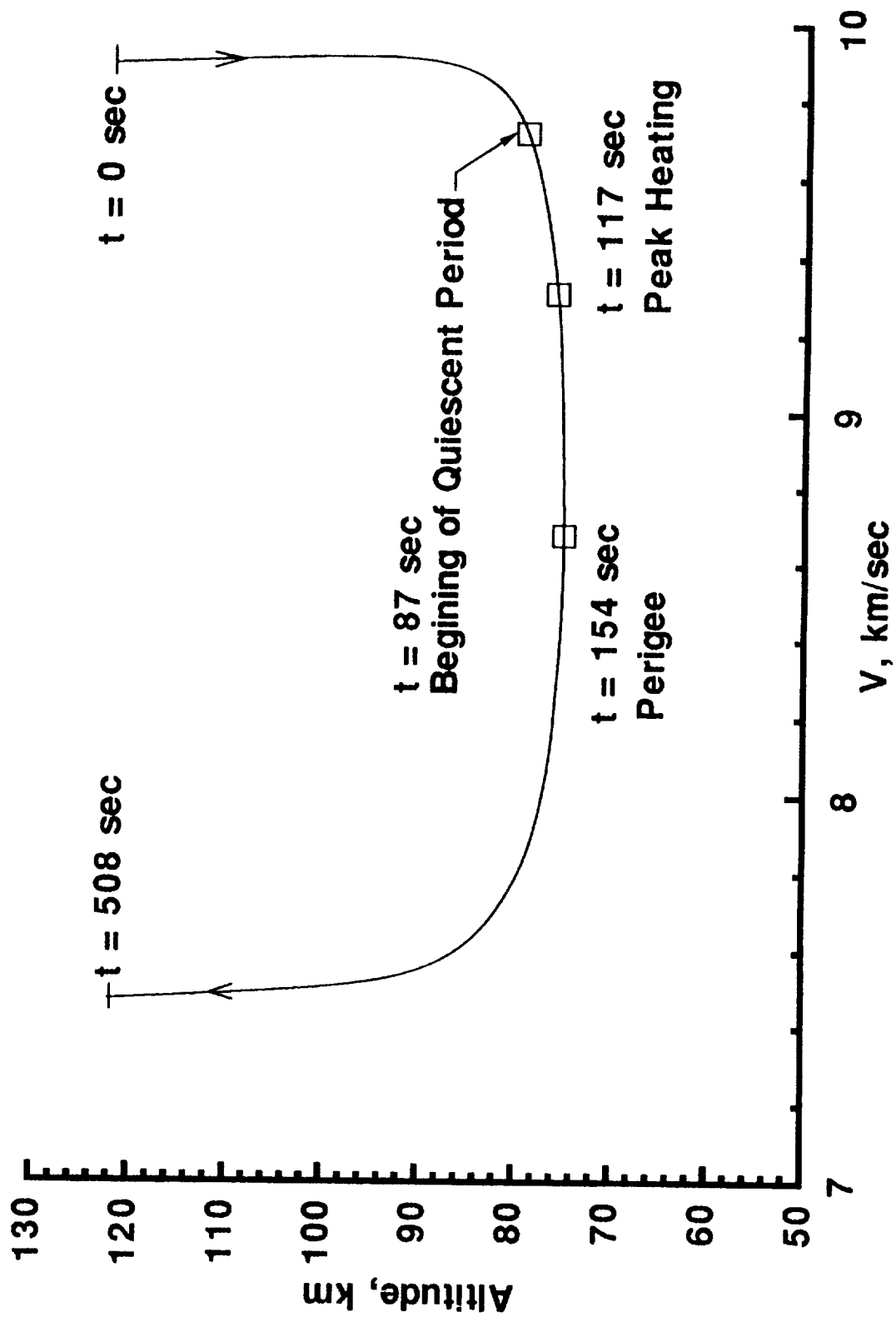
Figure 2. - Baseline 5A trajectory.
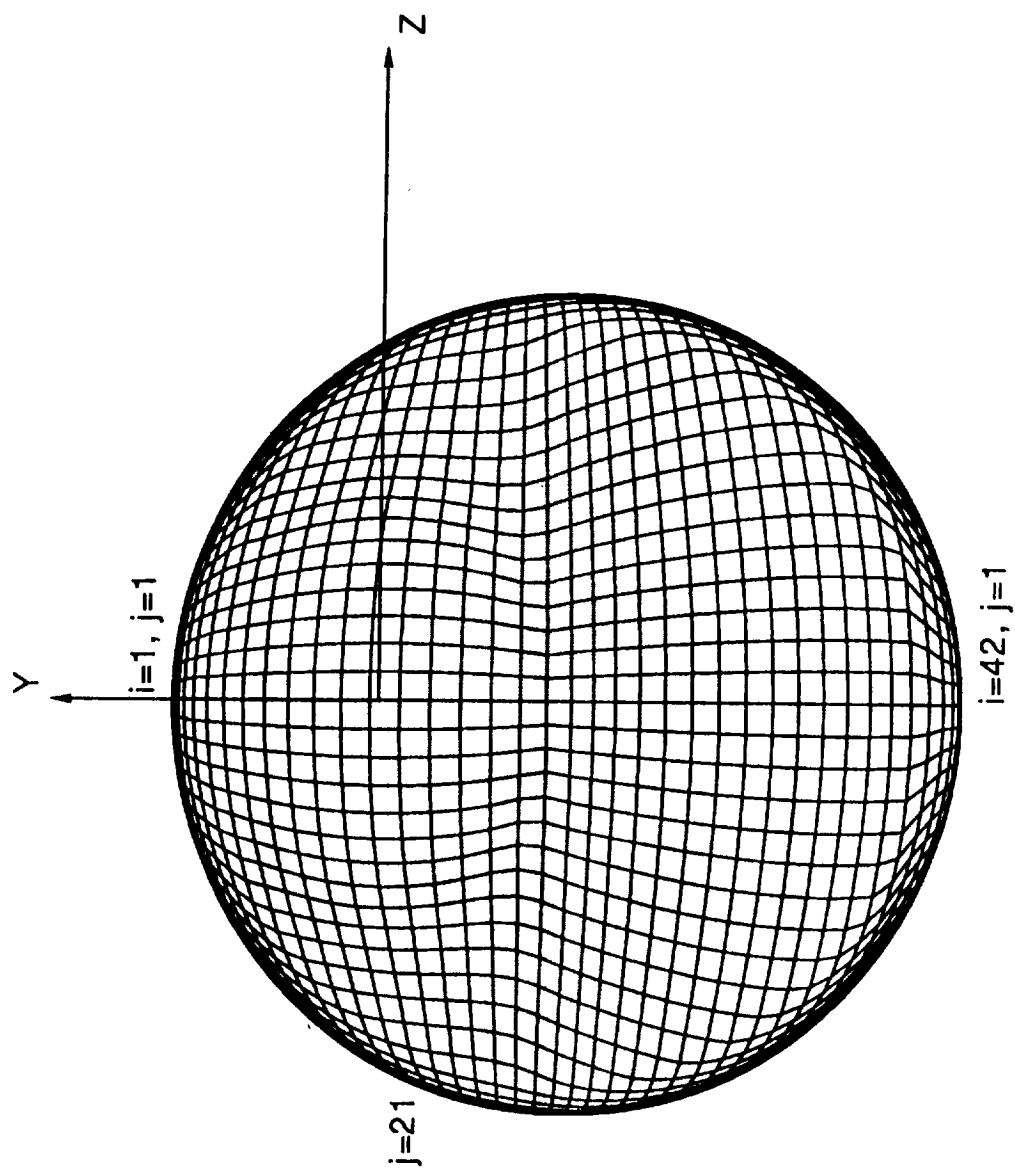
Figure 3. - Body Grid.
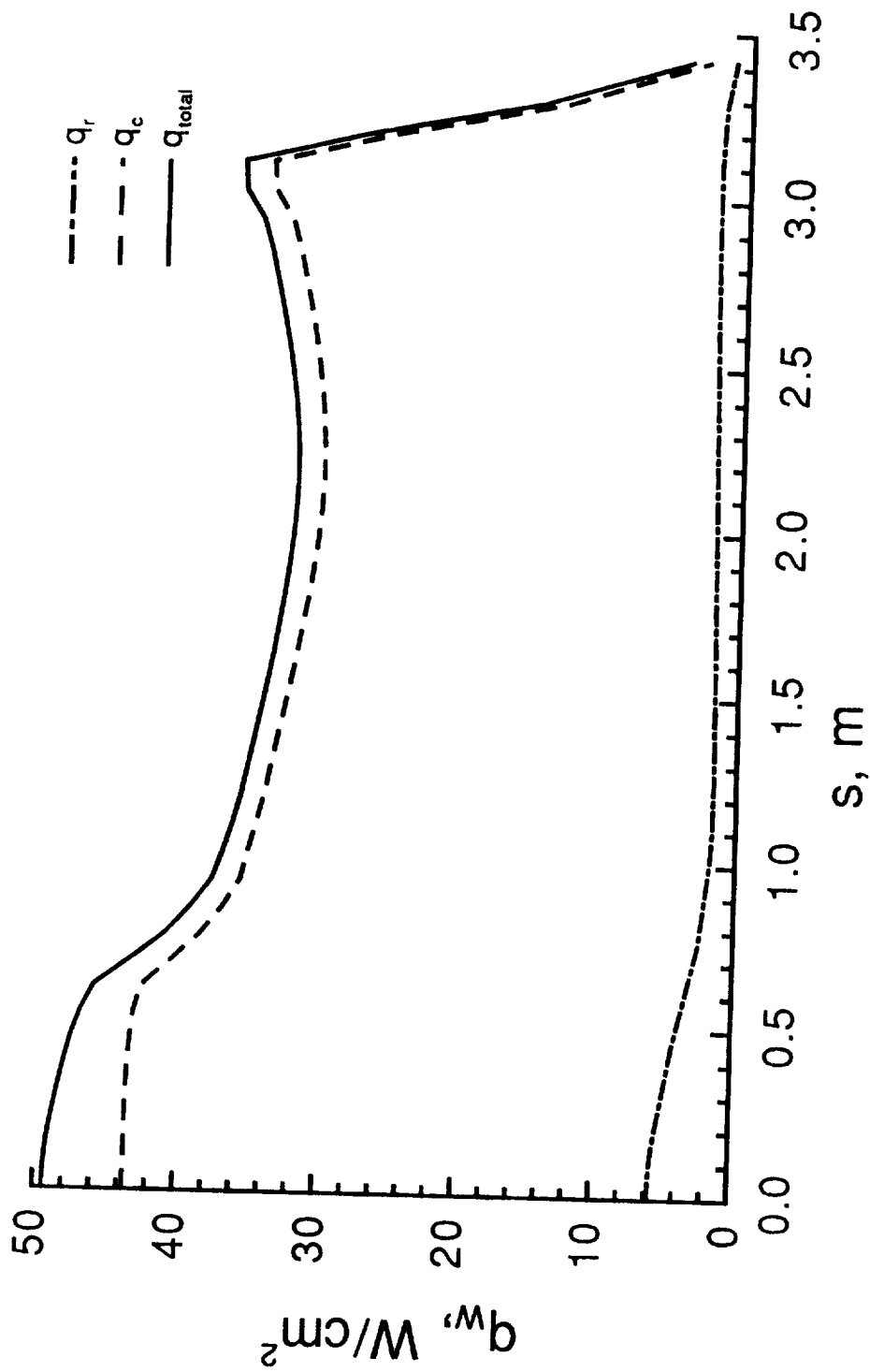
(a) $\phi = -90°$

Figure 4. - Heat Transfer at Peak Heating Point.
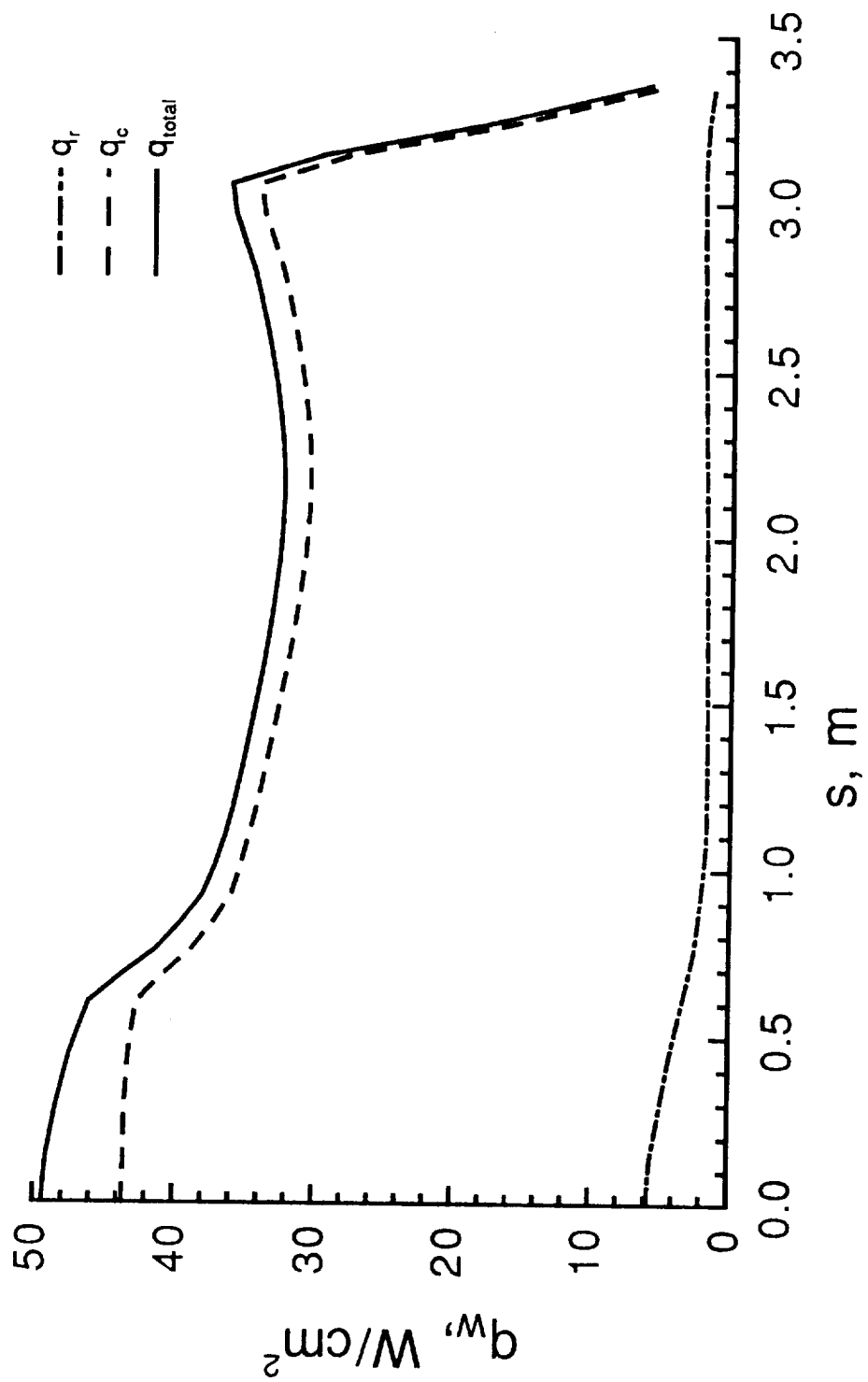
(b) $\phi = -80°$

Figure 4. - Continued.
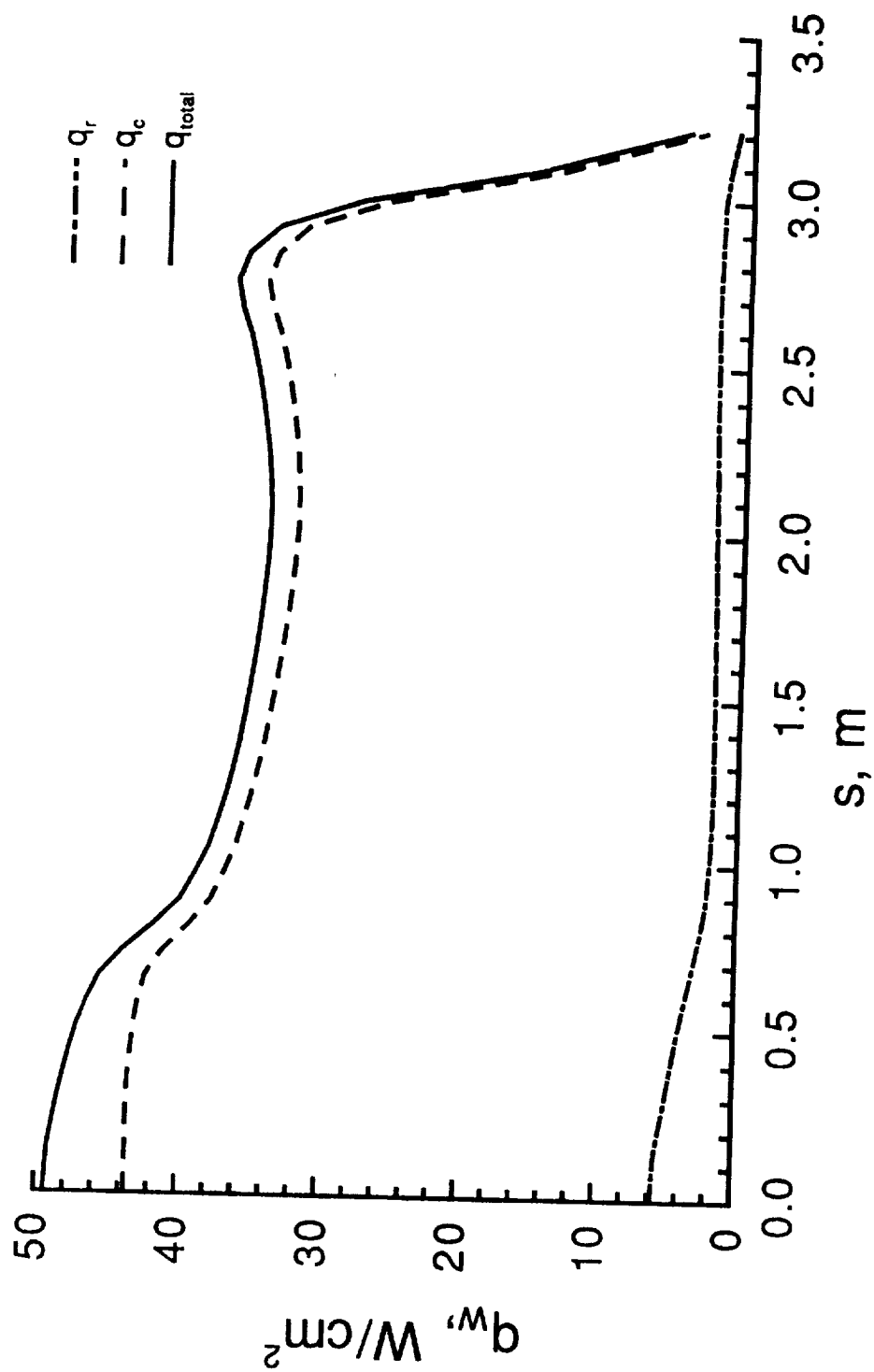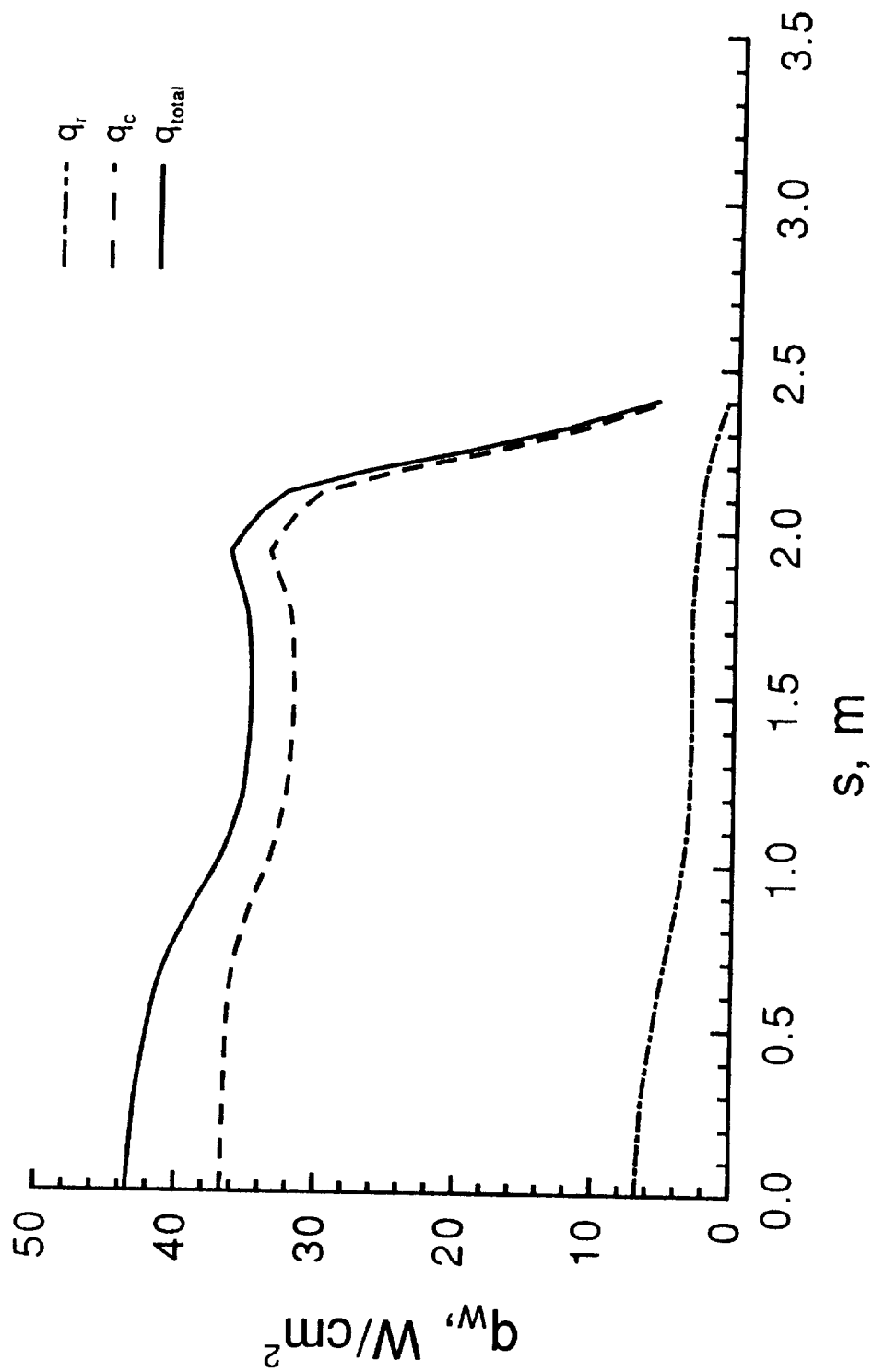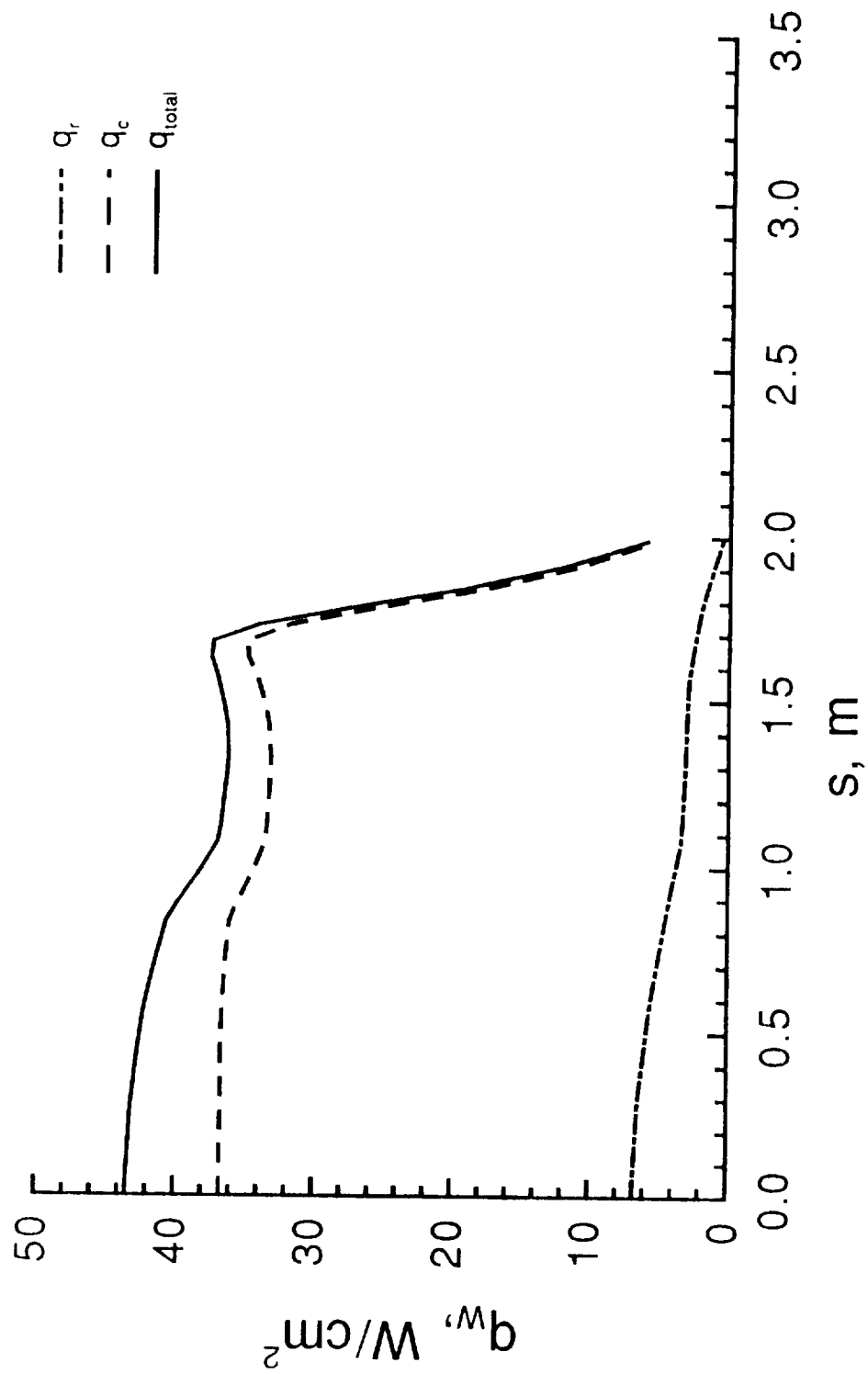
(c) $\phi = -60°$
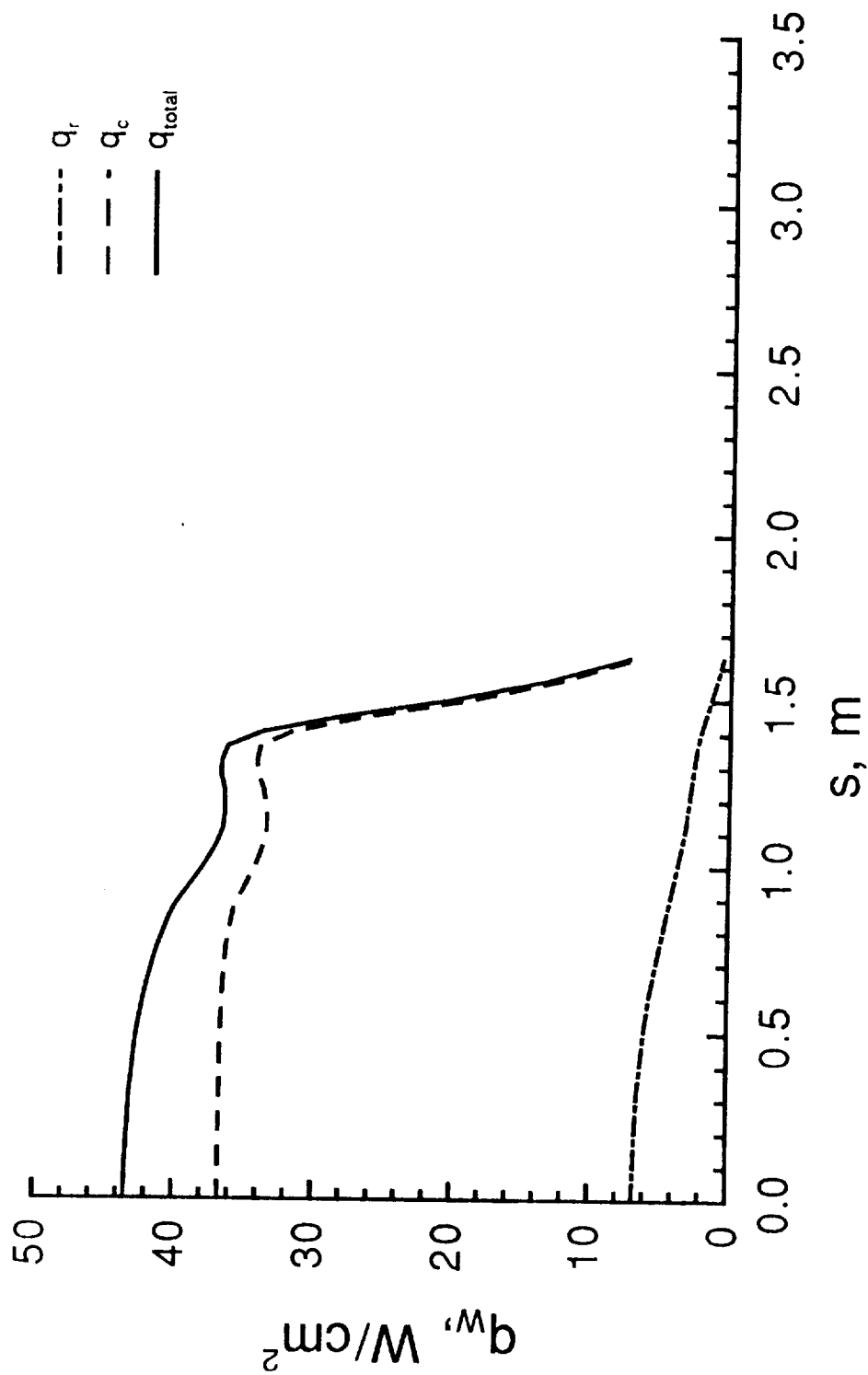
Figure 4. - Continued.
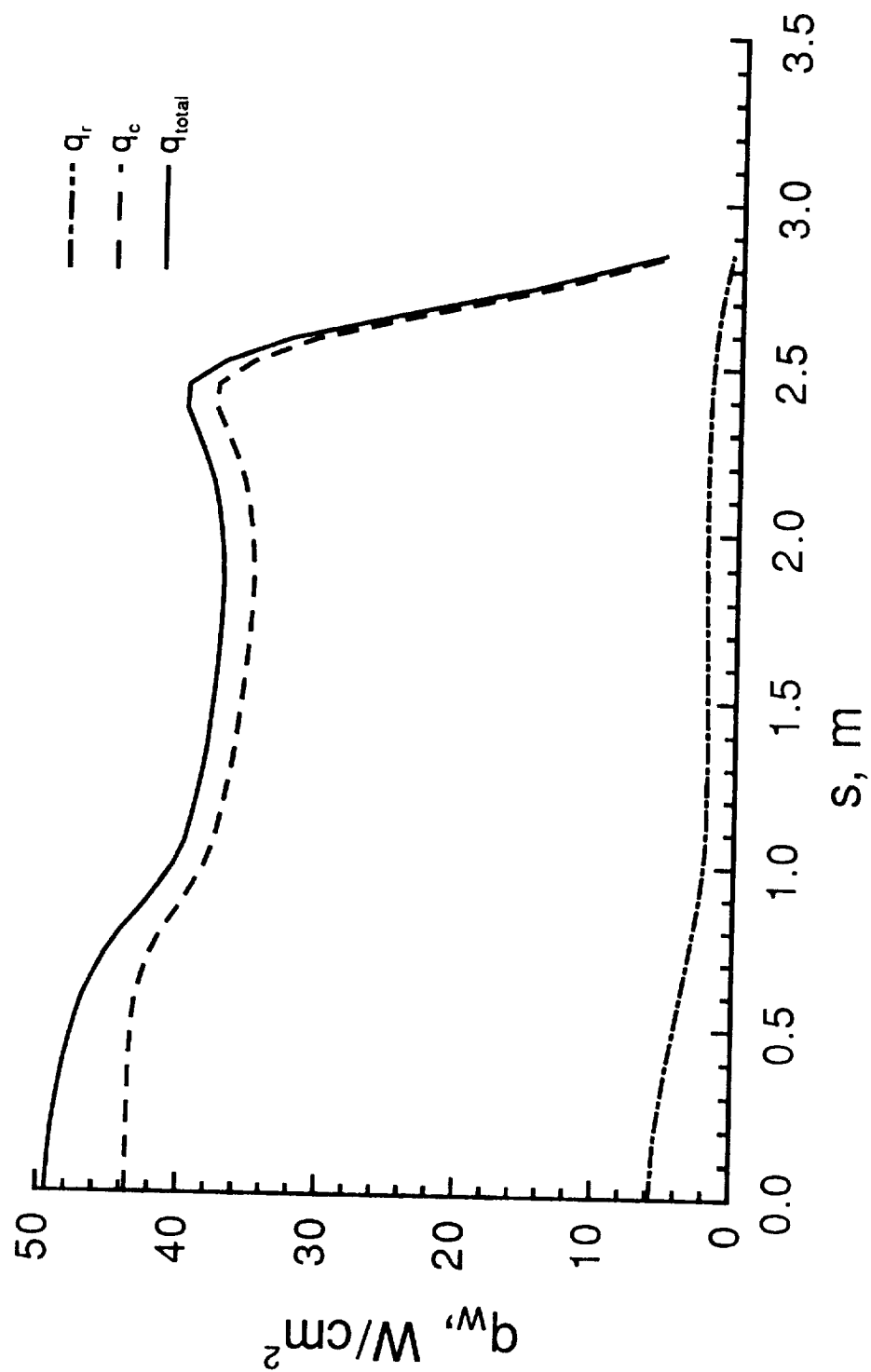
(d) $\phi = -40°$

Figure 4. - Continued.
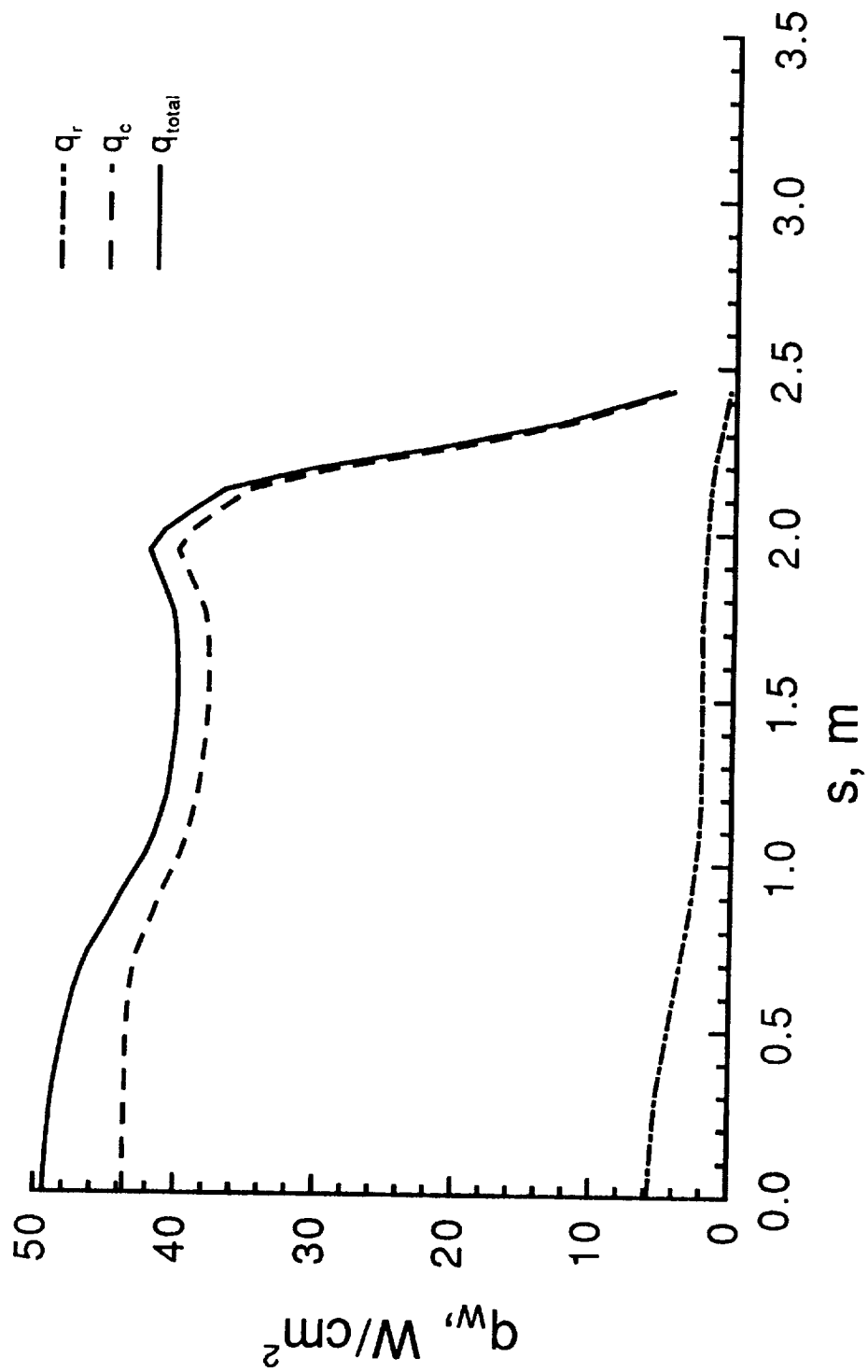
(e) $\phi = -20°$

Figure 4. - Continued.
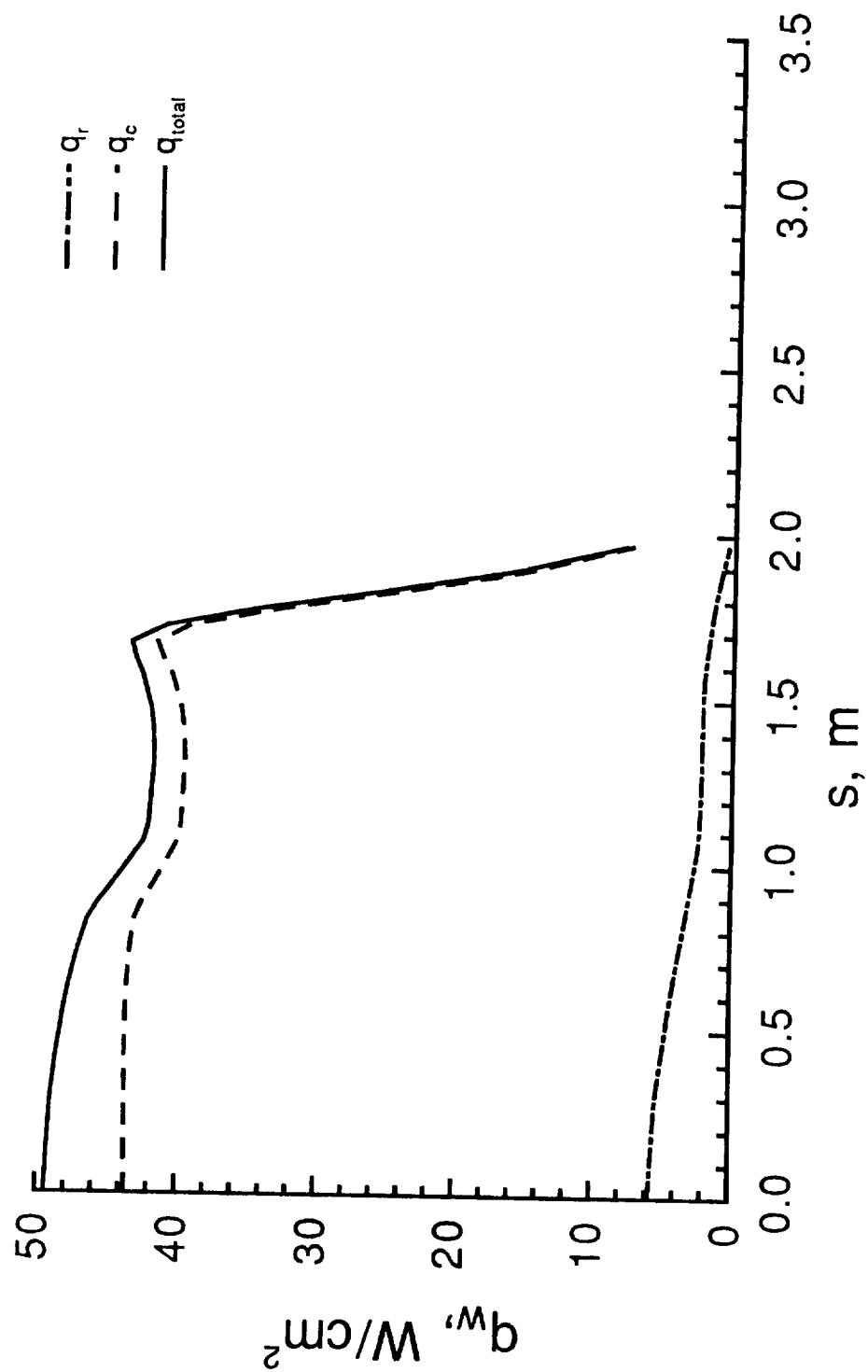
(f) $\phi = 0°$

Figure 4. - Continued.
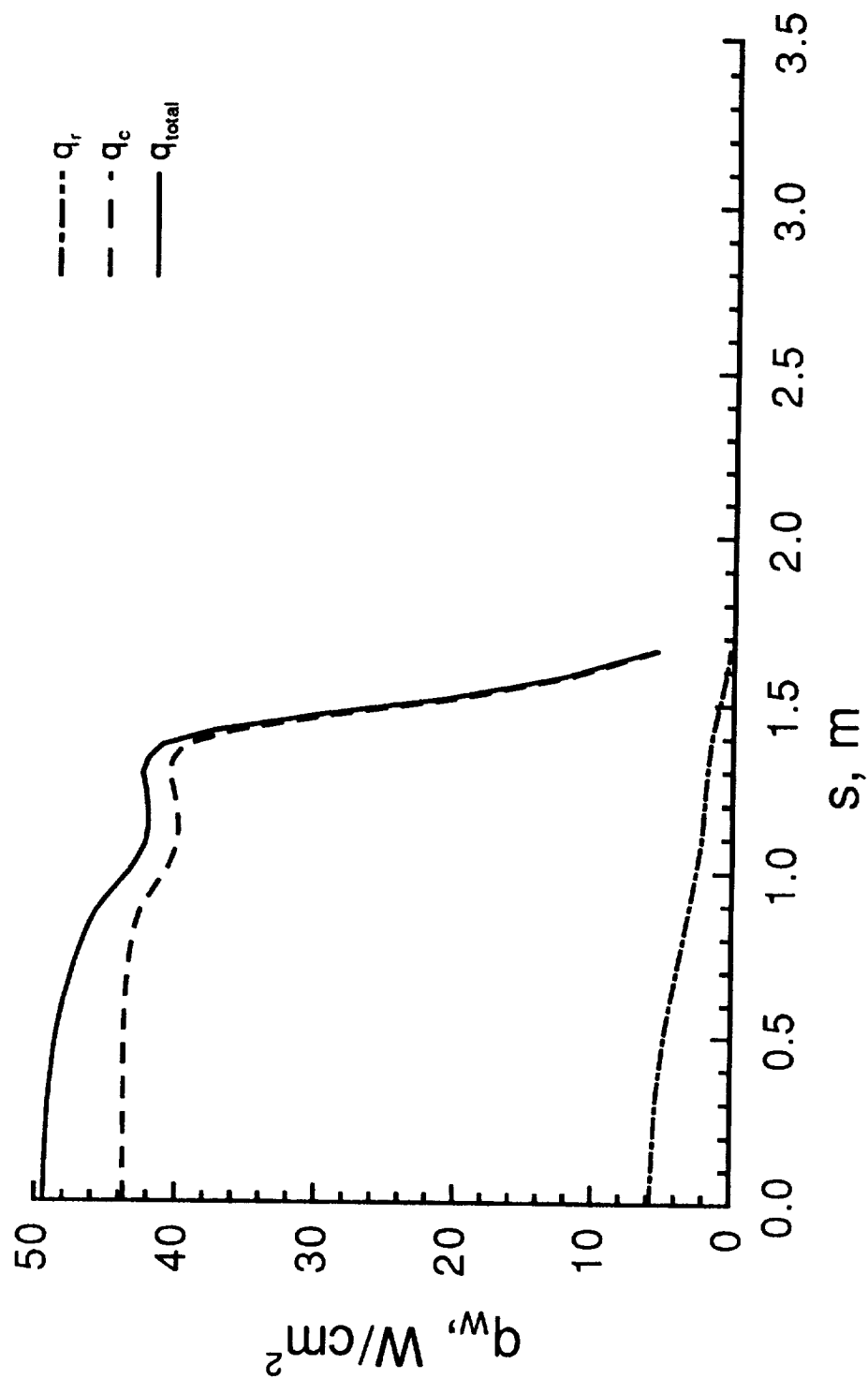
(g) $\phi = +20°$

Figure 4. - Continued.

(h) ϕ = +40°
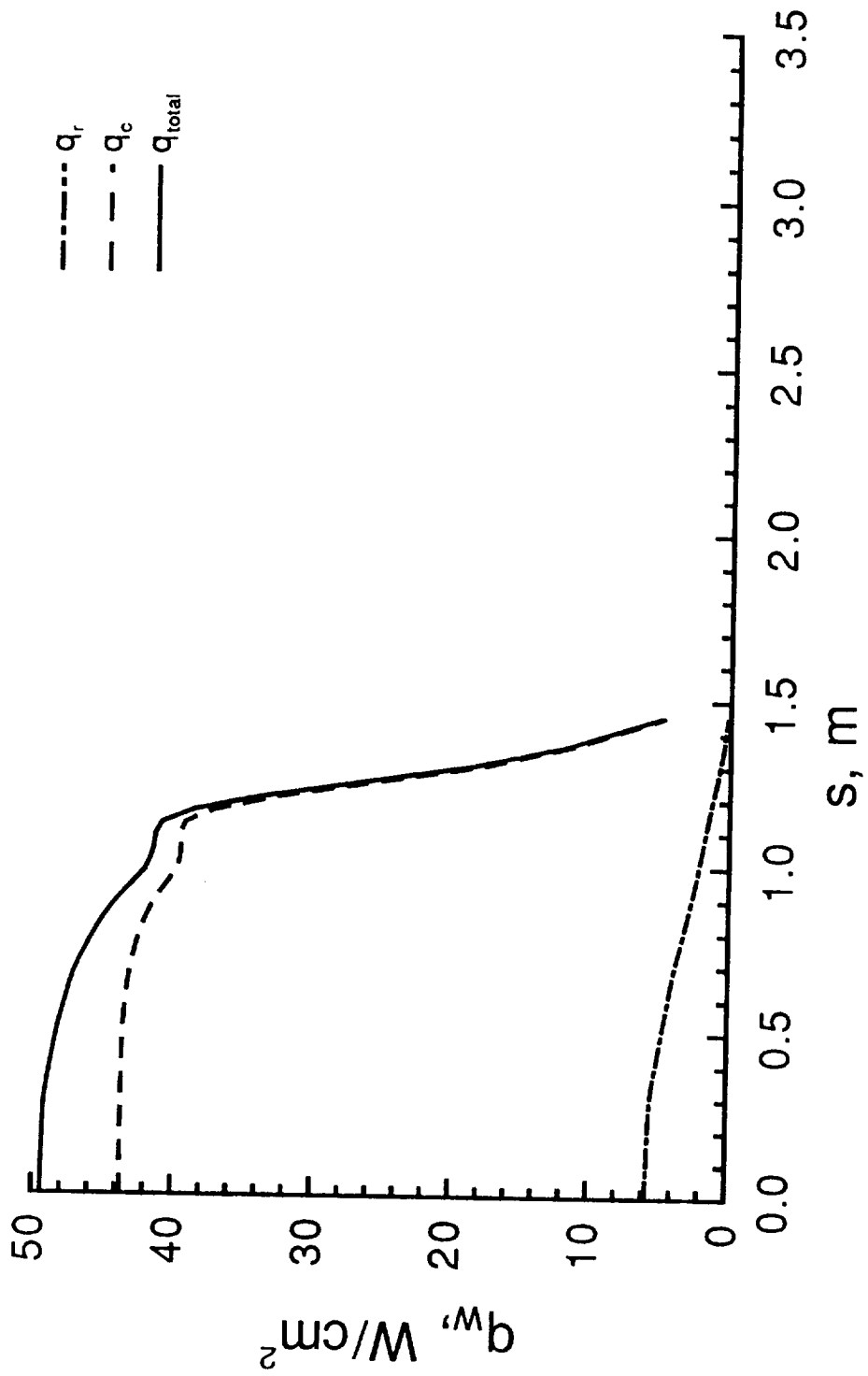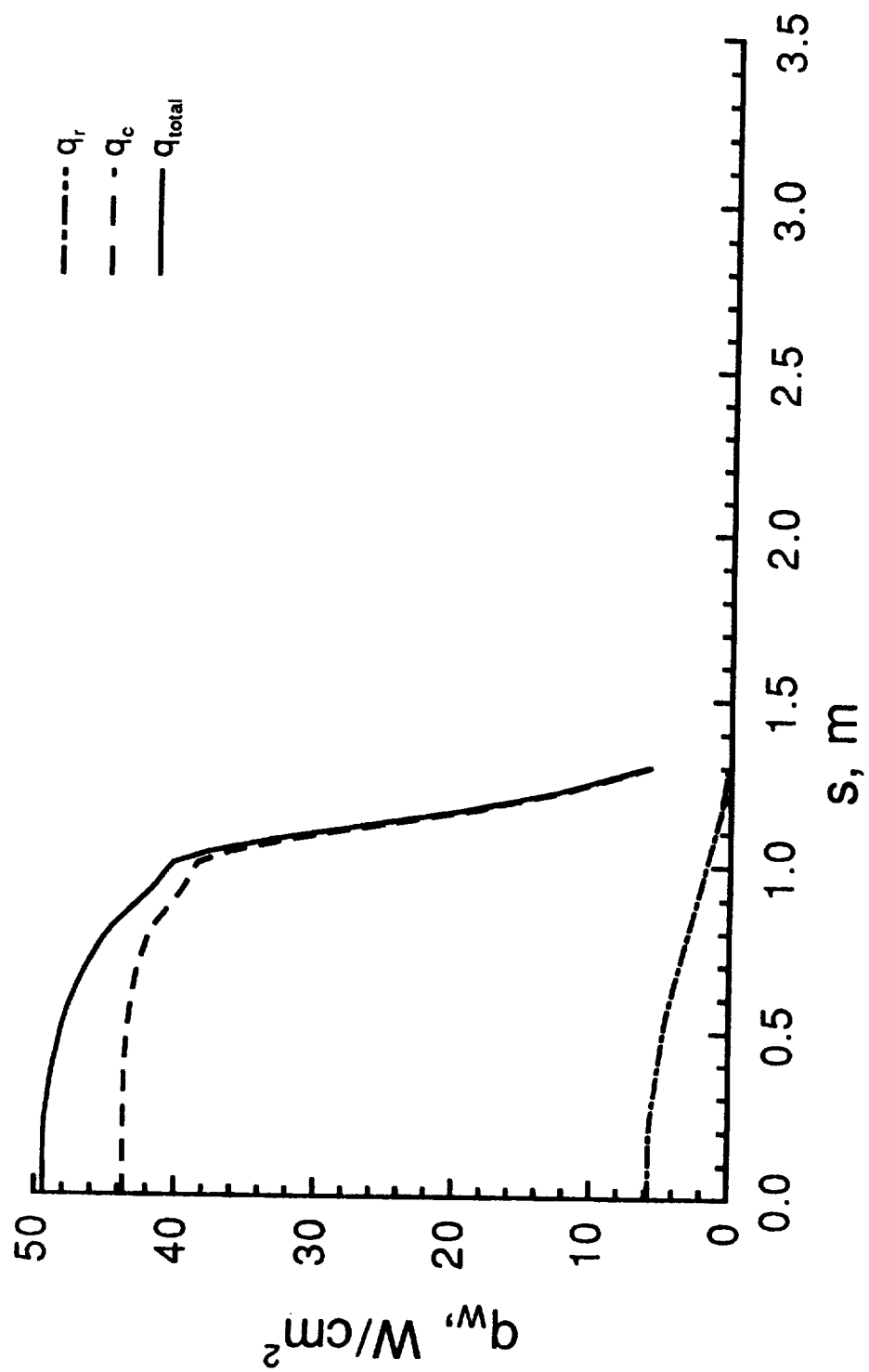
Figure 4. - Continued.

(i) $\phi = +60°$

Figure 4. - Continued.
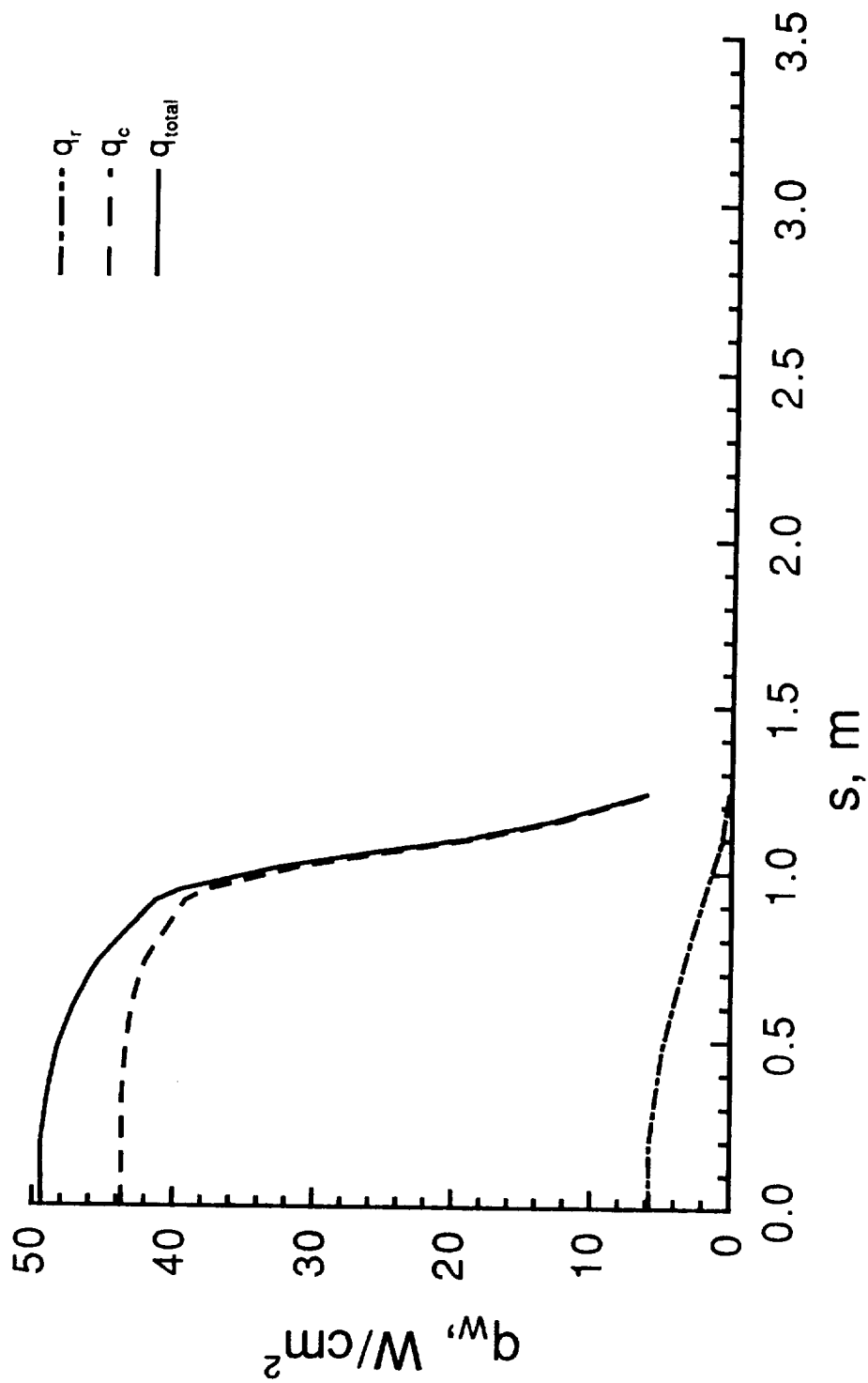
(j) $\phi = +80°$

Figure 4. - Continued.
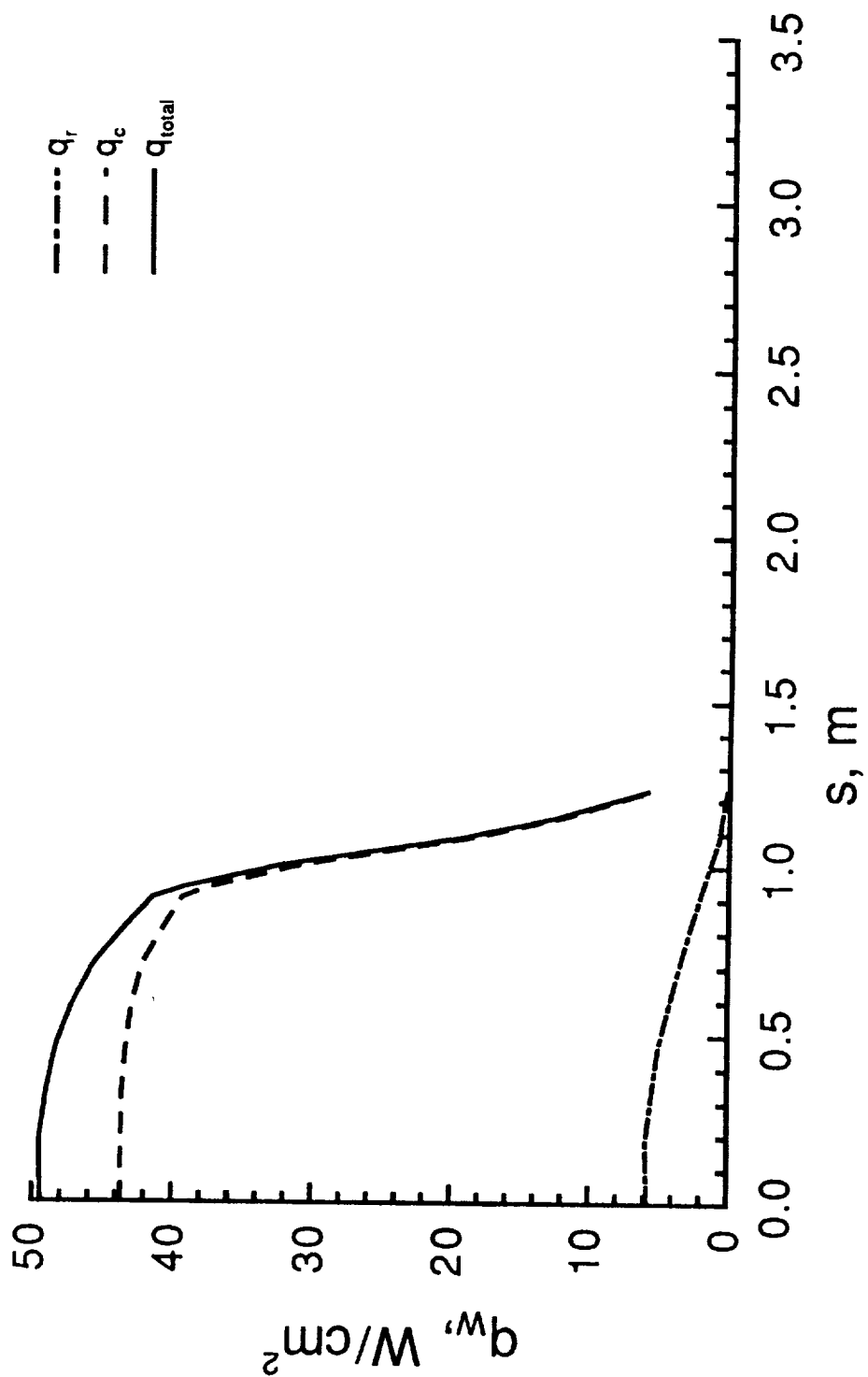
(k) $\phi = +90°$

Figure 4. - Concluded.

28
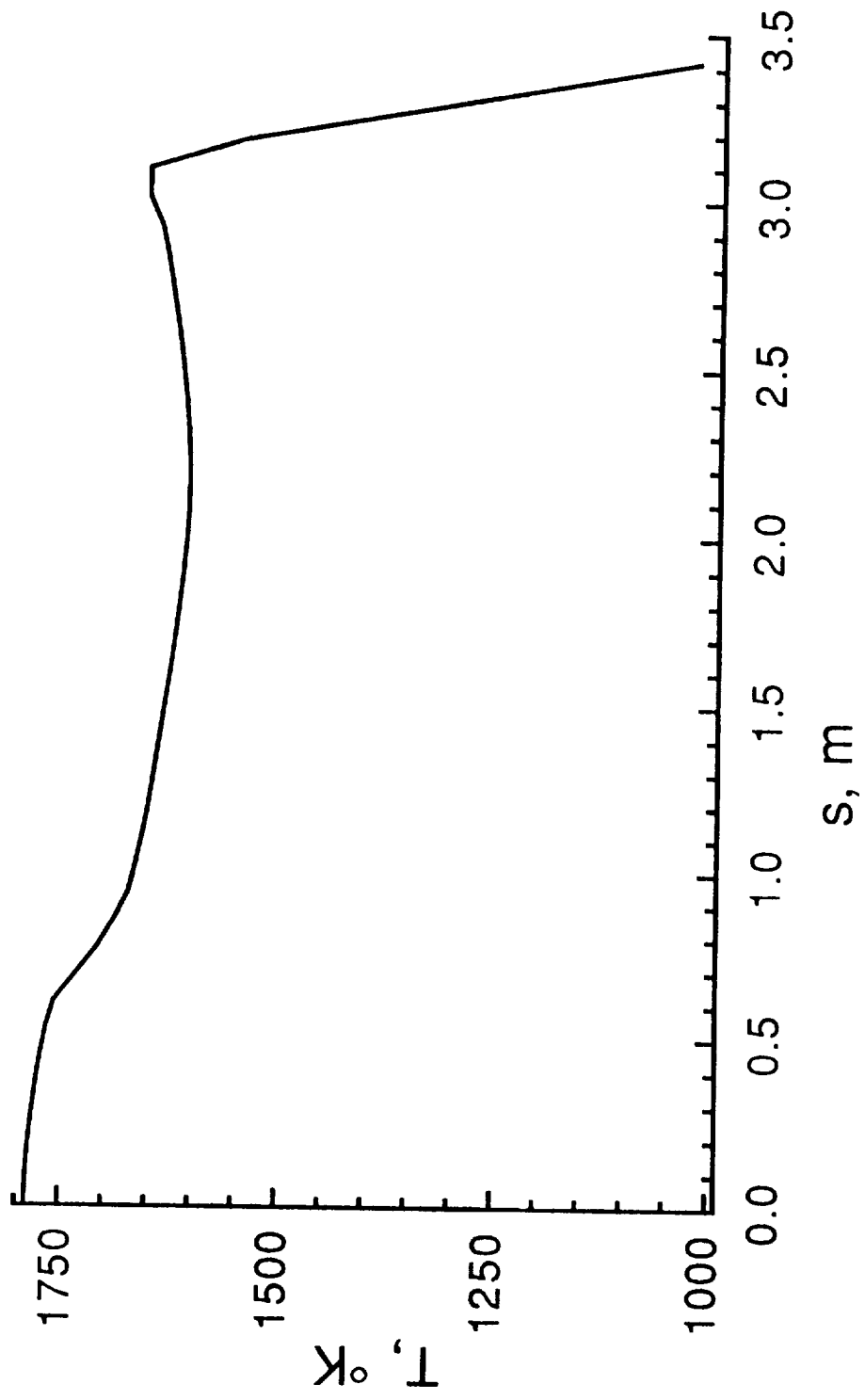
(a) $\phi = -90°$

Figure 5. - Wall Temperature at Peak Heating Point.

29
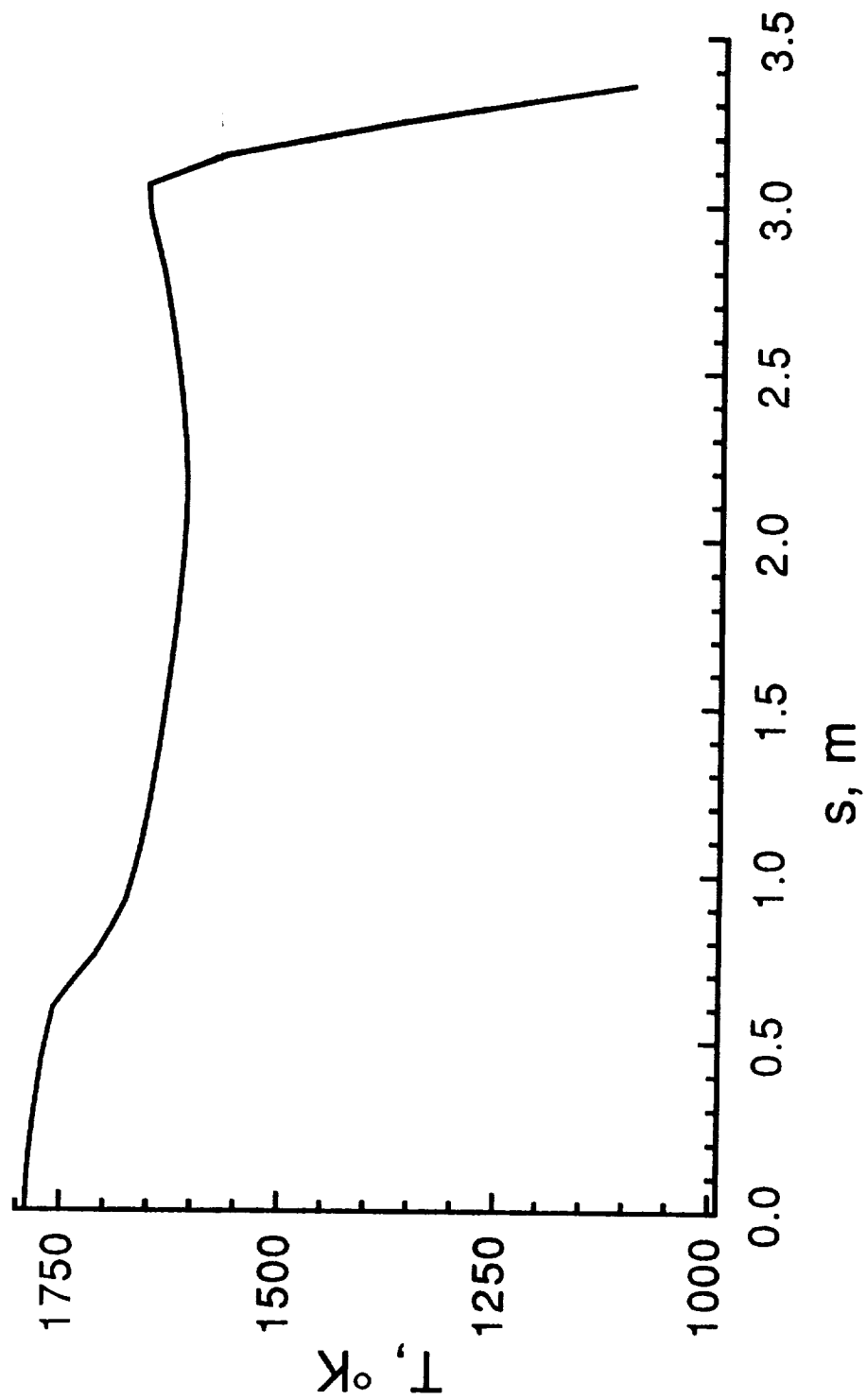
(b) $\phi = -80°$

Figure 5. - Continued.
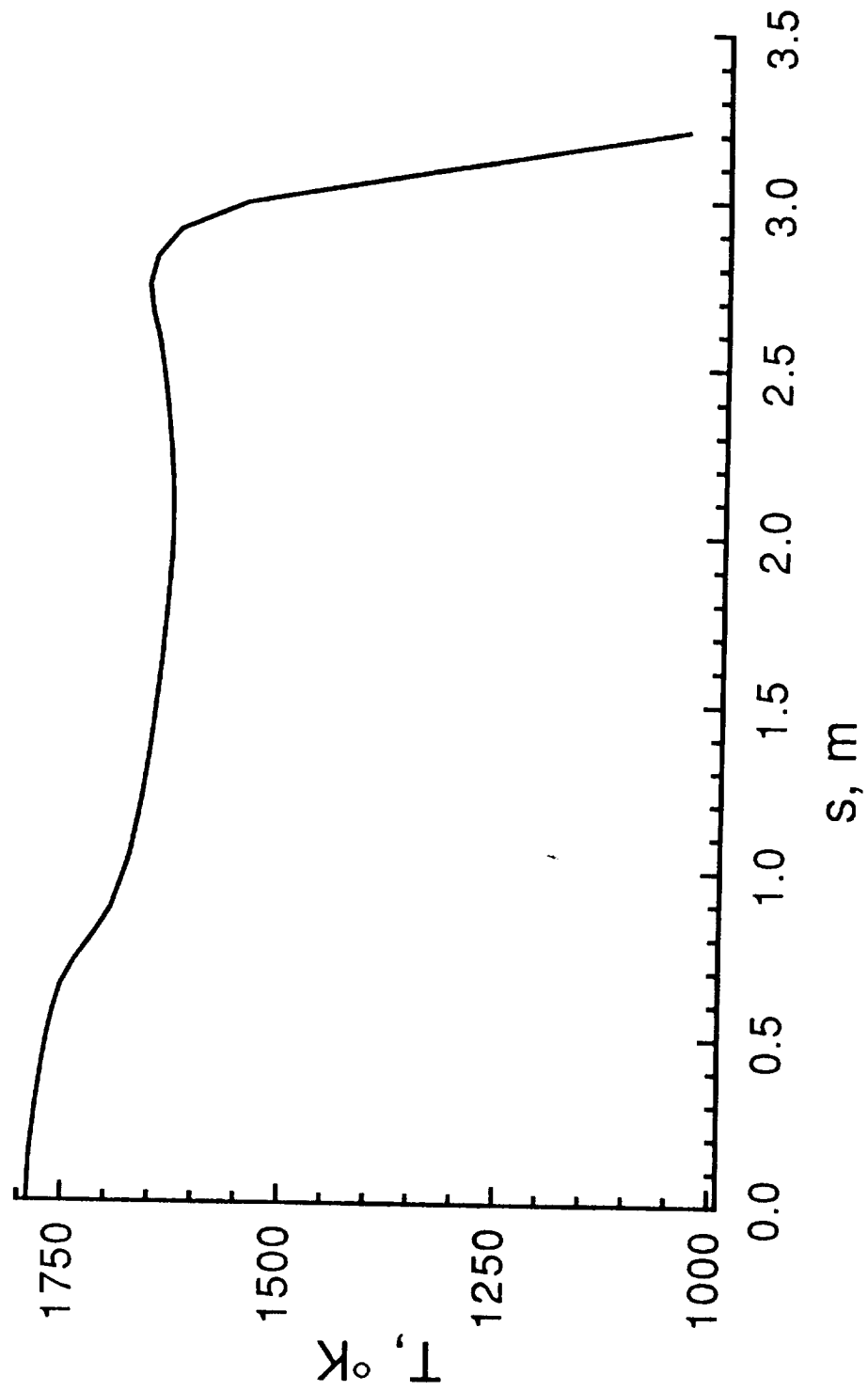
(c) $\phi = -60°$

Figure 5. - Continued.
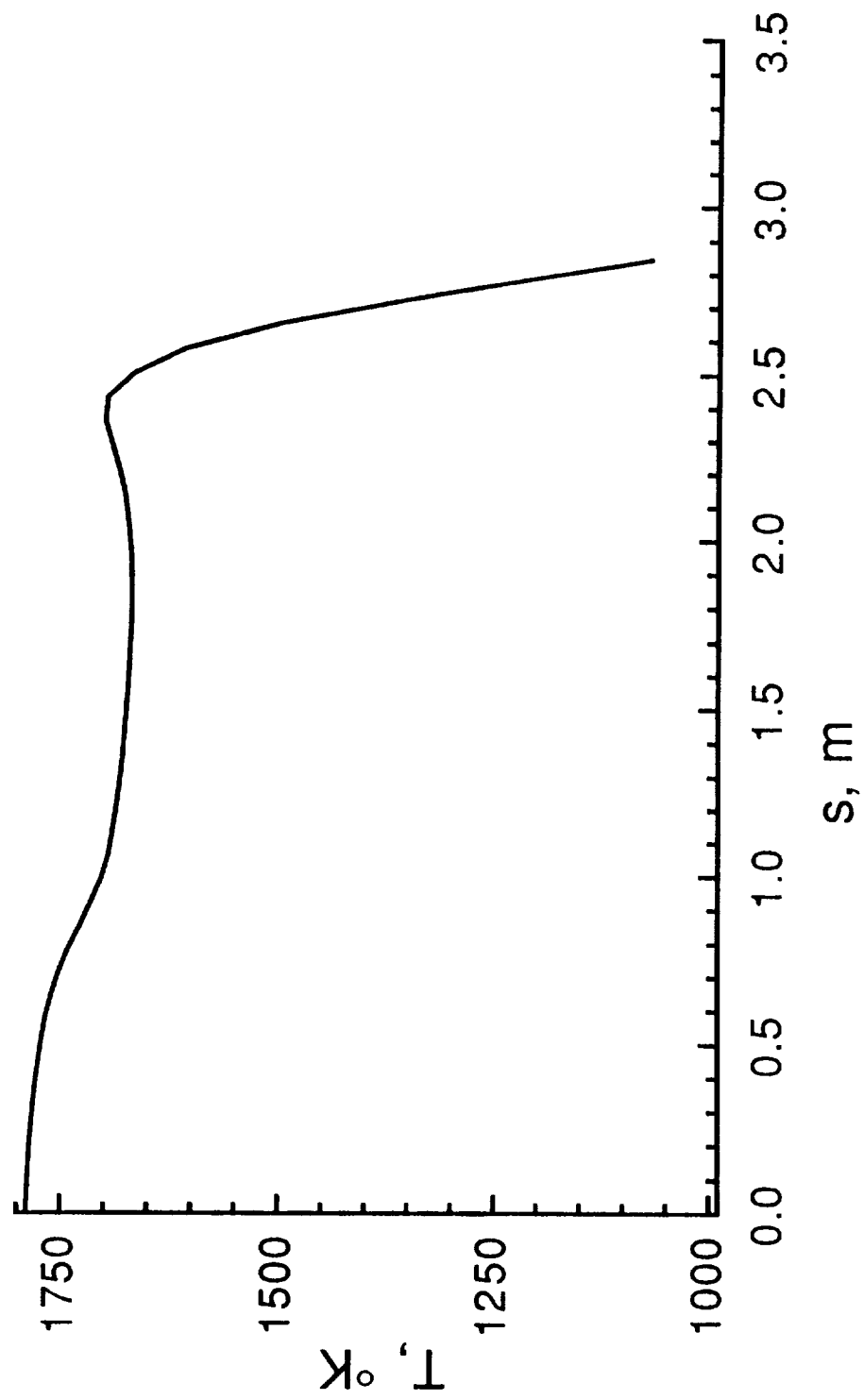
(d) $\phi = -40°$

Figure 5. - Continued.
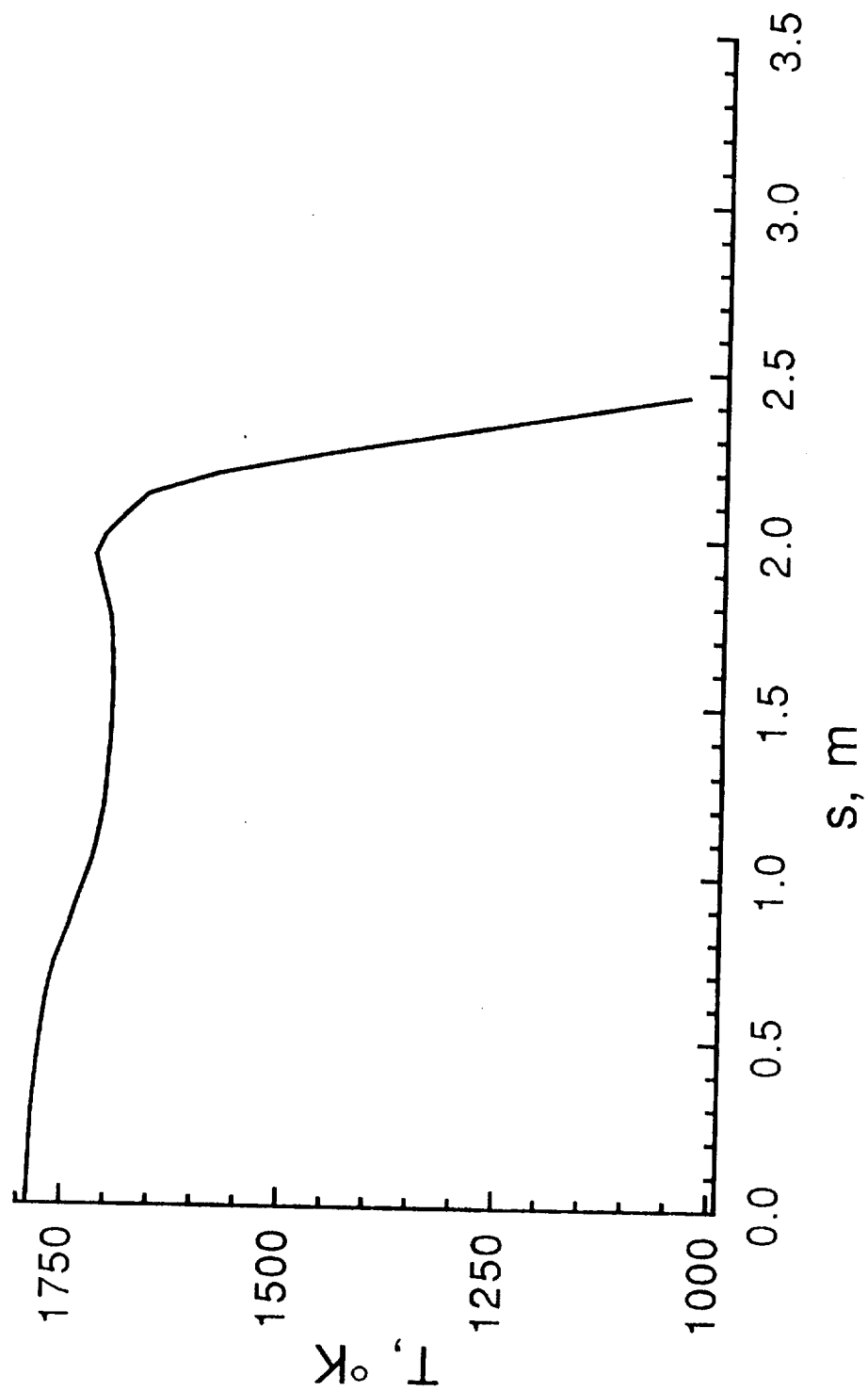
(e) $\phi = -20°$

Figure 5. - Continued.

33
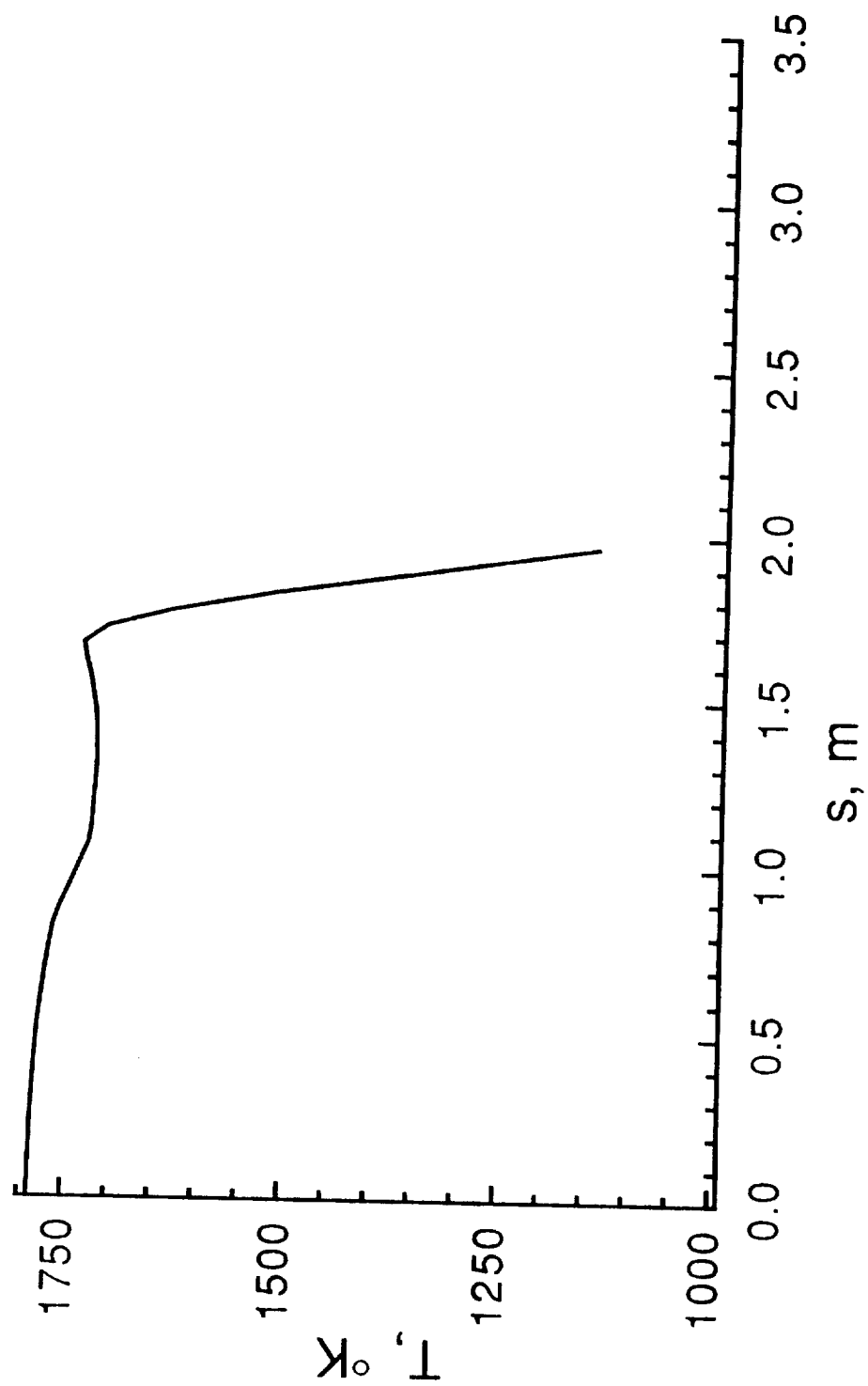
(f) $\phi = 0°$
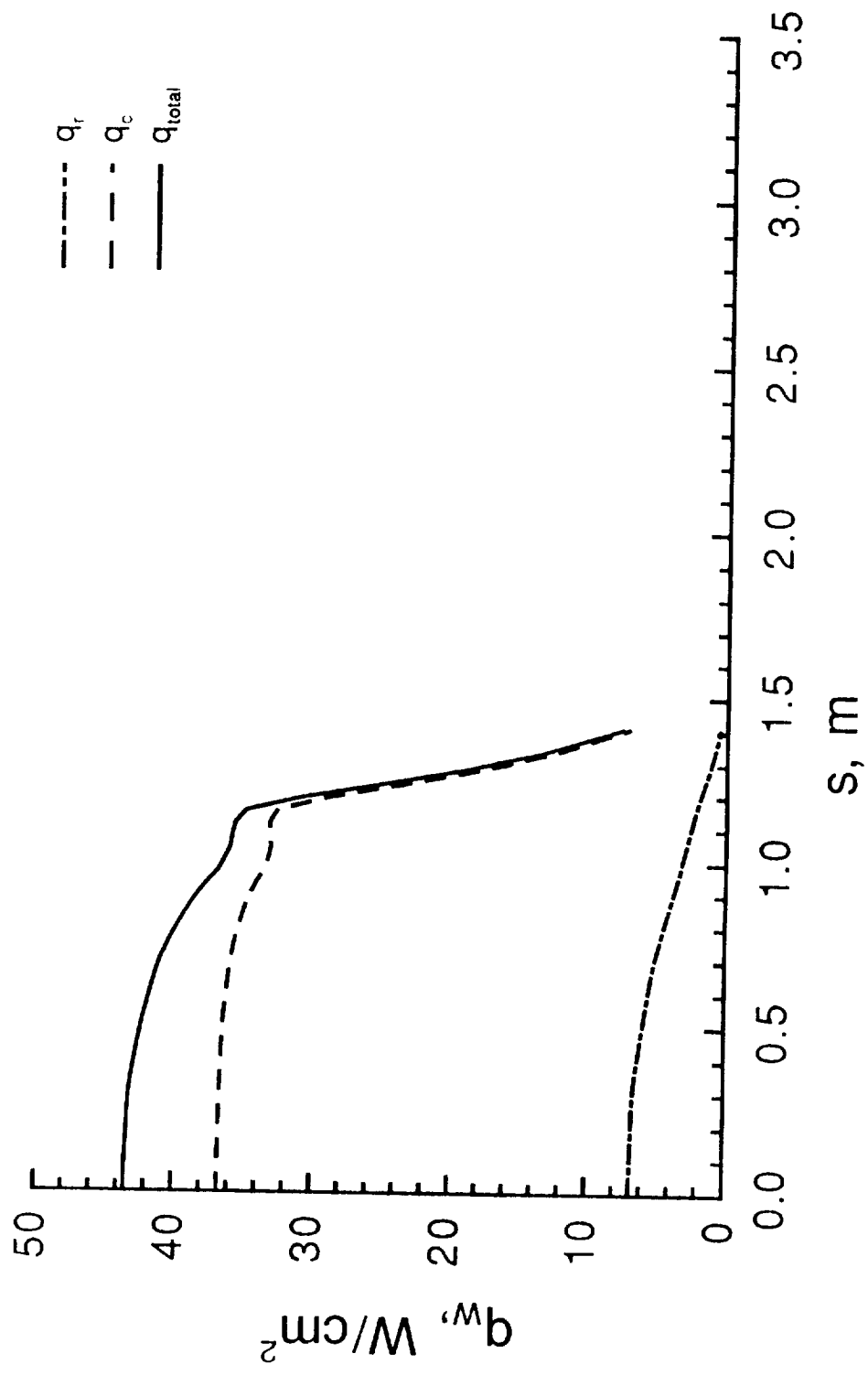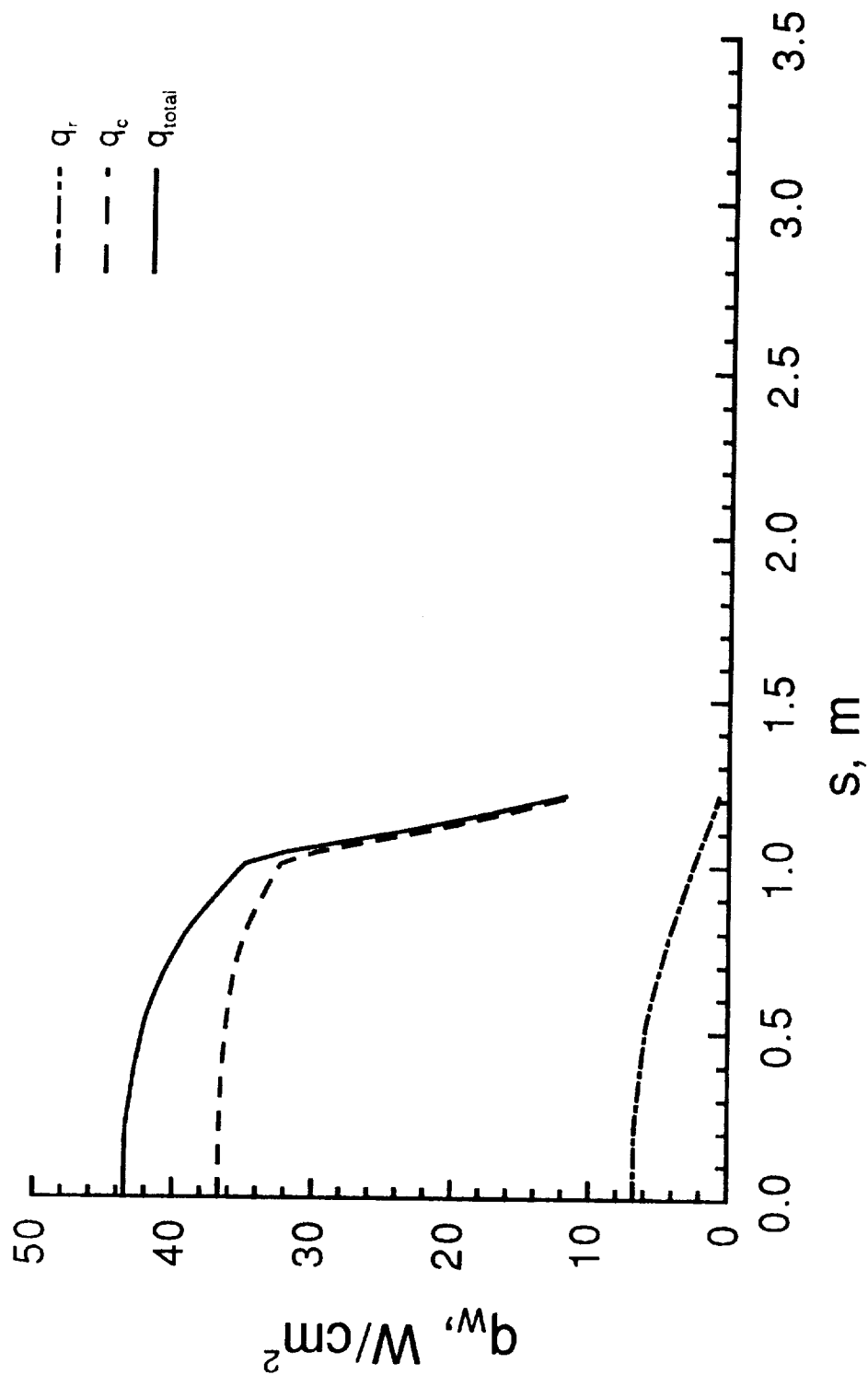
Figure 5. - Continued.
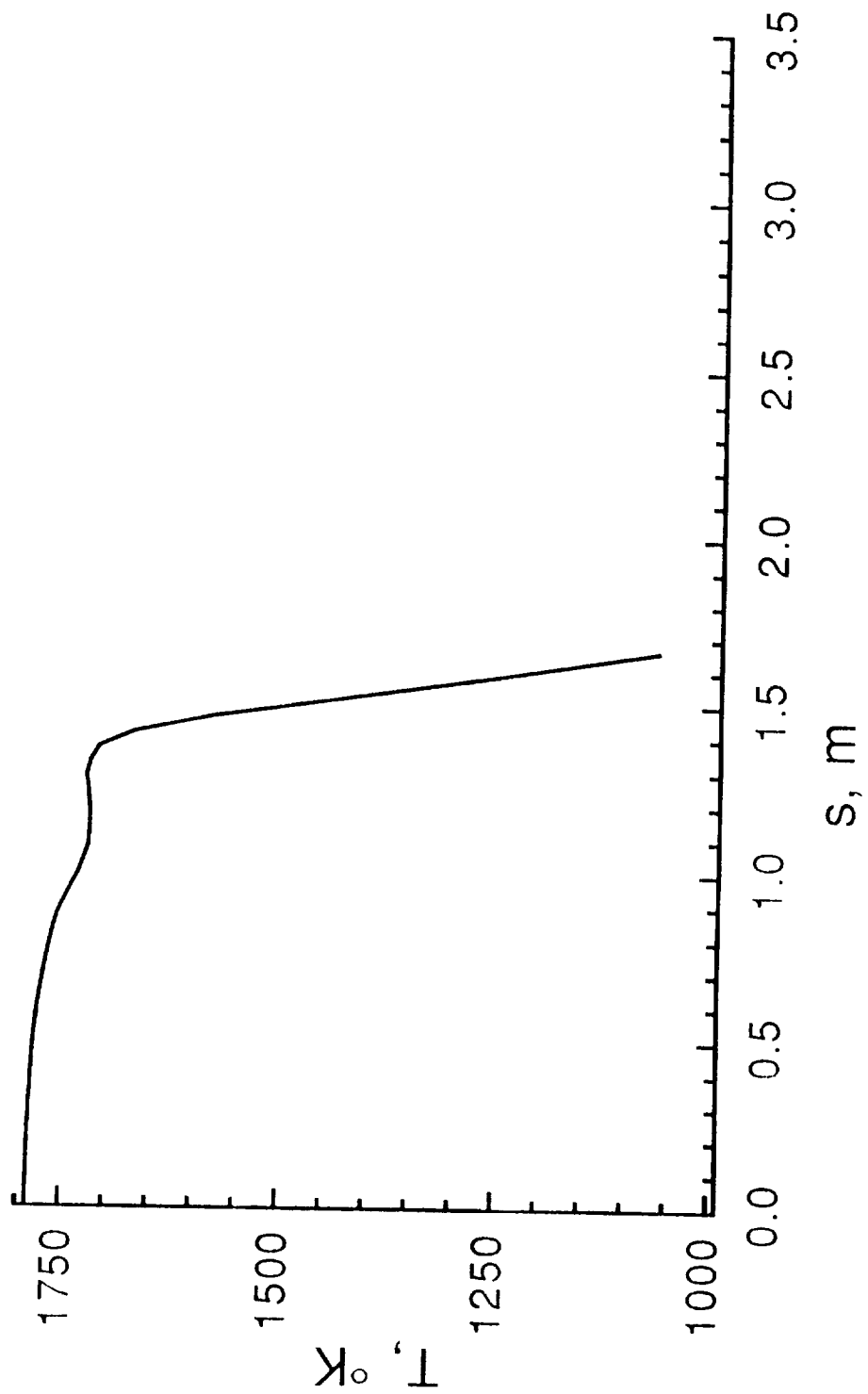
(g) $\phi = +20°$

Figure 5. - Continued.
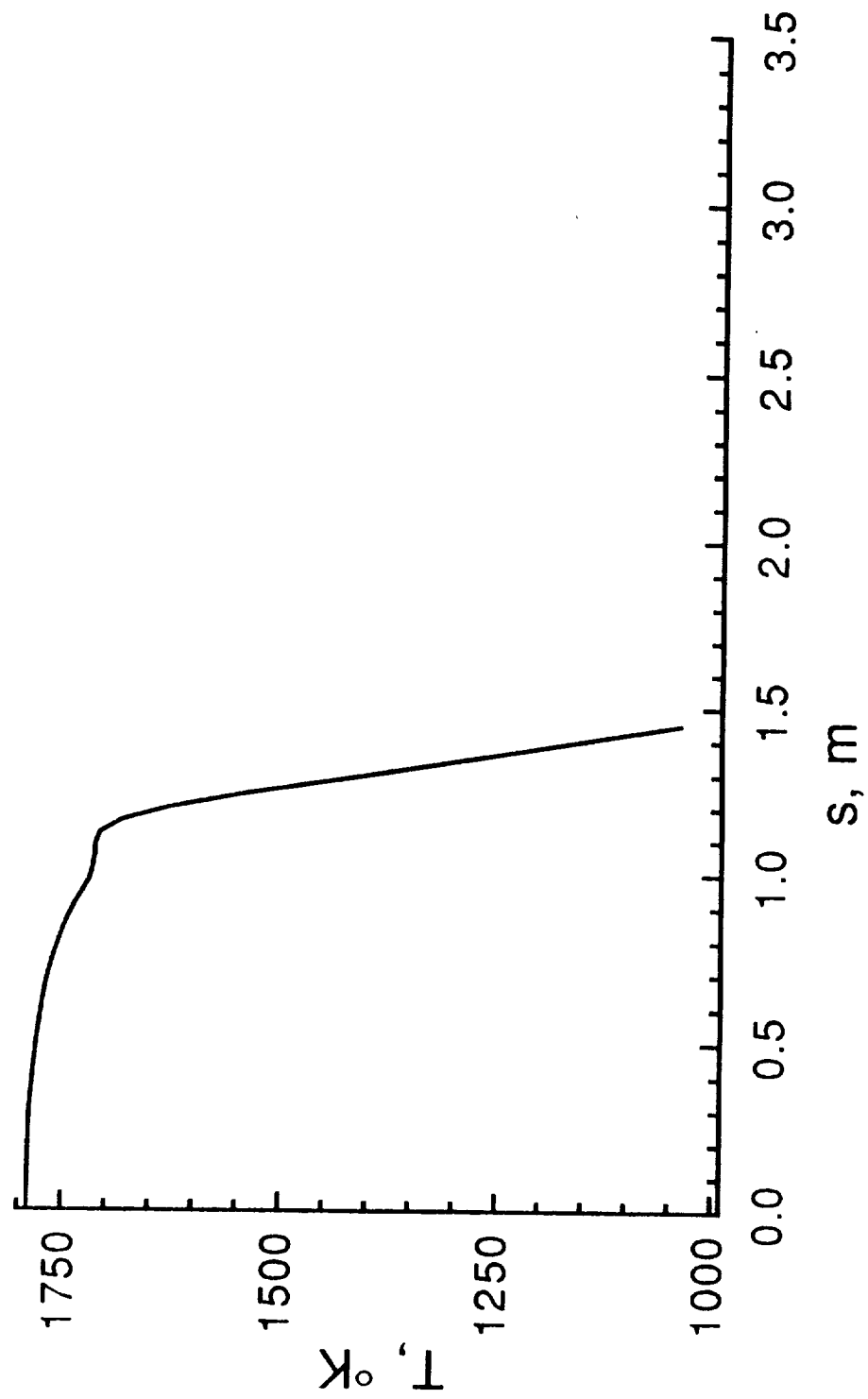
(h) $\phi = +40°$

Figure 5. - Continued.
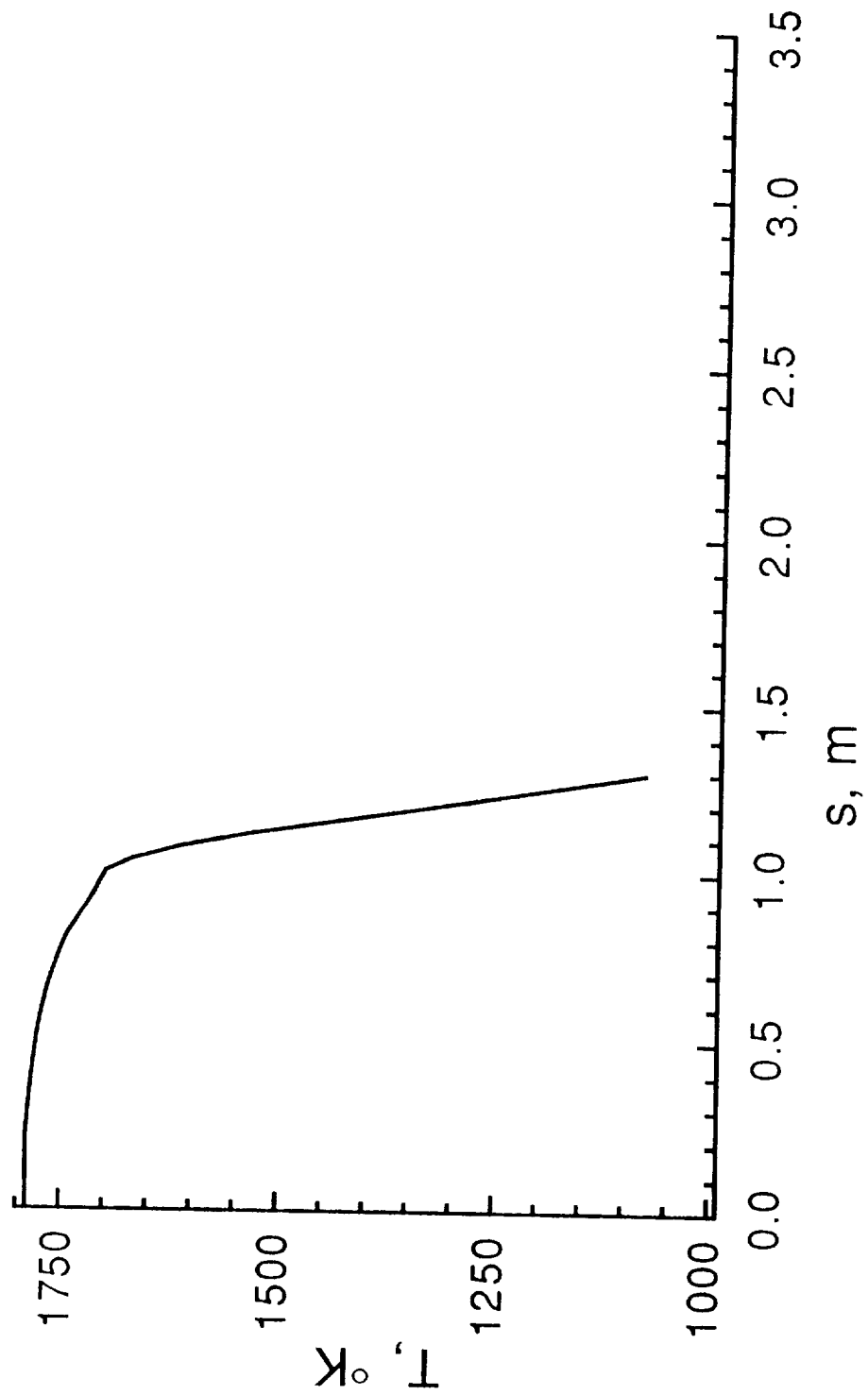
(i) $\phi = +60°$

Figure 5. - Continued.
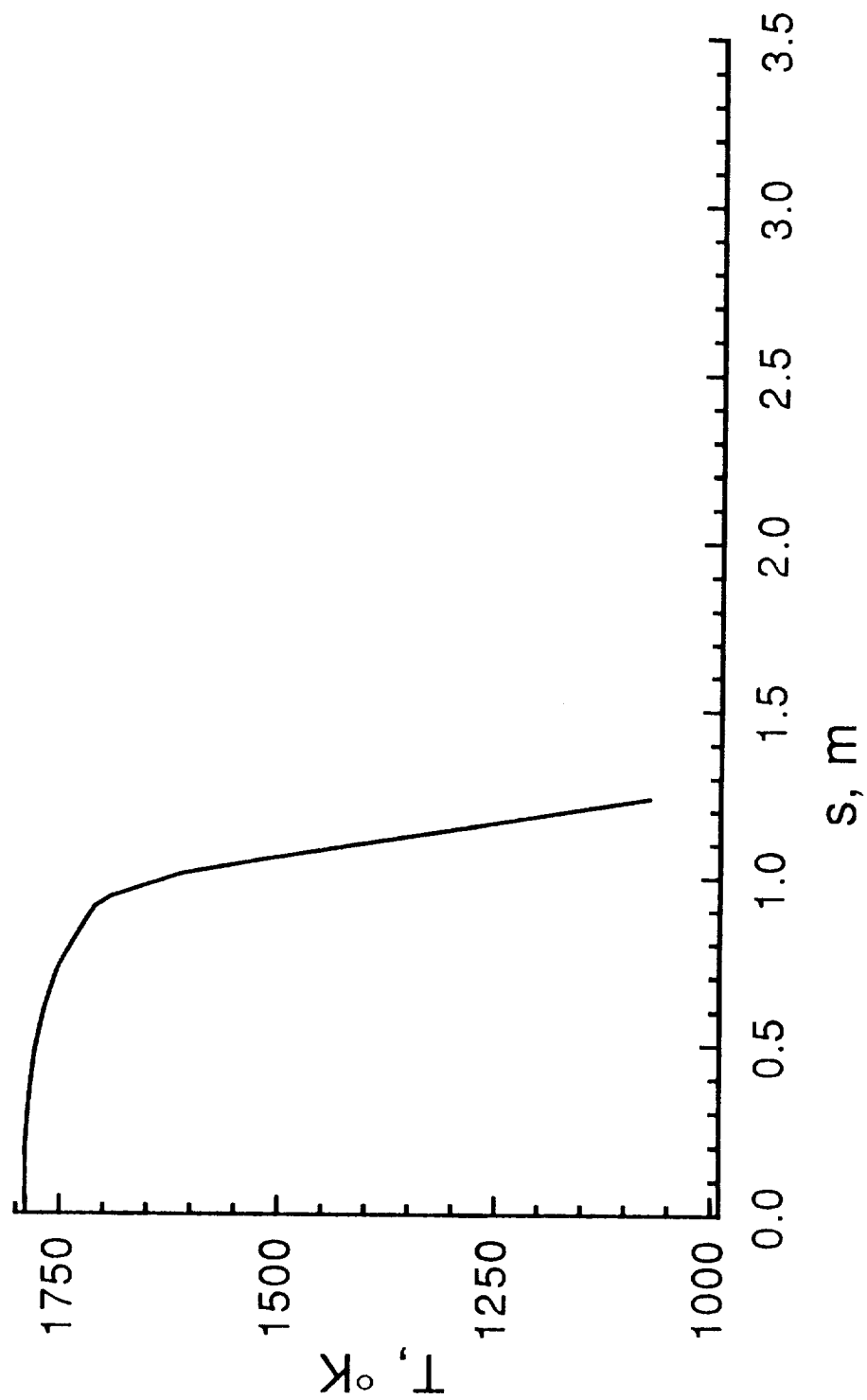
(j) $\phi = +80°$

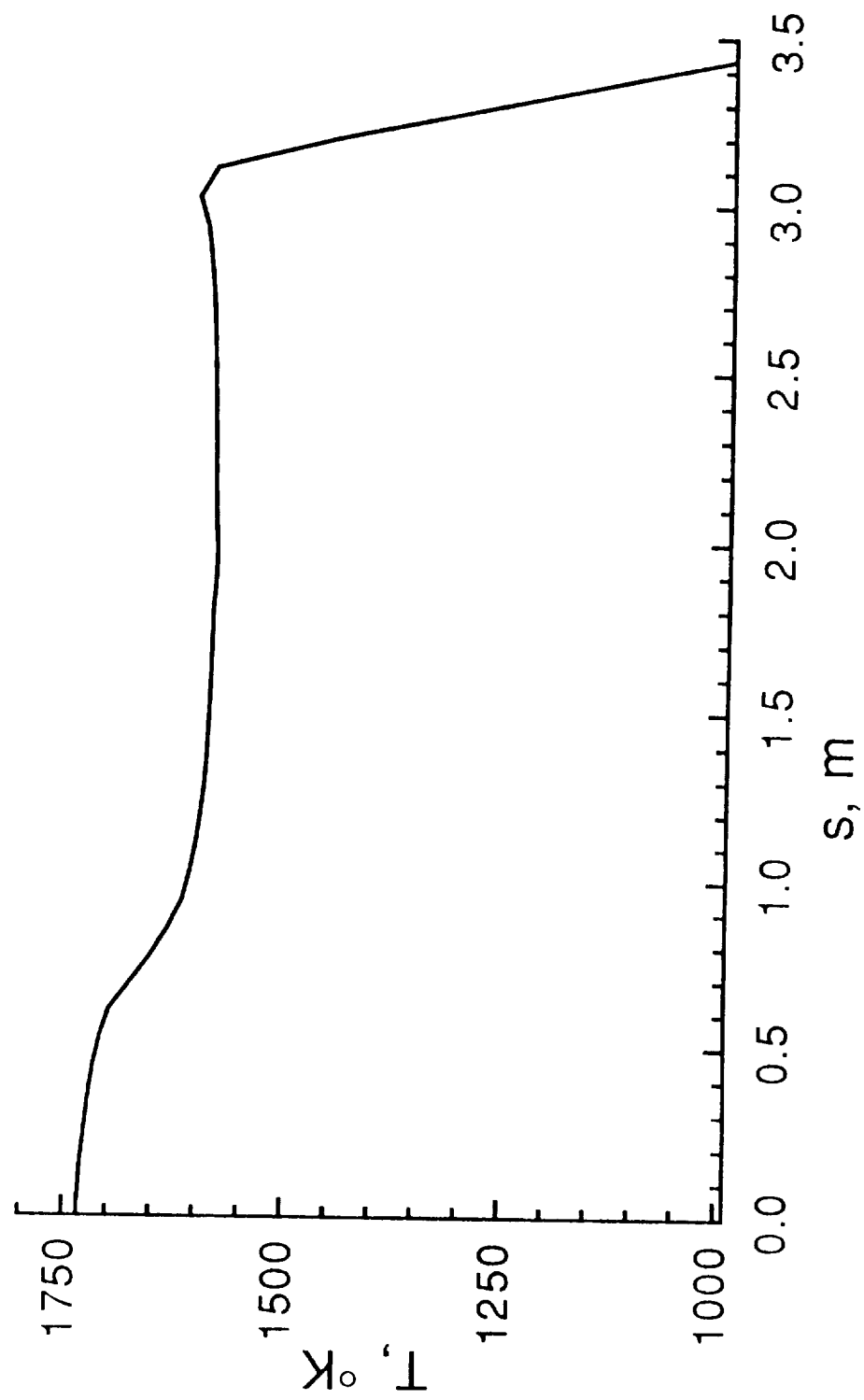Figure 5. - Continued.
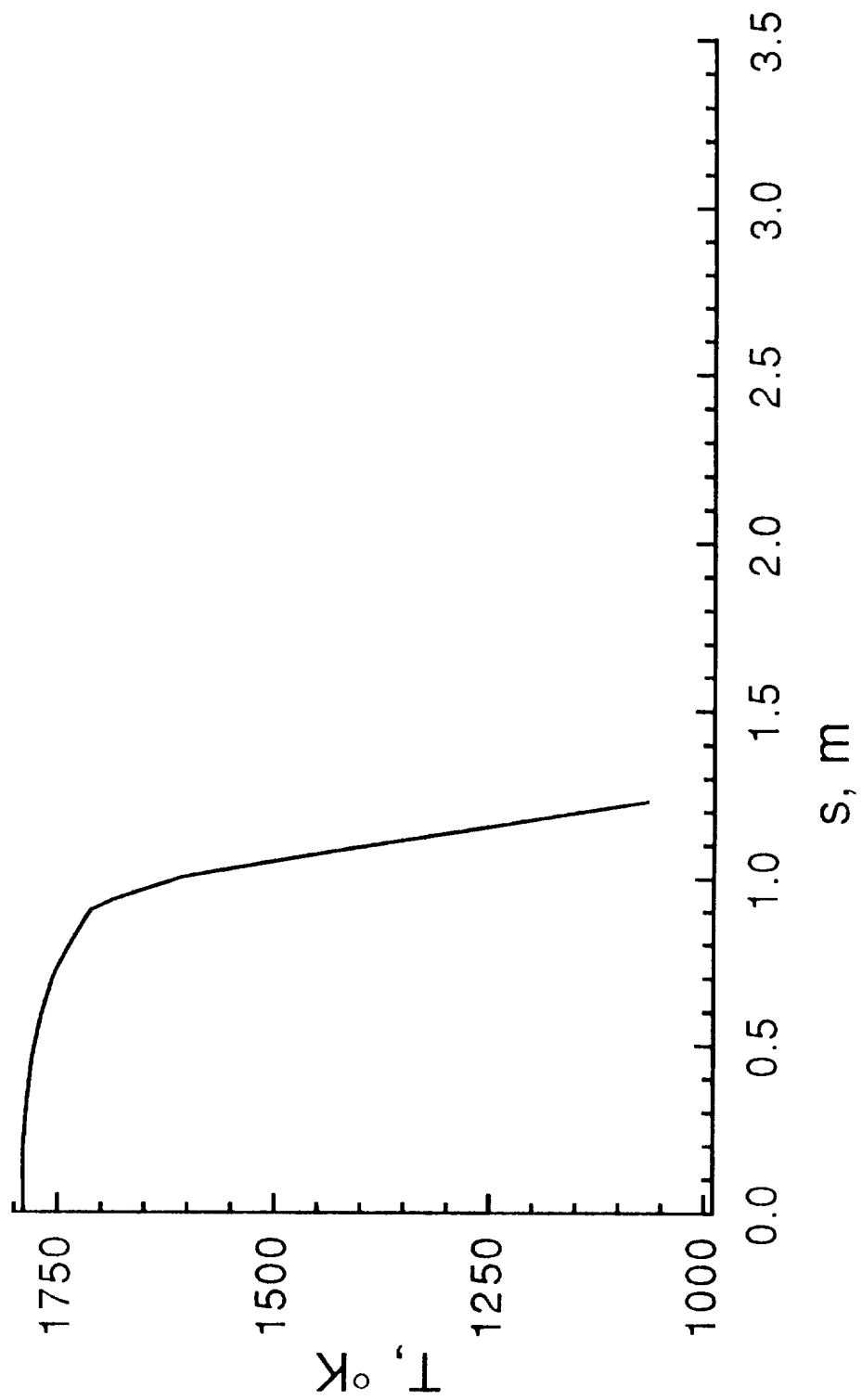
(k) $\phi = +90°$

Figure 5. - Concluded.
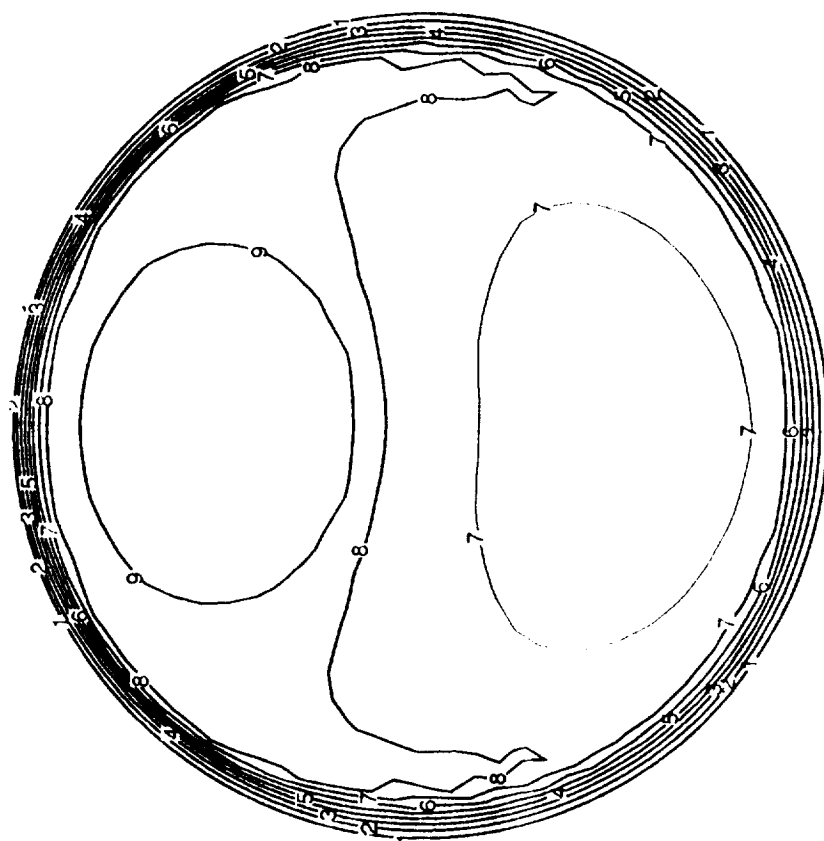
Level	q_{total}
9	45.00
8	40.00
7	35.00
6	30.00
5	25.00
4	20.00
3	15.00
2	10.00
1	5.00

(a) q_{total}

Figure 6. - Heat Transfer Contours at Peak Heating Point.
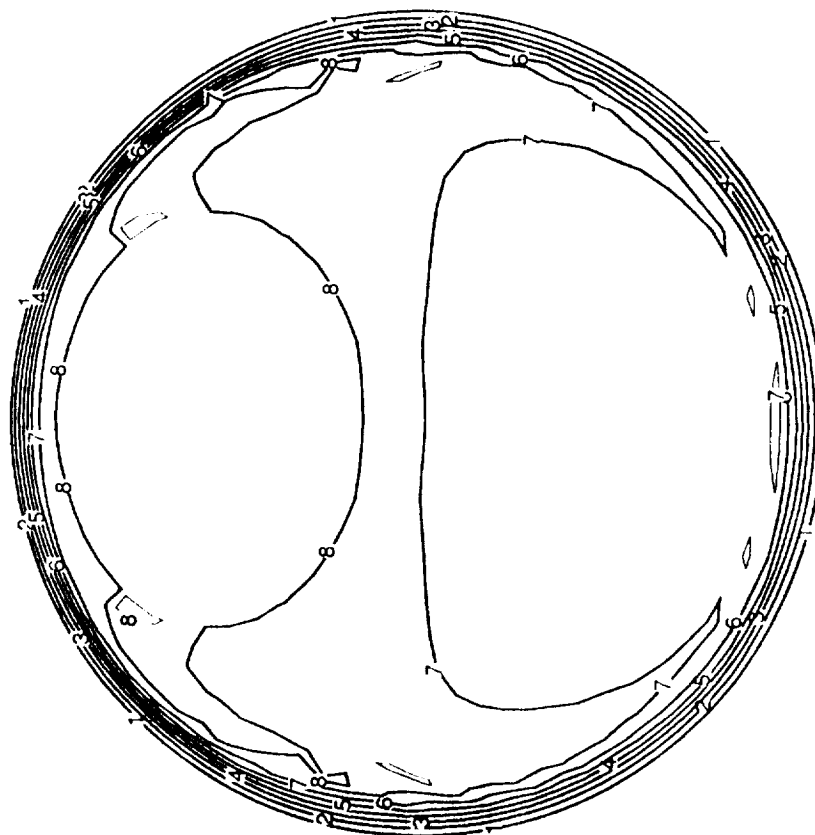
Level	q_c
9	45.00
8	40.00
7	35.00
6	30.00
5	25.00
4	20.00
3	15.00
2	10.00
1	5.00

(b) q_c

Figure 6. - Continued.

41

Level	q_r
9	5.40
8	4.80
7	4.20
6	3.60
5	3.00
4	2.40
3	1.80
2	1.20
1	0.60

(c) q_r

Figure 6. - Concluded.

Level	T (°K)
9	1750.
8	1700.
7	1650.
6	1600.
5	1550.
4	1500.
3	1450.
2	1400.
1	1350.
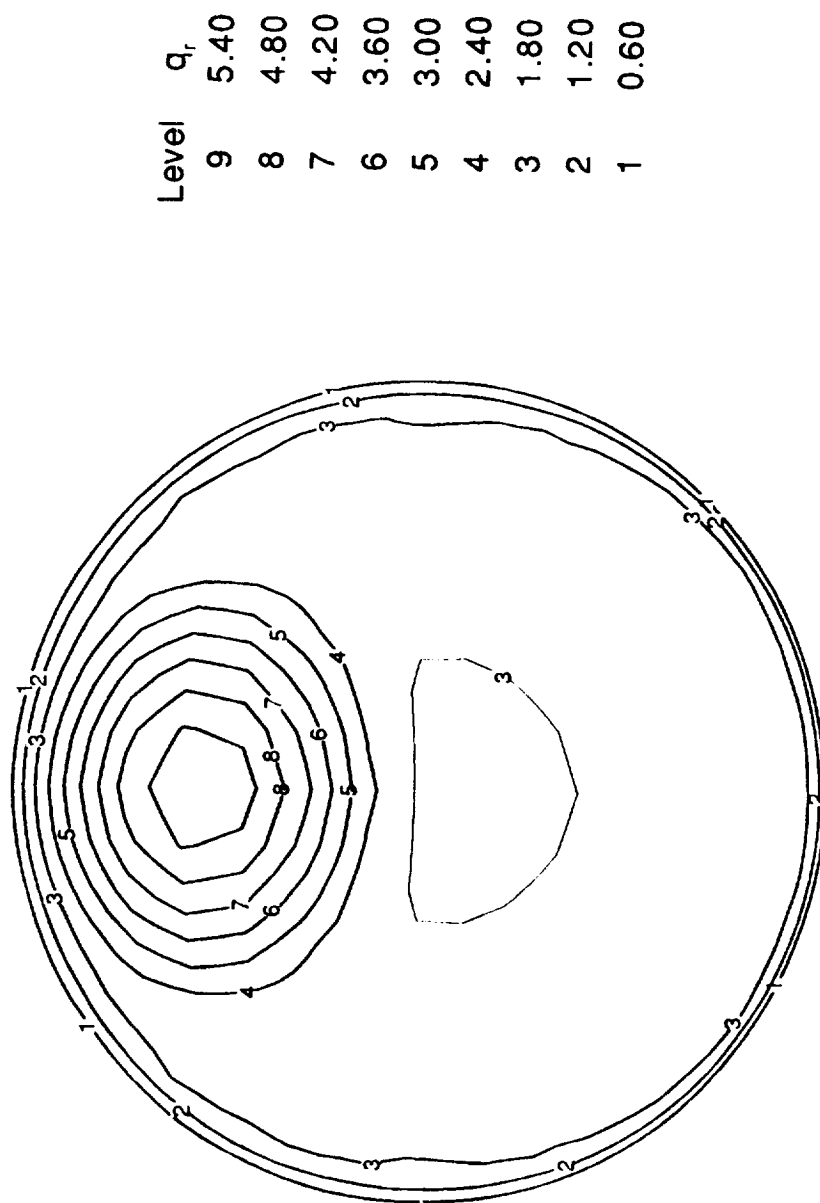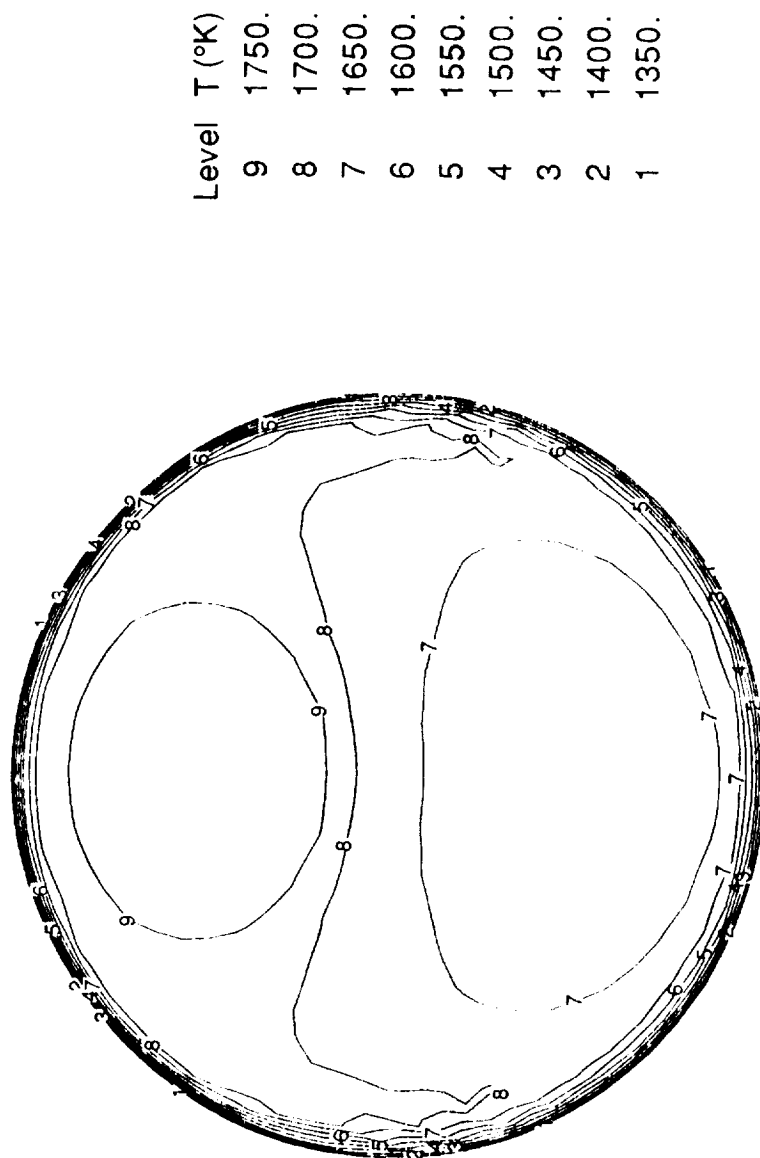
Figure 7. - Wall Temperature Contours at Peak Heating Point.
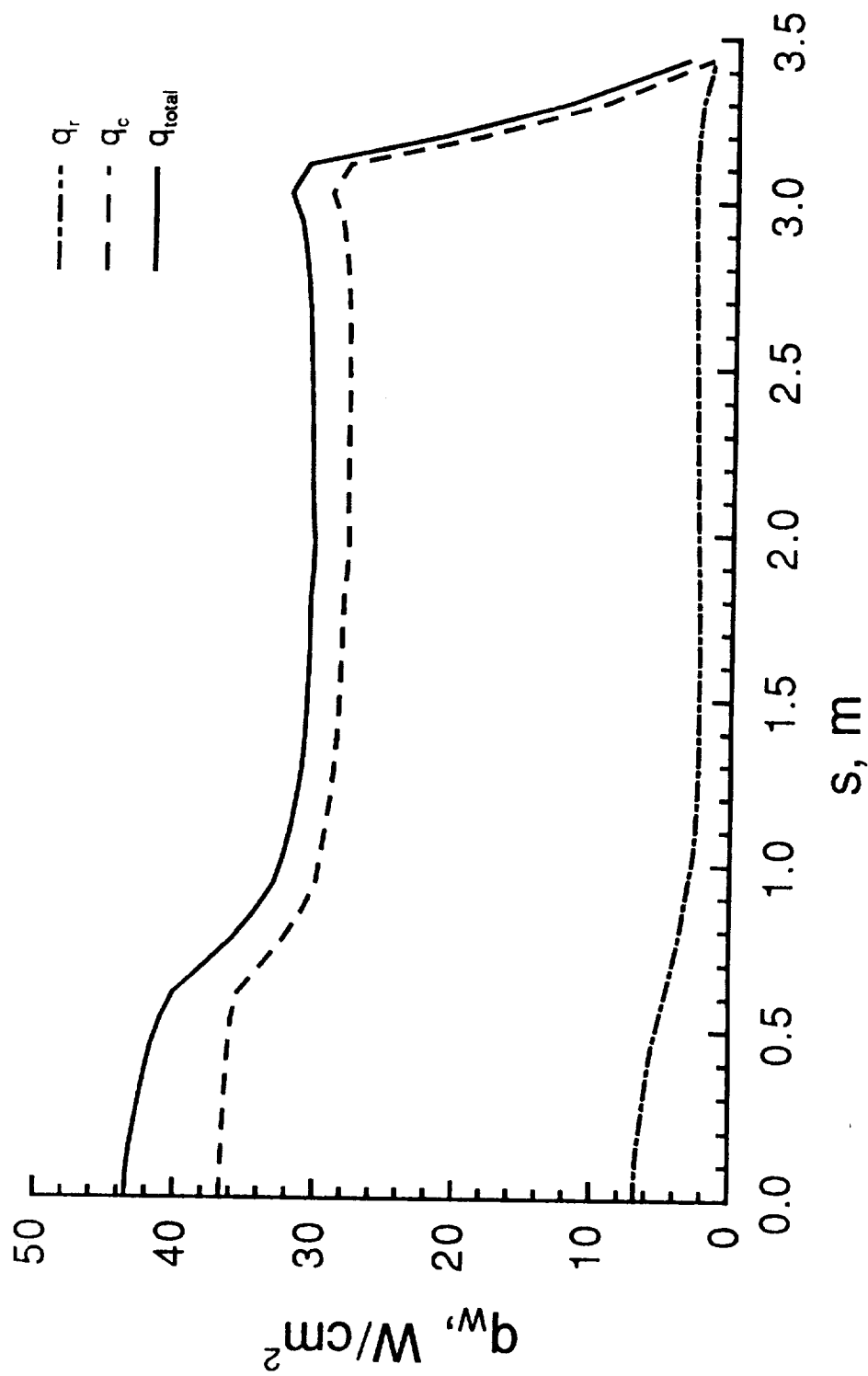
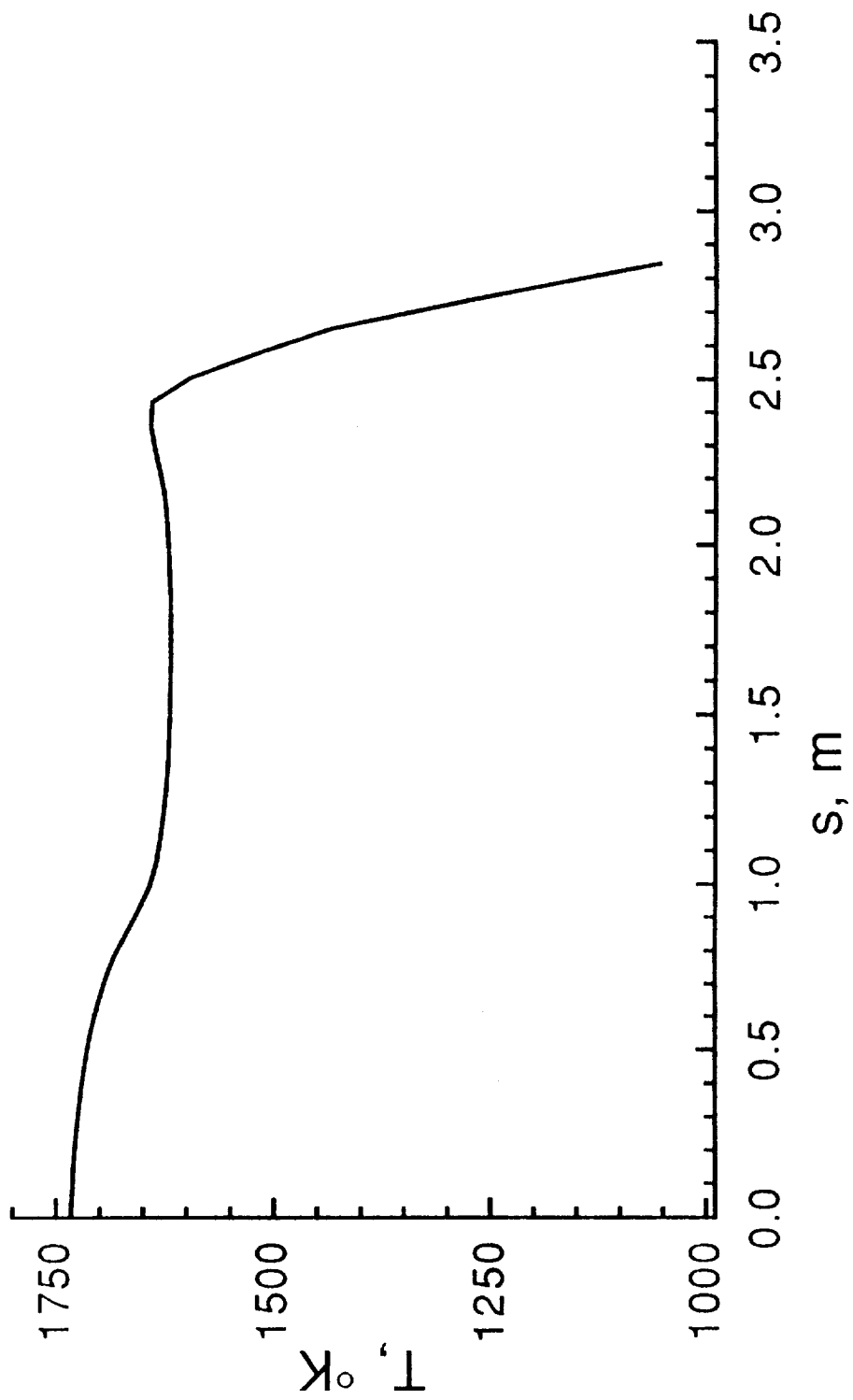Figure 8. - Heat Transfer at Start of Quiescent Period.

(a) ϕ = -90°
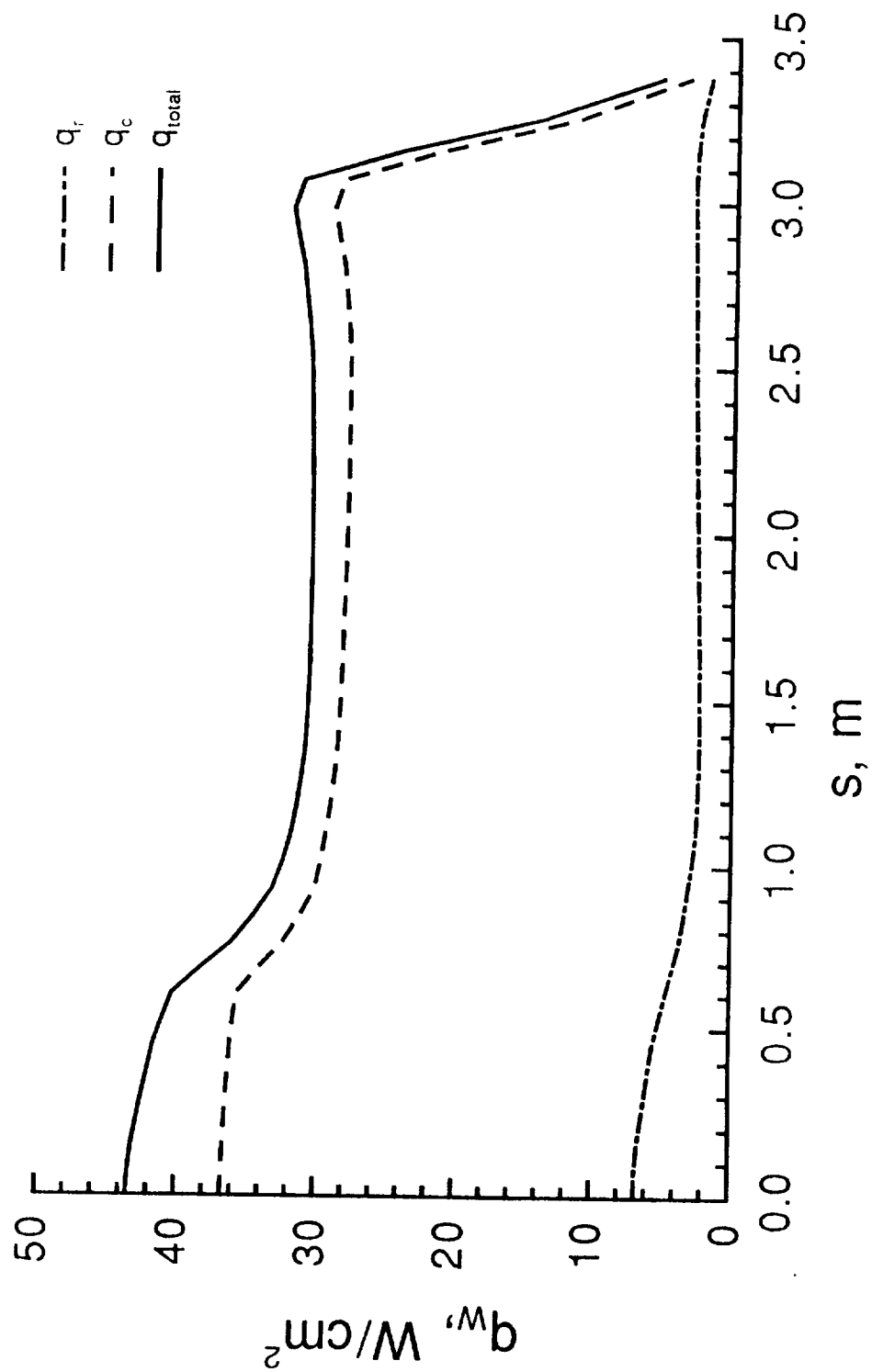
(b) $\phi = -80°$

Figure 8. - Continued.
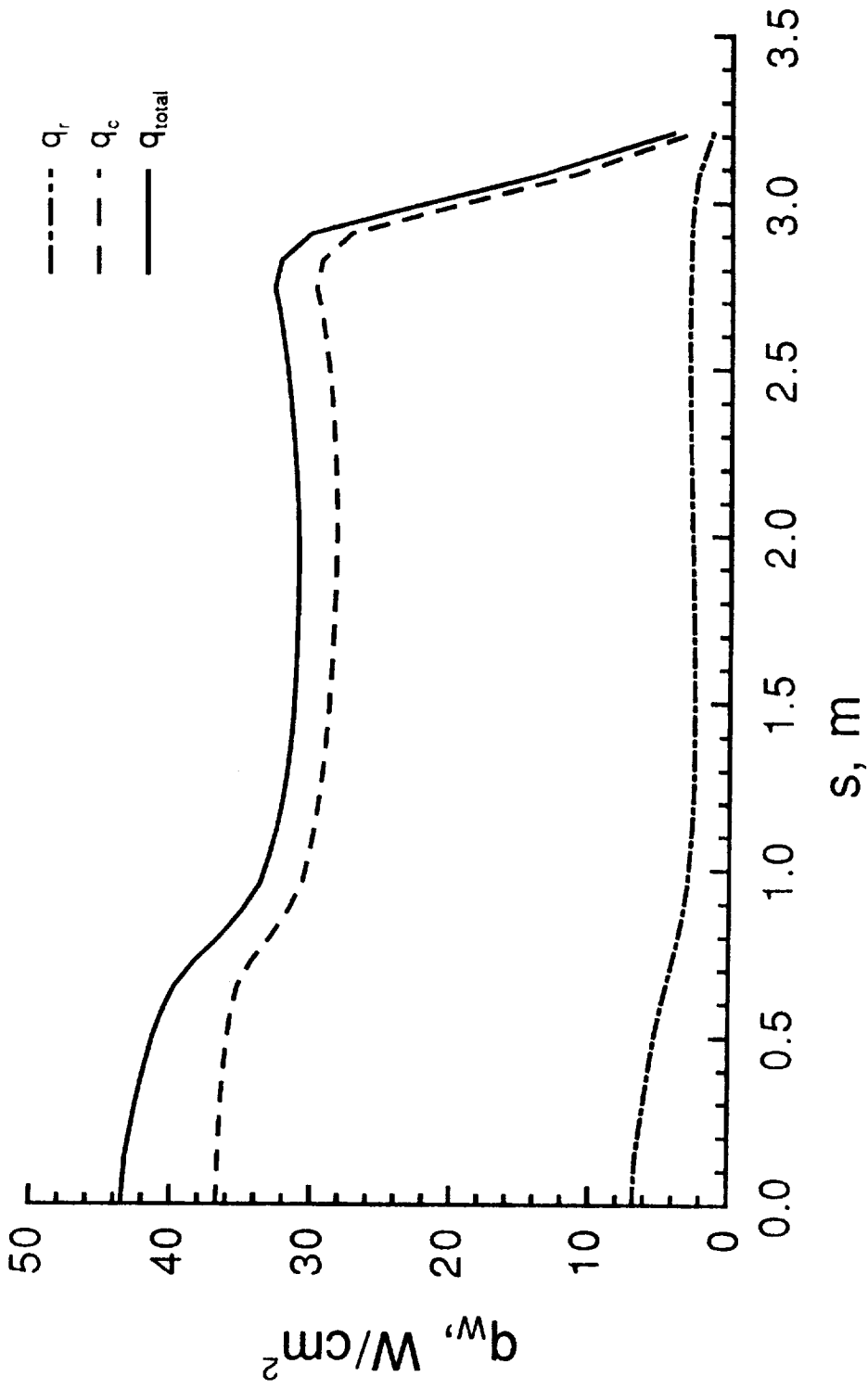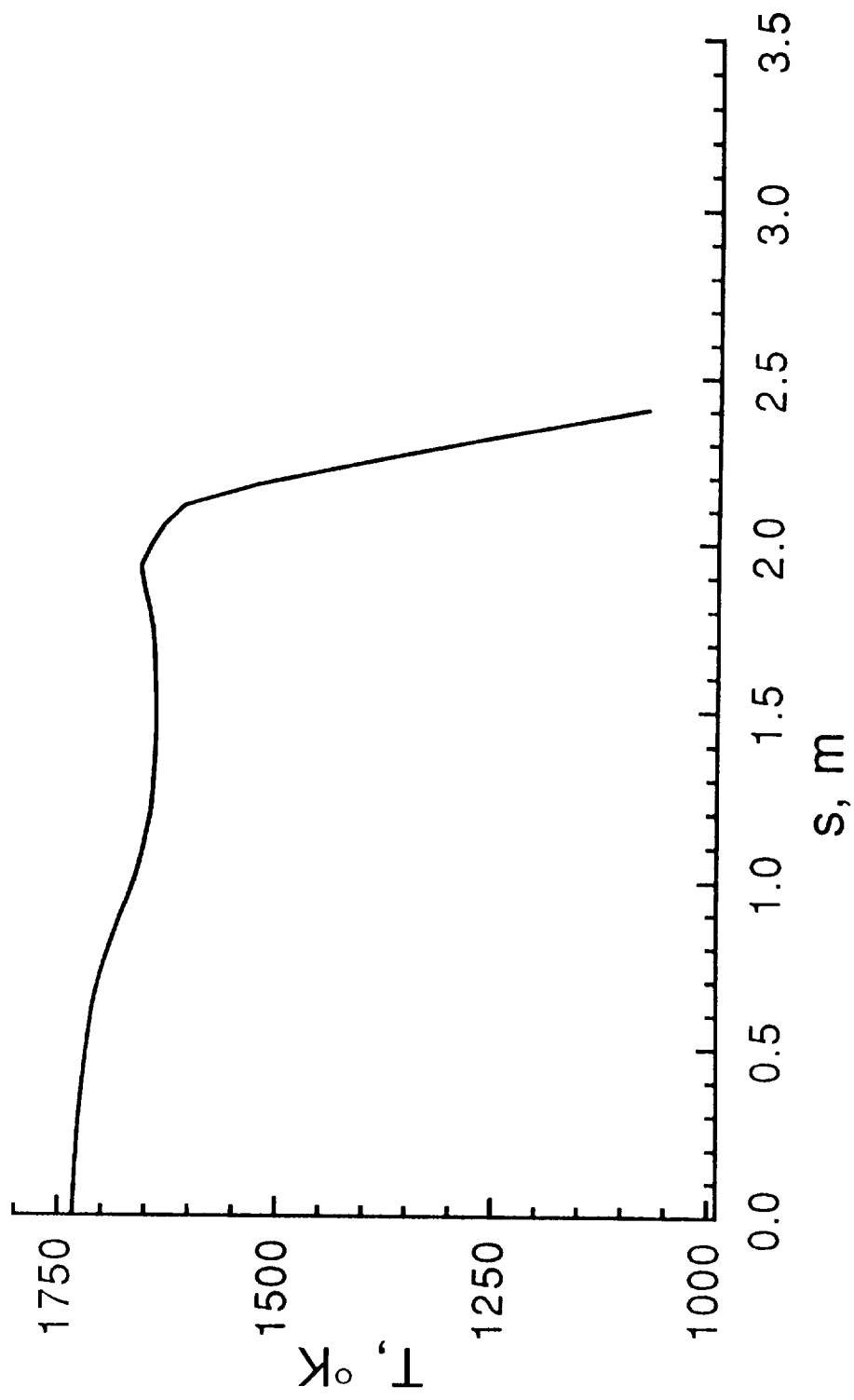
(c) $\phi = -60°$

Figure 8. - Continued.
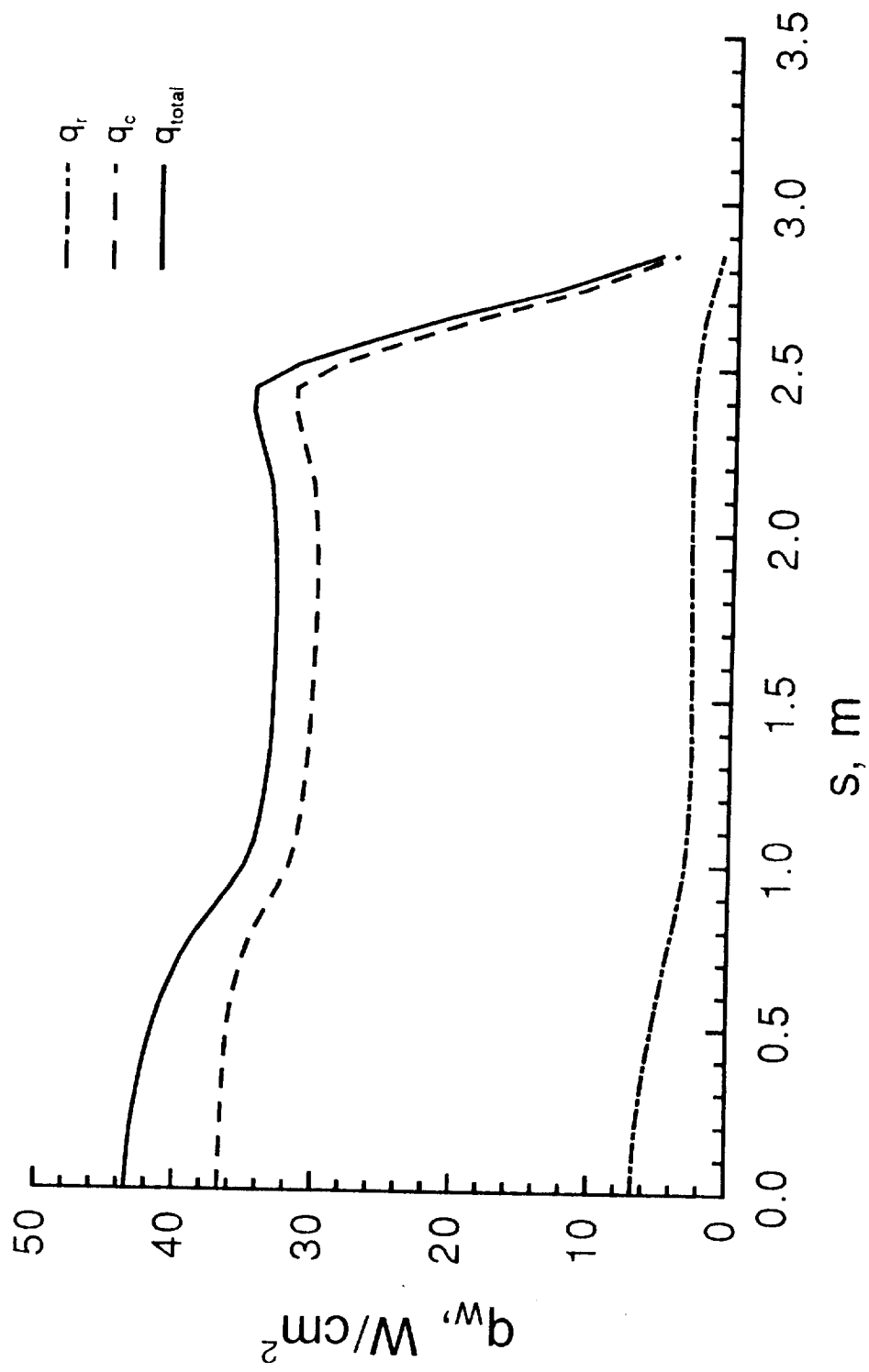
(d) $\phi = -40°$

Figure 8. - Continued.

(e) $\phi = -20°$

Figure 8. - Continued.

(f) $\phi = 0°$

Figure 8. - Continued.

(g) $\phi = +20°$

Figure 8. - Continued.

(h) $\phi = +40°$

Figure 8. - Continued.

(i) $\phi = +60°$

Figure 8. - Continued.
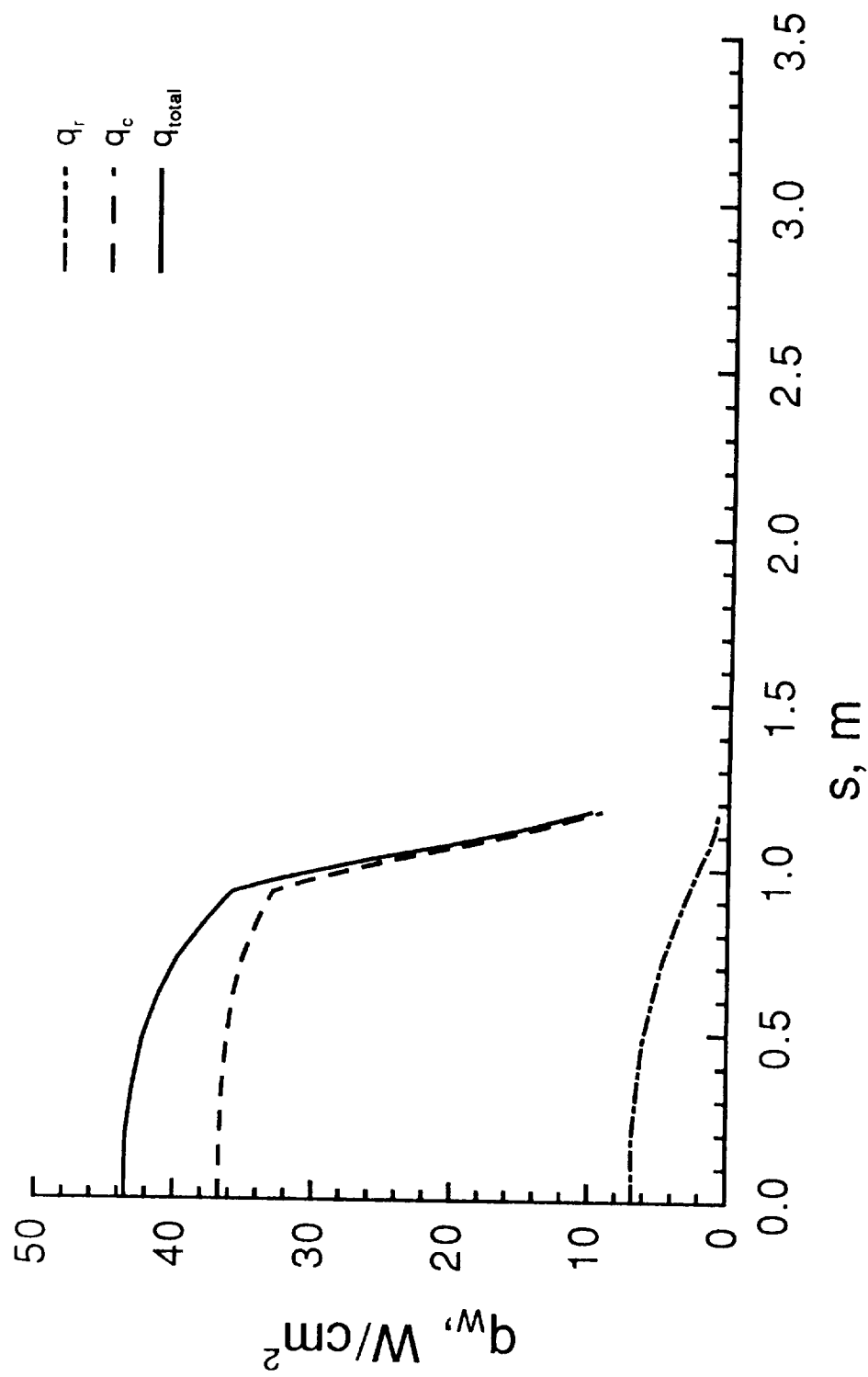
(j) $\phi = +80°$

Figure 8. - Continued.
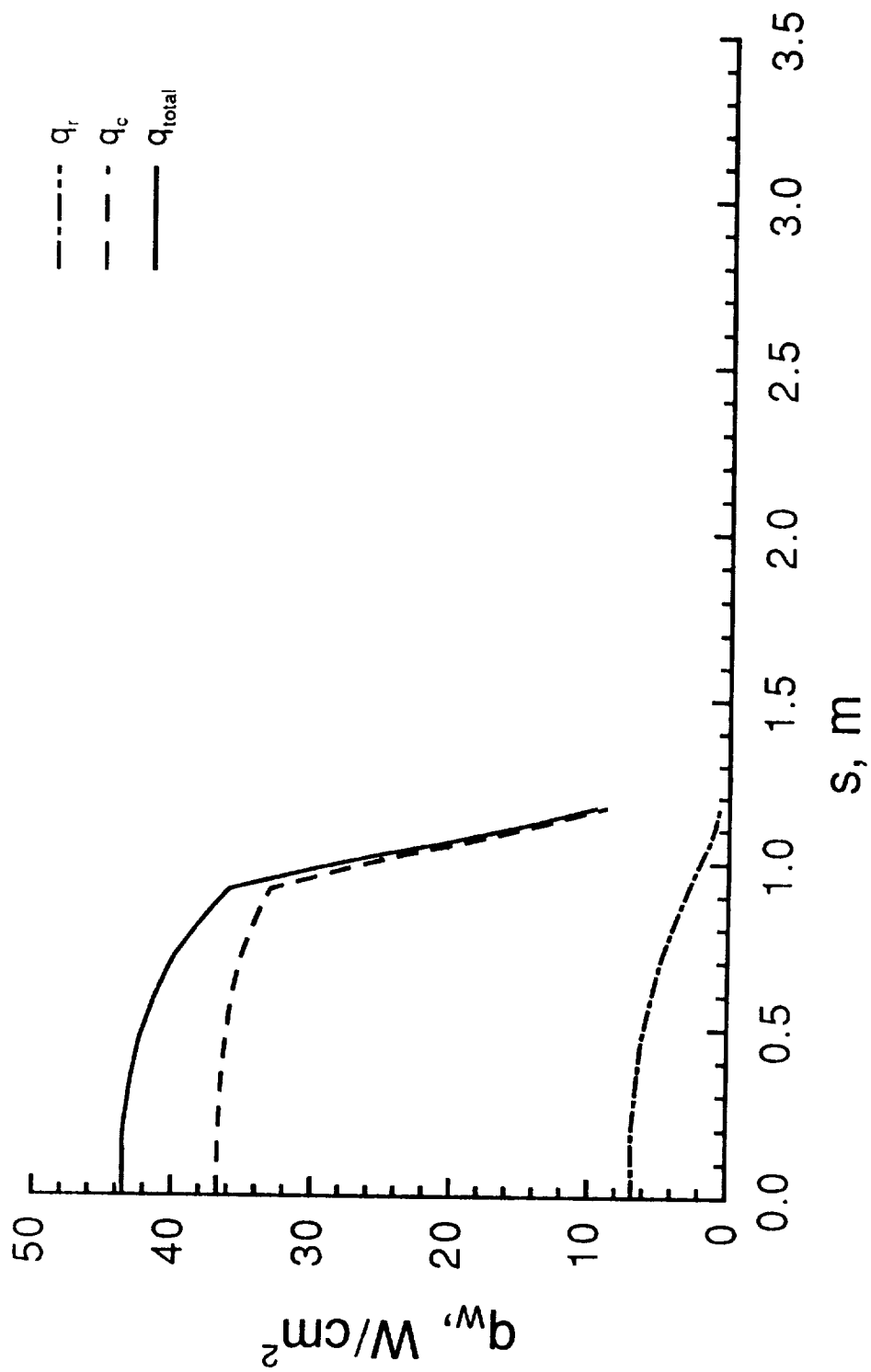
(k) $\phi = +90°$

Figure 8. - Concluded.

(a) $\phi = -90°$

Figure 9. - Wall Temperature at Start of Quiescent Period.
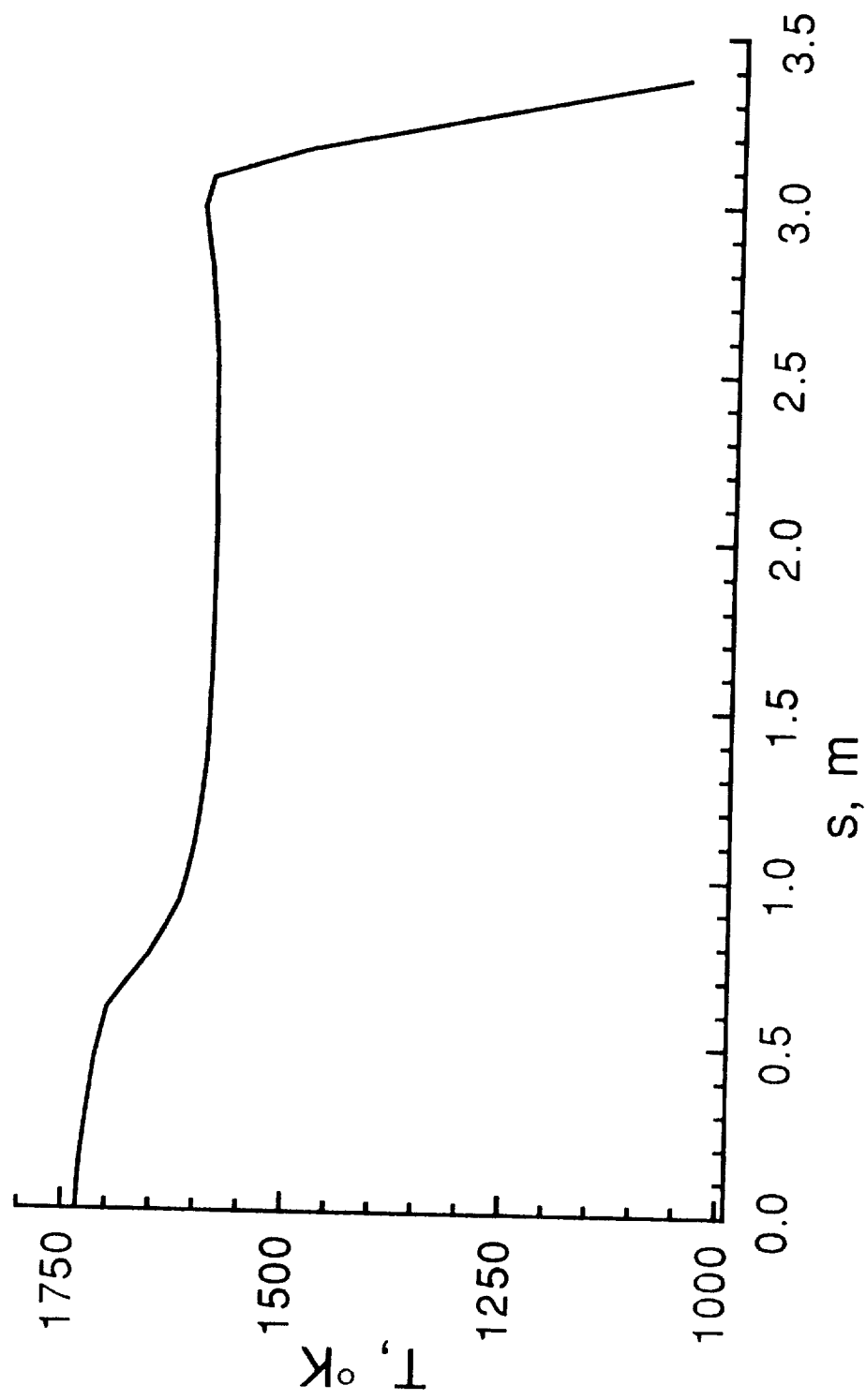
(b) $\phi = -80°$

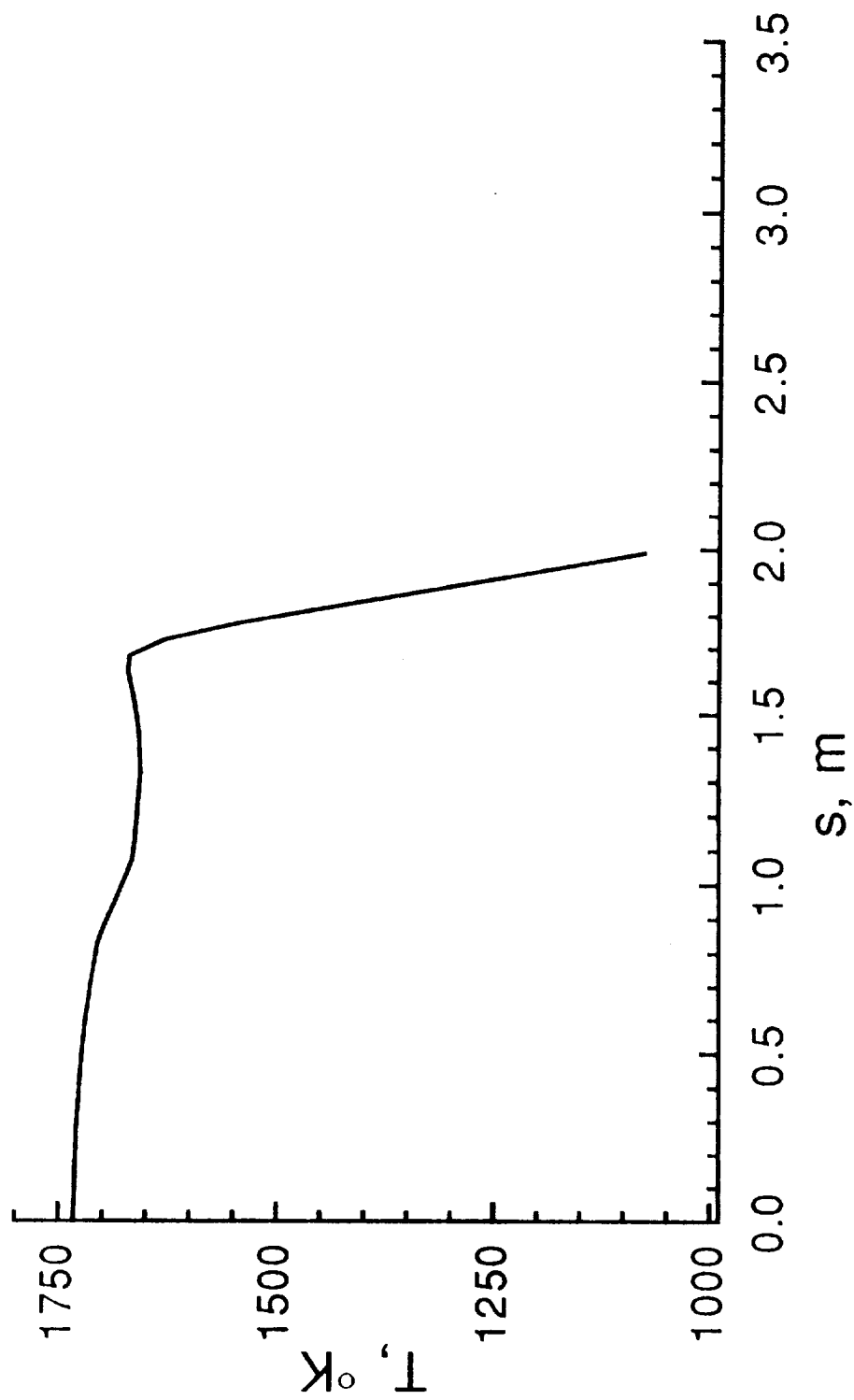Figure 9. - Continued.
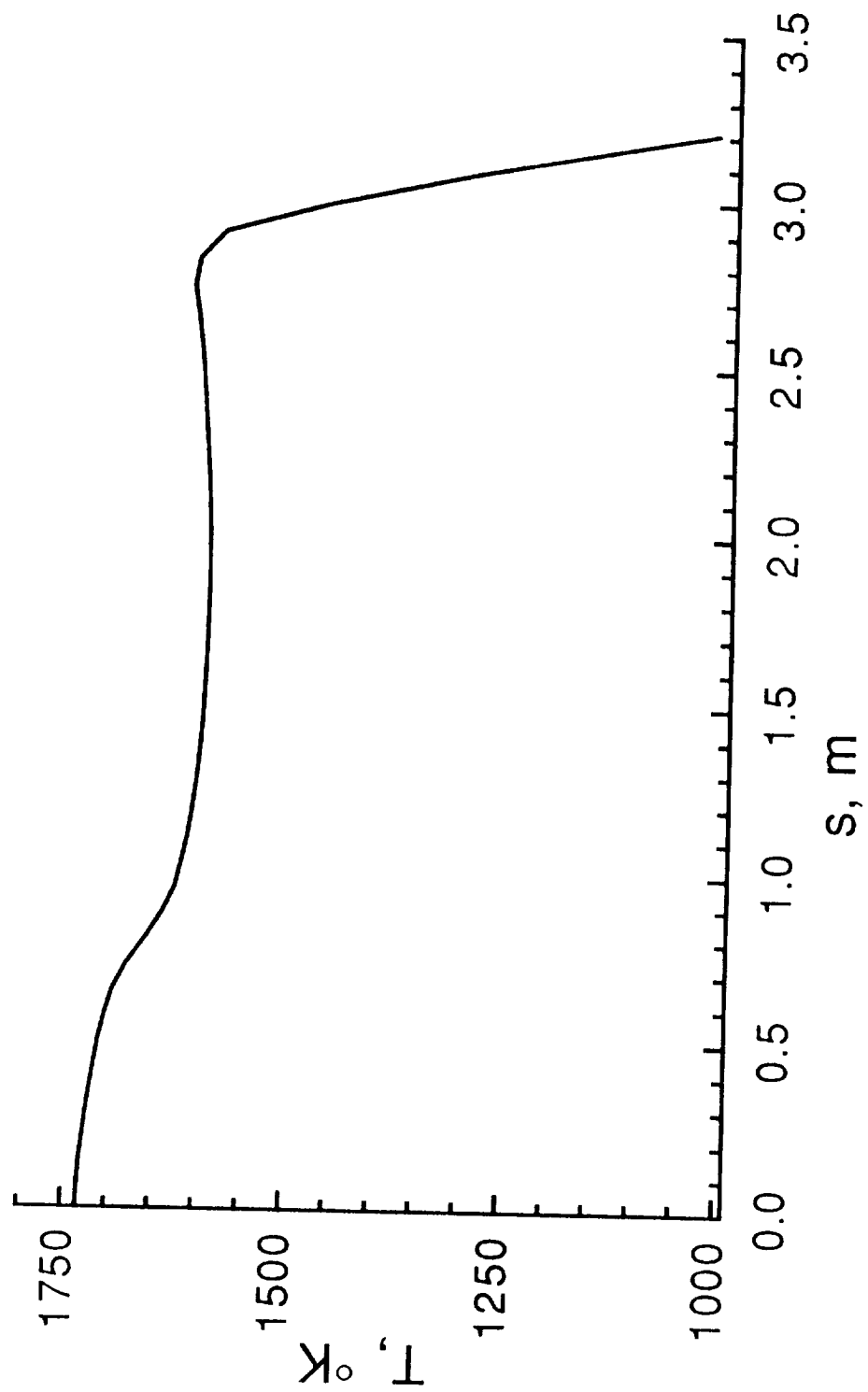
(c) $\phi = -60°$

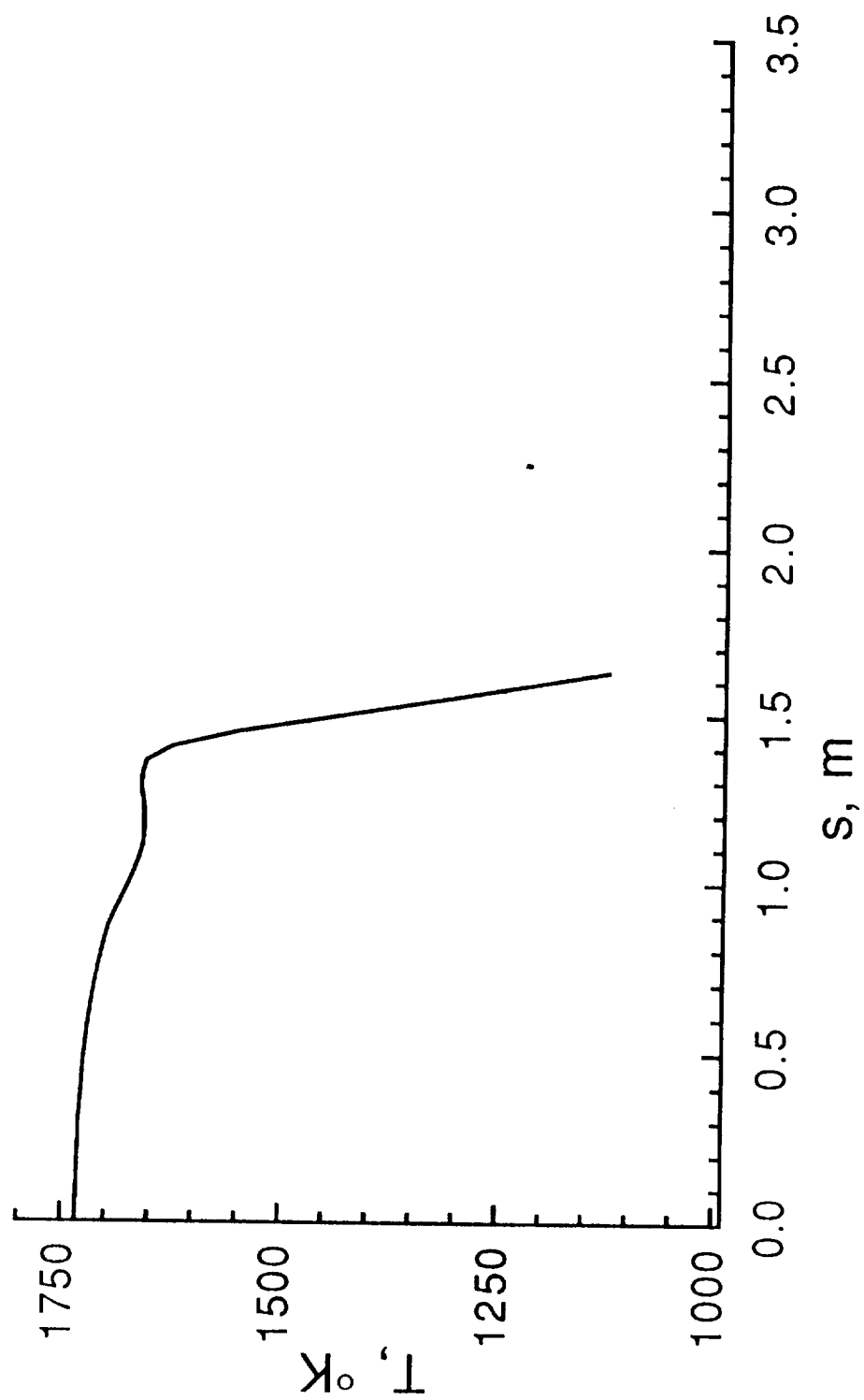Figure 9. - Continued.

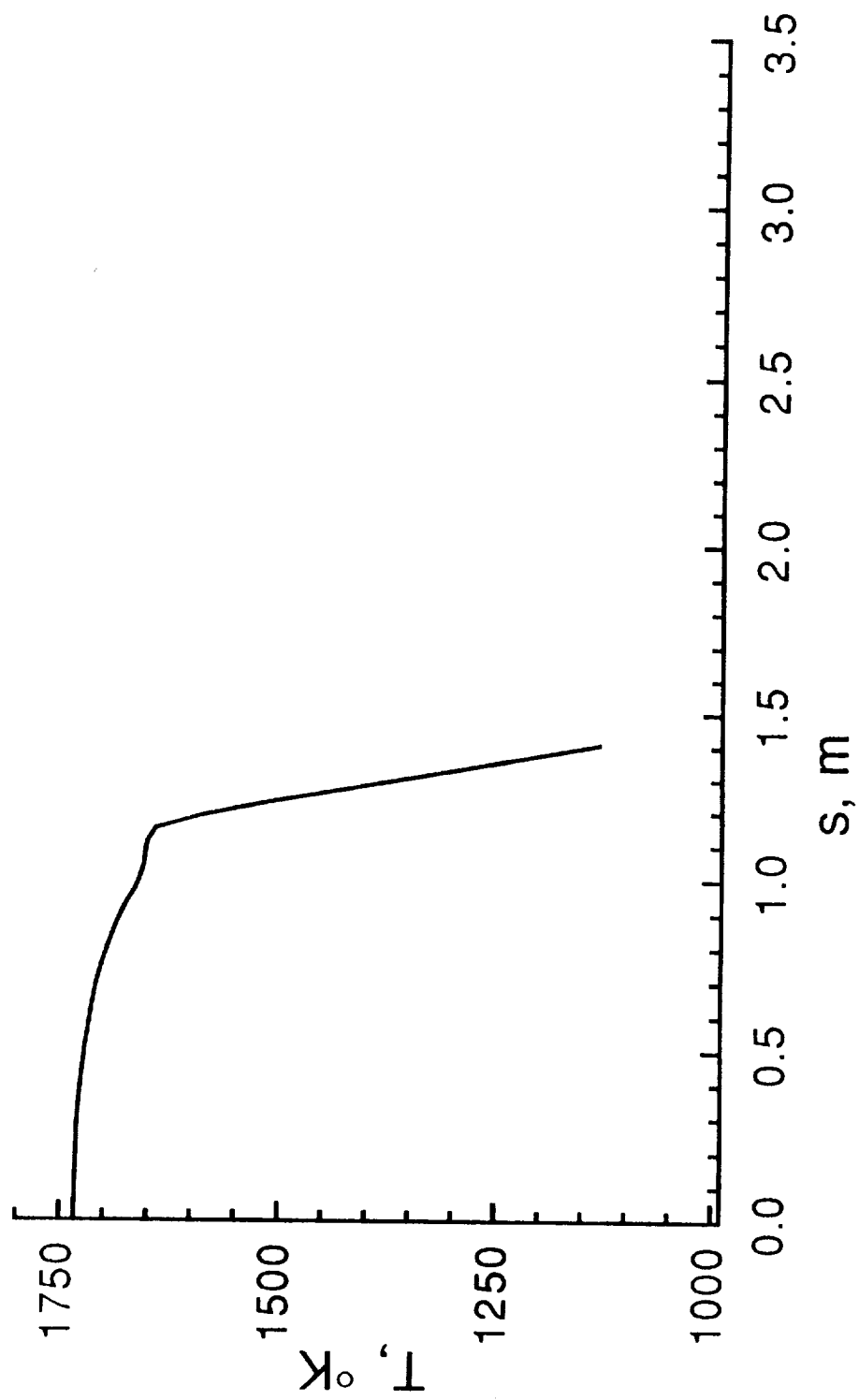(d) $\phi = -40°$

Figure 9. - Continued.

(e) φ = -20°

Figure 9. - Continued.

(f) $\phi = 0°$

Figure 9. - Continued.
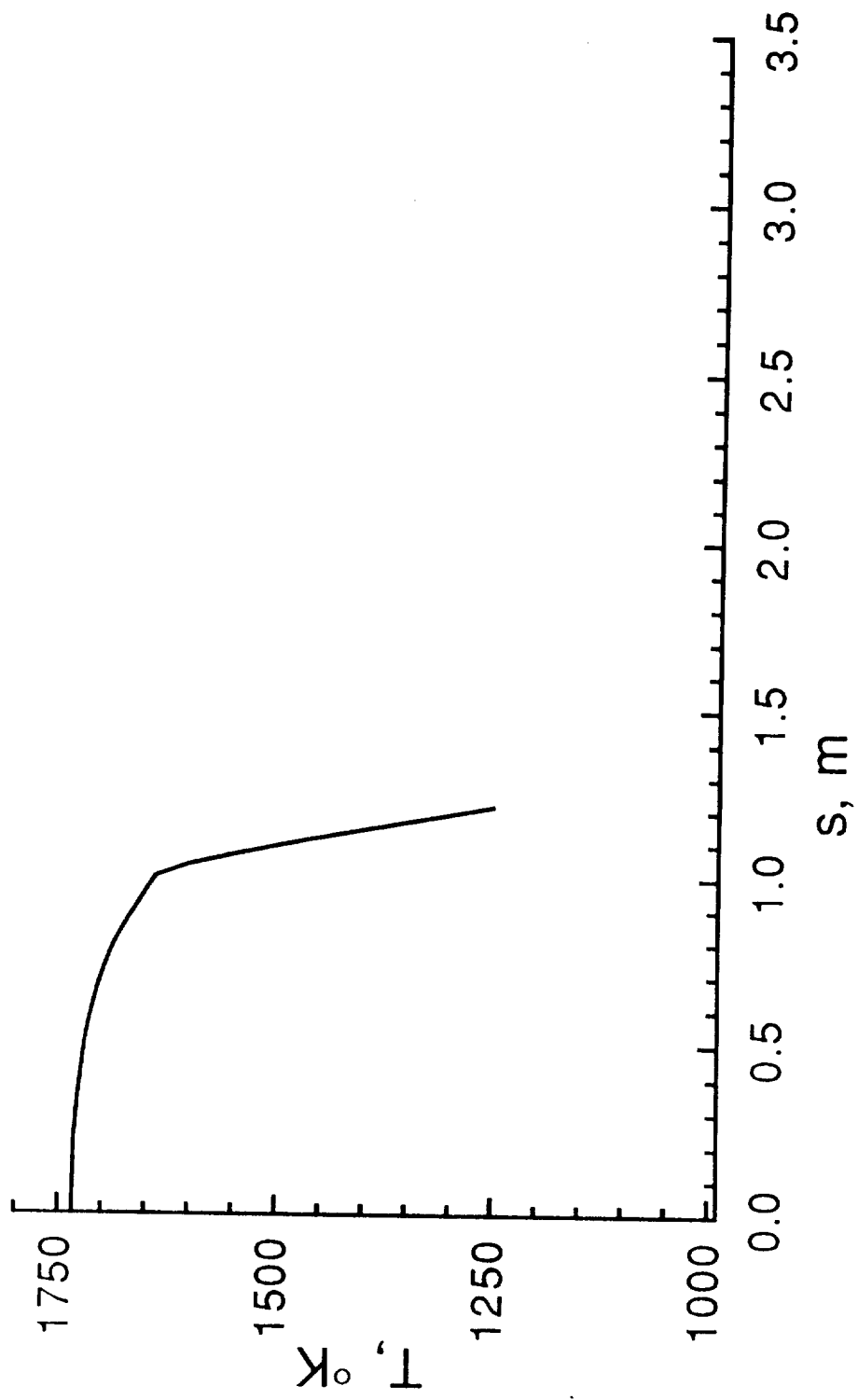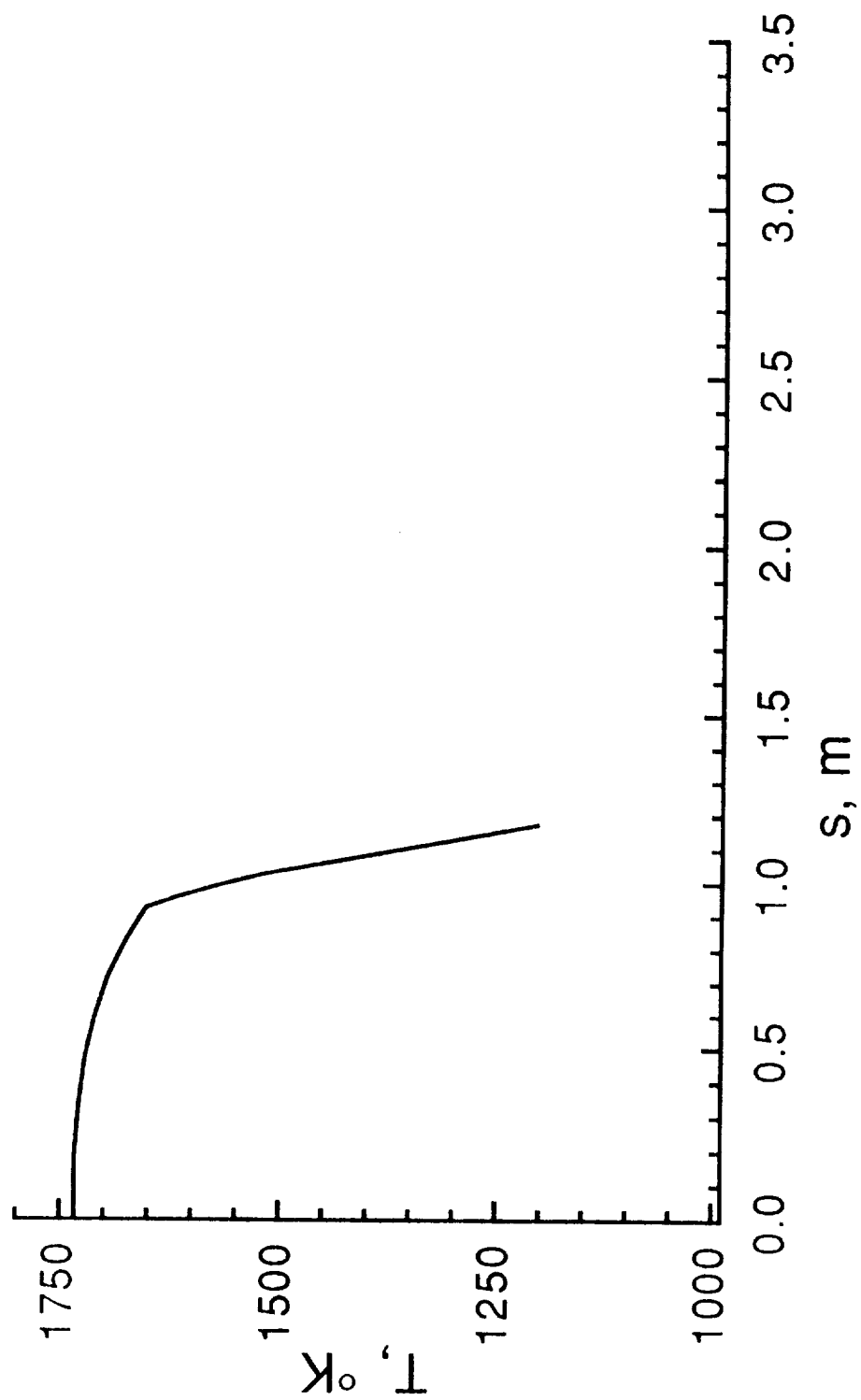
(g) φ = +20°

Figure 9. - Continued.

(h) $\phi = +40°$

Figure 9. - Continued.

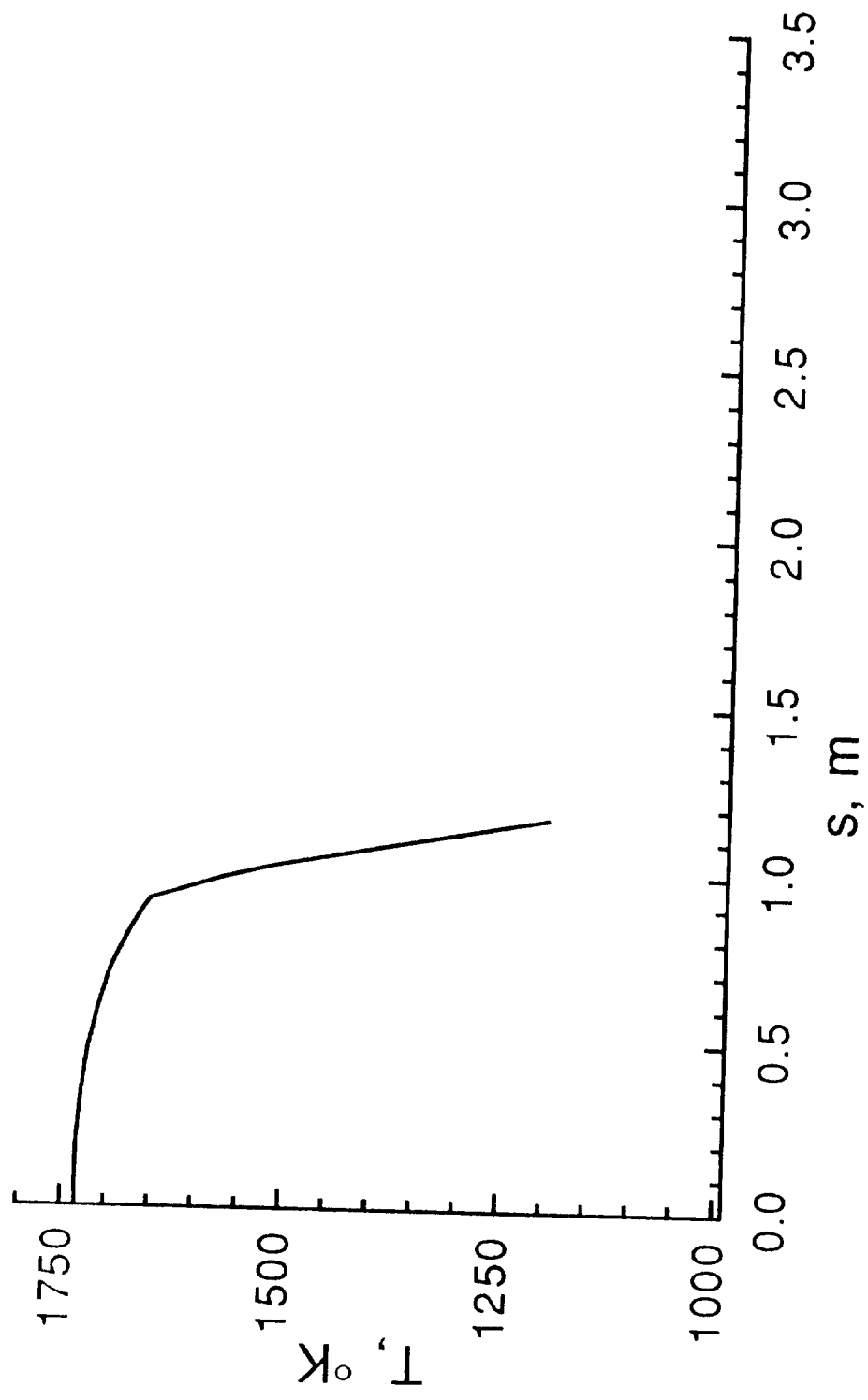(i) $\phi = +60°$

Figure 9. - Continued.

(j) $\phi = +80°$

Figure 9. - Continued.

(k) $\phi = +90°$

Figure 9. - Concluded.

Level	q_{total}
9	45.00
8	40.00
7	35.00
6	30.00
5	25.00
4	20.00
3	15.00
2	10.00
1	5.00
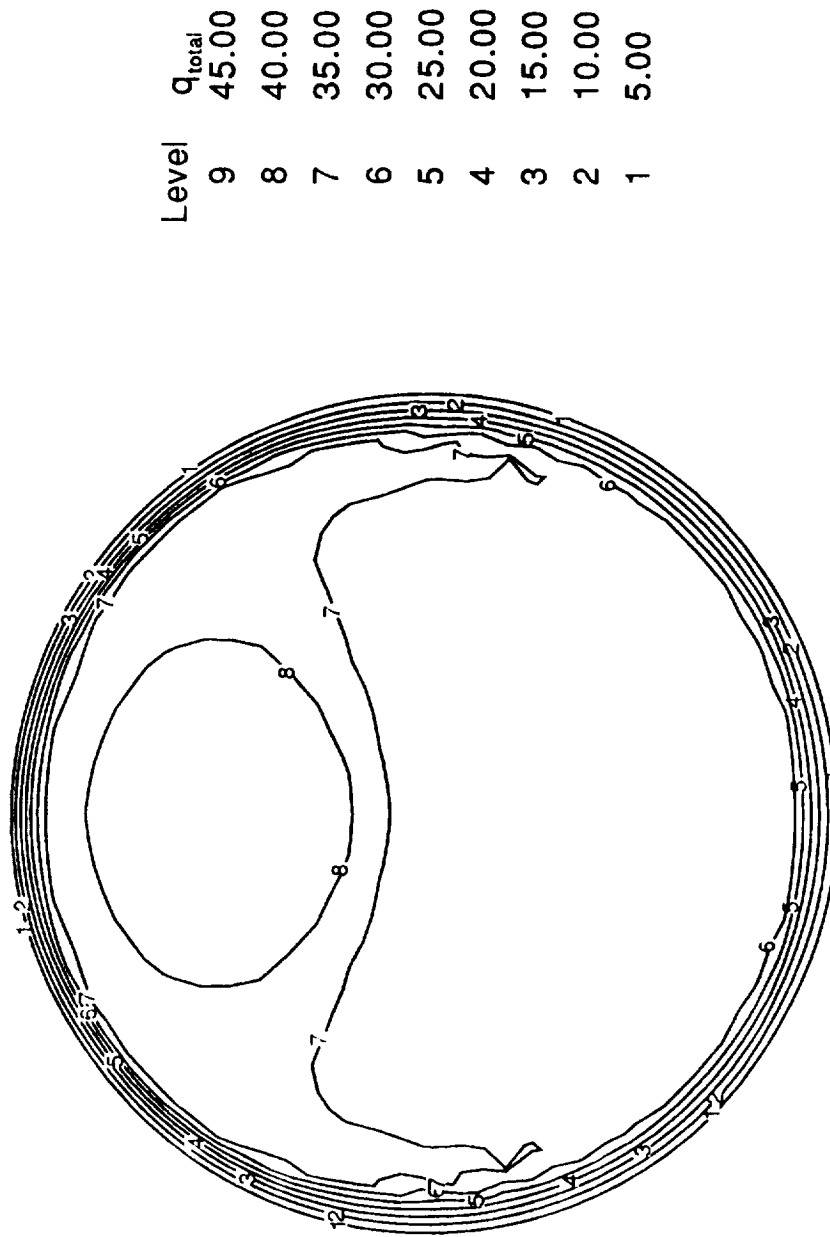
(a) q_{total}

Figure 10. - Heat Transfer Contours at Start
of Quiescent Period.

Level	q_c
9	45.00
8	40.00
7	35.00
6	30.00
5	25.00
4	20.00
3	15.00
2	10.00
1	5.00

(b) q_c

Figure 10. - Continued.

Level	q_r
9	5.40
8	4.80
7	4.20
6	3.60
5	3.00
4	2.40
3	1.80
2	1.20
1	0.60
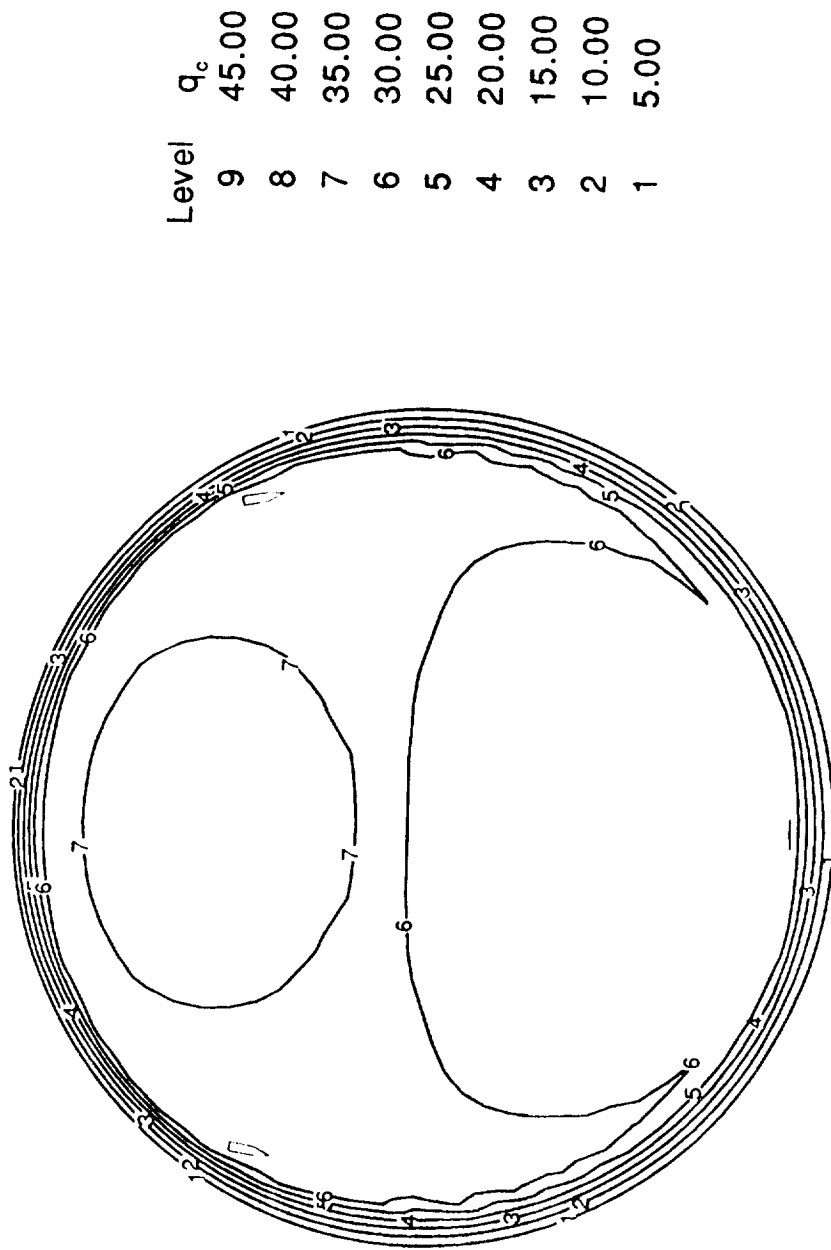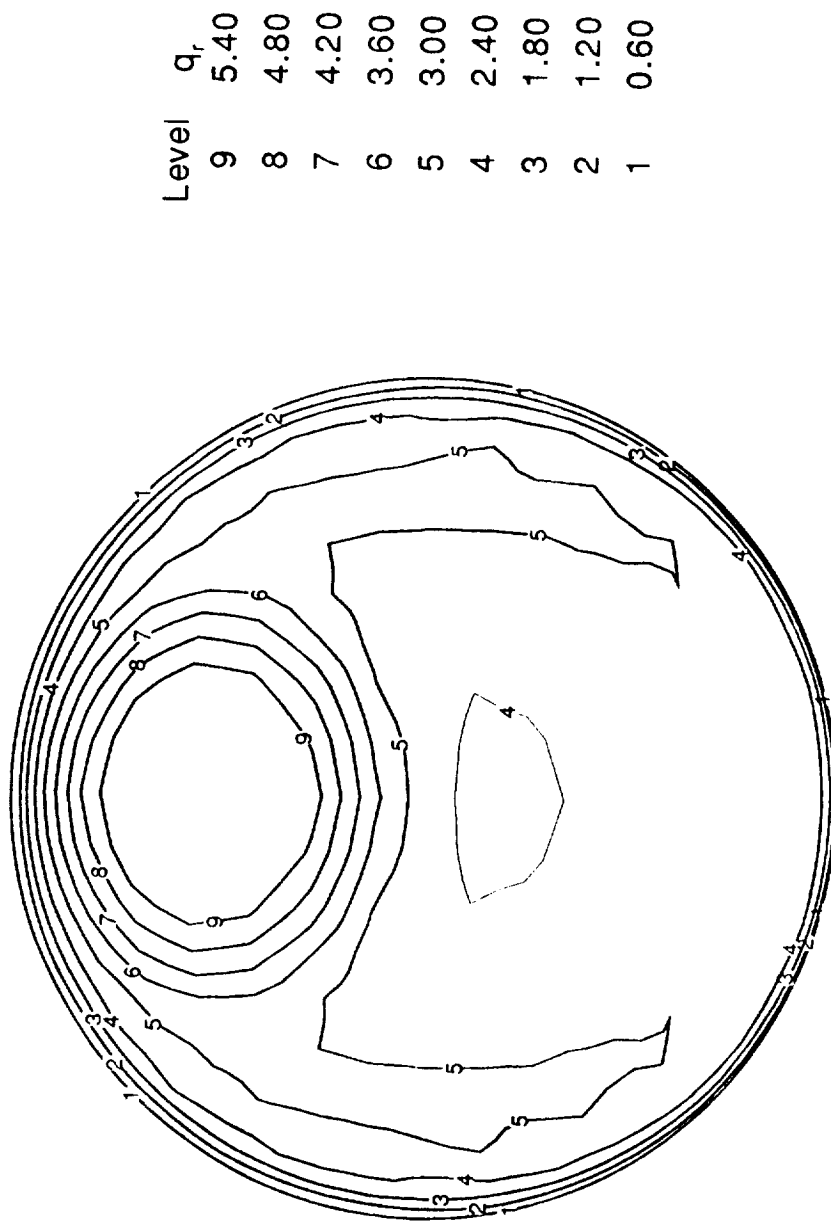
(c) q_r

Figure 10. - Concluded.
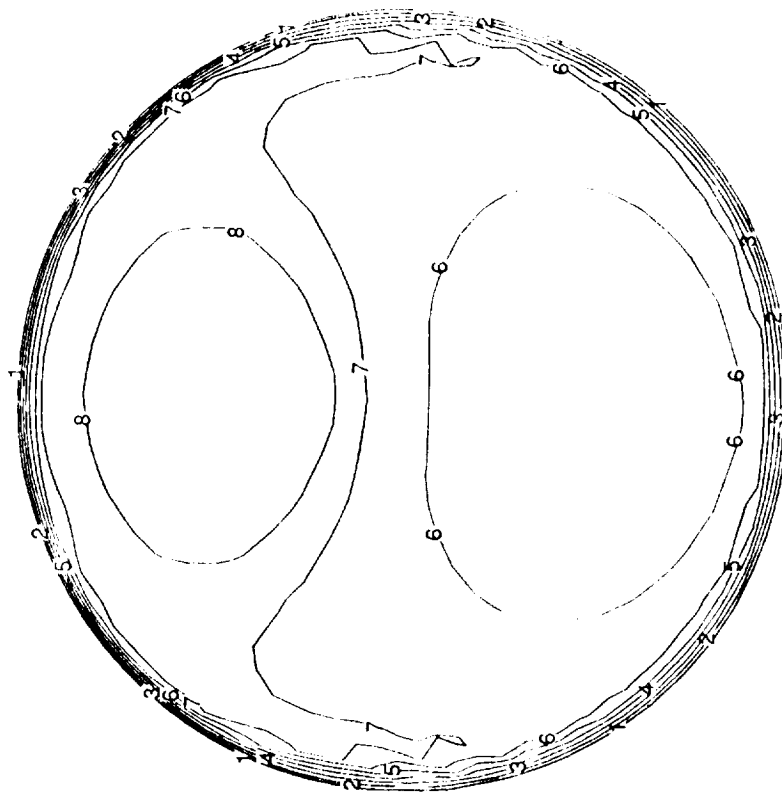
Level	T (°K)
9	1750.
8	1700.
7	1650.
6	1600.
5	1550.
4	1500.
3	1450.
2	1400.
1	1350.

Figure 11. – Wall Temperature Contours at Start of Quiescent Period.

Report Documentation Page

1. Report No. NASA TM-104103	2. Government Accession No.	3. Recipient's Catalog No.
4. Title and Subtitle Calculation of Convective and Radiative Heating on the Forebody Heatshield of the Aeroassist Flight Experiment Vehicle		5. Report Date May 1991
		6. Performing Organization Code
7. Author(s) H. Harris Hamilton II and Robert B. Greendyke		8. Performing Organization Report No.
		10. Work Unit No. 506-40-91-01
9. Performing Organization Name and Address NASA Langley Research Center Hampton, VA 23665-5225		11. Contract or Grant No.
		13. Type of Report and Period Covered Technical Memorandum
12. Sponsoring Agency Name and Address National Aeronautics and Space Administration Washington, DC 20546-0001		14. Sponsoring Agency Code

15. Supplementary Notes

H. Harris Hamilton: Langley Research Center, Hampton, Virginia.
Robert B. Greendyke: Analytical Services and Materials, Incorporated, Hampton, Virginia.

16. Abstract

The total (convective and radiative) heating is calculated over the entire forebody heatshield of the AFE vehicle. The convective heating is calculated using a three-dimensional Navier-Stokes code (LAURA) which includes both chemical and thermal nonequilibrium effects. The flowfield solution is then used to provide inputs to a nonequilibrium air radiation code (NEQAIR) to calculate the nonequilibrium radiative heating. Results are presented at two points on the current Baseline 5A trajectory corresponding to the start of the primary data taking period and peak heating.

17. Key Words (Suggested by Author(s)) AFE Nonequilibrium Convective heating Radiative heating	18. Distribution Statement Unclassified-Unlimited Subject Category 34

19. Security Classif. (of this report) Unclassified	20. Security Classif. (of this page) Unclassified	21. No. of pages 70	22. Price A04

NASA FORM 1626 OCT 86